TASOPT 2.00
Transport Aircraft System OPTimization

Technical Description

Mark Drela
20 Mar 10

Appendices A–F present the theory behind the TASOPT methodology and code. Appendix A describes the bulk of the formulation, while Appendices B–F develop the major sub-models for the engine, fuselage drag, BLI accounting, etc.

Contents

Appendix A

TASOPT — Transport Aircraft System OPTimization

A.1 Introduction

A.1.1 Background

There is a vast body of work on conceptual and preliminary aircraft design. The more traditional approaches of e.g. Roskam [1], Torrenbeek [2], Raymer [3], have relied heavily on historical weight correlations, empirical drag build-ups, and established engine performance data for their design evaluations. The ACSYNT program [4],[5] likewise relies on such models, with a more detailed treatment of the geometry via its PDCYL [6] extension.

More recently, optimization-based approaches such as those of Knapp [7], the WINGOP code of Wakayama [8],[9], and in particular the PASS program of Kroo [10] perform tradeoffs in a much more detailed geometry parameter space, but still rely on simple drag and engine performance models.

The recent advent of turbofan engines with extremely high bypass ratios (Pratt geared turbofan), advanced composite materials (Boeing 787), and possibly less restrictive operational restrictions (Free-Flight ATC concept), make it of great interest to re-examine the overall aircraft/engine/operation system to maximize transportation efficiency. NASA's N+1,2,3 programs are examples of research efforts towards this goal. In addition, greater emphasis on limiting noise and emissions demands that such aircraft design examination be done under possibly stringent environmental constraints. Optimally exploiting these new factors and constraints on transport aircraft is a major motivation behind TASOPT's development.

A.1.2 Summary

Overall approach

To examine and evaluate future aircraft with potentially unprecedented airframe, engine, or operation parameters, it is desirable to dispense with as many of the historically-based

methods as possible, since these cannot be relied on outside of their data-fit ranges. The approach used by TASOPT is to base most of the weight, aerodynamic, and engine-performance prediction on low-order models which implement fundamental structural, aerodynamic, and thermodynamic theory and associated computational methods. Historical correlations will be used only where absolutely necessary, and in particular only for some of the secondary structure and for aircraft equipment. Modeling the bulk of the aircraft structure, aerodynamics, and propulsion by fundamentals gives considerable confidence that the resulting optimized design is realizable, and not some artifact of inappropriate extrapolated data fits.

Airframe structure and weight

The airframe structural and weight models used by TASOPT treat the primary structure elements as simple geometric shapes, with appropriate load distributions imposed at critical loading cases. The fuselage is assumed to be a pressure vessel with one or more "bubbles", with added bending loads, with material gauges sized to obtain a specified stress at specified load situations. The wing is assumed to be cantilevered or to have a single support strut, whose material gauges are also sized to obtain a specified stress. The resulting fuselage, wing, and tail material volumes, together with specified material density, then gives the primary structural weight. Only the secondary structural weights and non-structural and equipment weights are estimated via historical weight fractions.

Aerodynamic performance

The wing airfoil performance is represented by a parameterized transonic airfoil family spanning a range of thicknesses, whose performance is determined by 2D viscous/inviscid CFD calculation for a range of lift coefficients and Mach numbers. Together with suitable sweep corrections, this gives reliable profile+wave drag of the wing in cruise and high climb and high descent. The fuselage drag is likewise obtained from compressible viscous/inviscid CFD, suitably simplified with axisymmetric-based approximations. A side benefit is that detailed knowledge of the fuselage boundary layers makes it possibly for TASOPT to reliably predict the benefits of boundary layer ingestion in fuselage-mounted engines.

The drag of only the minor remaining components such as nacelles is obtained by traditional wetted area methods, but corrected for supervelocities estimated with vortex sheet models. Induced drag is predicted by fairly standard Trefftz-Plane analysis.

The primary use of CFD-level results in the present TASOPT method makes it more widely applicable than the previous more traditional approaches which have typically relied on wetted-area methods for major components of the configuration.

Engine performance

A fairly detailed component-based turbofan model, such as described by Kerrebrock [11], is used to both size the engines for cruise, and to determine their off-design performance at takeoff, climb, and descent. The model includes the effects of turbine cooling flows, allowing realistic simultaneous optimization of cycle pressure ratios and operating temperatures

together with the overall airframe and its operating parameters. The overall aircraft and engine system is actually formulated in terms of dissipation and power rather than drag and thrust [12], which allows a rigorous examination of advanced propulsion systems using boundary layer ingestion.

The use of component-based engine simulation in the present TASOPT method differs from previous approaches which typically have relied on simple historical regressions or established engine performance maps. The more detailed treatment is especially important for examining designs with extreme engines parameters which fall outside of historical databases.

Mission profiles

Integration of standard trajectory equations over a parameterized mission profile provides the required mission weight, which completes the overall sizing approach. The end result is a defined aircraft and engine combination which achieves the specified payload and range mission. Off-design missions are also addressed, allowing the possibility of minimizing fuel burn for a collection of fleet missions rather than for just the aircraft-sizing mission.

Takeoff and noise

A takeoff performance model is used to determine the normal takeoff distance and the balanced field length of any given design. The balanced field length can be included as a constraint in overall TASOPT optimization. Noise estimates are also calculated using a few published methods, e.g. [13], [14], [15]. These are used only for run-time rough estimates, and are not well suited for use as constraints. Much more detailed noise analyses can typically be performed as a post-processing step using the ANOPP method, for example.

Restriction to wing+tube aircraft

The description of the structural and aerodynamic models above explains why TASOPT is restricted to tube+wing configurations — most other configurations would be quite difficult or impossible to treat with these models. For example, a joined-wing configuration [16] has a relatively complex structure with out-of-plane deformations and the possibility of coupled twist/bend buckling in the presence of eccentricity from the airloads, which requires a greatly more complex structural analysis than straightforward beam theory. A blended-wing-body configuration [17] with non-circular cabin cross sections likewise has non-obvious critical load cases and load paths, and its transonic aerodynamics are dominated by 3D effects. For these reasons such non-traditional configurations are simply outside the scope of the present work.

A.2 Model Derivation

A.2.1 Weight Breakdown

The weight breakdown is summarized in Figure A.1, to serve as a convenient reference.

W_{MTO}

W_{pay} — 1

W_{fuse}:
- W_{padd} — f_{padd}
- W_{apu} — f_{apu}
- W_{fix}
- W_{shell}:
  - W_{skin} — 1
  - f_{string}
  - f_{frame}
  - f_{fadd}
  - W_{db}
- W_{window}
- W_{insul}
- W_{seat}
- W_{floor}
- W_{cone} — f_{cone}
- W_{hbend} — f_{hbend}
- W_{vbend} — f_{vbend}

W_{wing}:
- W_{wcap} — 1 — 1
- W_{wweb}
- W_{wadd}:
  - W_{flap} — f_{flap}
  - W_{slat} — f_{slat}
  - W_{aile} — f_{aile}
  - W_{lete} — f_{lete}
  - W_{ribs} — f_{ribs}
  - W_{spoi} — f_{spoi}
  - W_{watt} — f_{watt}
  - f_{wadd} — f_{wing}

W_{strut} — f_{strut}

W_{tail}:
W_{htail}:
- W_{hcap} — 1
- W_{hweb}
- W_{hadd} — f_{hadd} — f_{htail}

W_{vtail}:
- W_{vcap} — 1
- W_{vweb}
- W_{vadd} — f_{vadd} — f_{vtail}

W_{eng}:
- W_{ebare} — 1
- W_{eadd} — f_{eadd} — 1
- W_{nace} — f_{eng}
- W_{pylon} — f_{pylon}

W_{fuel}:
- W_{burn} — 1 — f_{fuel}
- W_{reserve} — f_{reserve}

W_{hpesys} — f_{hpesys}
W_{lgnose} — f_{lgnose}
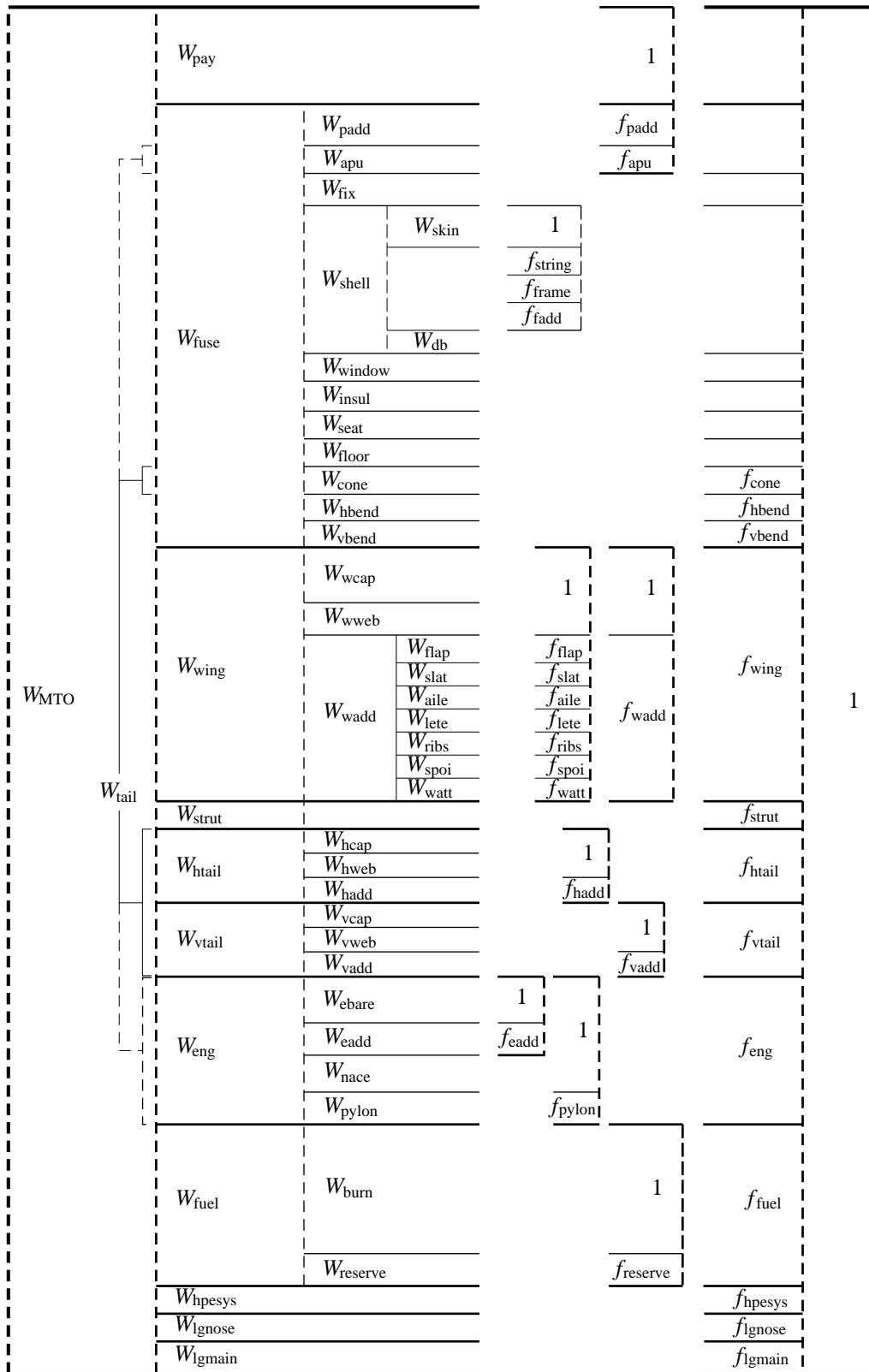W_{lgmain} — f_{lgmain}

1

Figure A.1: Aircraft weights and weight fractions breakdown.

A.2.2   Fuselage pressure and torsion loads

The fuselage is modeled as a side-by-side "double-bubble" pressure vessel with an ellipsoidal nose endcap and a hemispherical tail endcap, which is subjected to pressurization, bending,

and torsion loads, as shown in Figures A.2 and A.3. The loaded cylindrical length of the pressure vessel shell is from x_{shell_1} to x_{shell_2}.

$$l_{\text{shell}} \;\; = \;\; x_{\text{shell}_2} - x_{\text{shell}_1} \tag{A.1}$$

The horizontal-axis moment $\mathcal{M}_{\text{h}(x)}$ distributions on the front and back bending fuselage are assumed to match at location x_{wing}, as shown in Figure A.2. Theoretically this is the wing's net lift–weight centroid, which varies somewhat depending the fuel fraction in the wings, the wing's profile pitching moment and hence the flap setting, and on the aircraft C_L. For simplicity it will be approximated as the wing's area centroid. Note that for a swept wing the wing box location x_{wbox} will be centered somewhat ahead of x_{wing}, but it will then also impart a pitch-axis moment at its location, so that the front and back $\mathcal{M}_{\text{h}(x)}$ distributions must still match at x_{wing}.
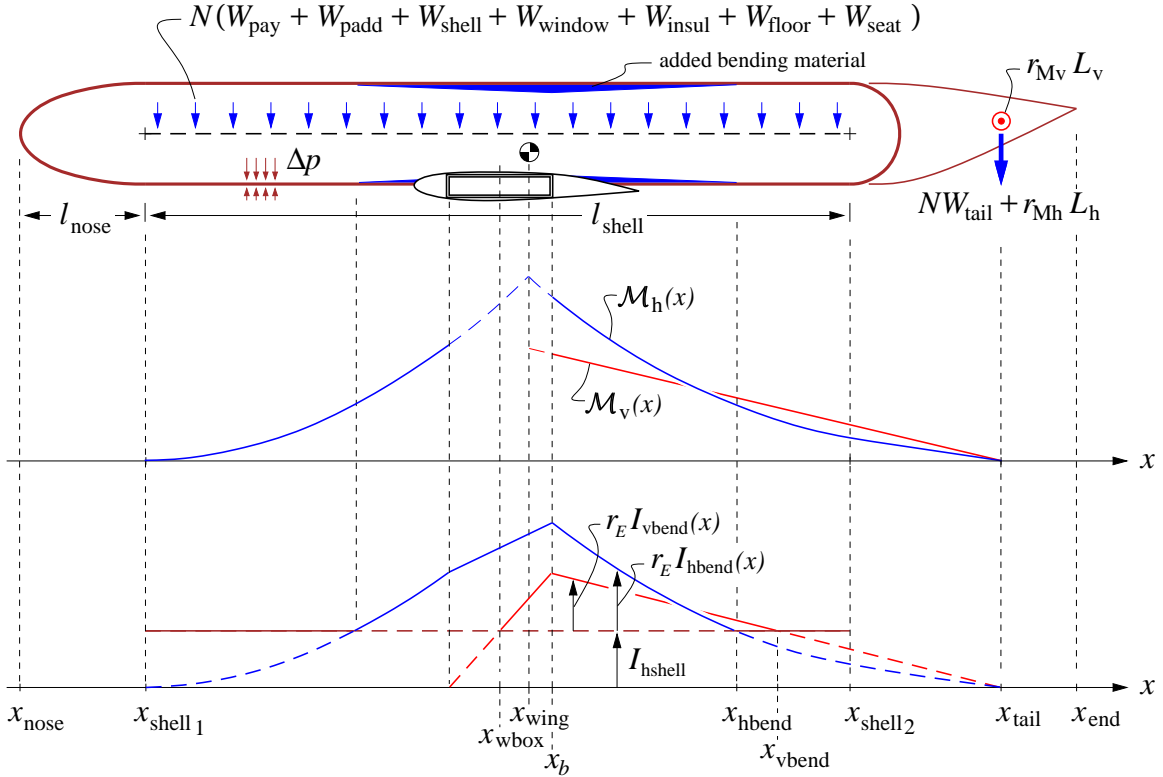
Figure A.2: Fuselage layout, loads, and bending moment and inertia distributions. Bending material and $r_E I_{\text{hbend}(x)}$ is added wherever the horizontal-axis bending moment $\mathcal{M}_{\text{h}(x)}$ exceeds the capability of the pressure vessel's bending inertia I_{hshell}, and likewise for the vertical-axis moment and inertia.

Figure A.3 shows the fuselage cross section. The pressure-vessel skin and endcaps have a uniform thickness t_{skin}, while the center tension web has an average thickness t_{db}. The cross-sectional area of the skin is A_{skin}, and has stiffening stringers which have a "smeared" average area $A_{\text{skin}} f_{\text{string}} \rho_{\text{skin}} / \rho_{\text{bend}}$, specified via the empirical stringer/skin weight fraction f_{string}. The enclosed area S_{skin} enters the torsional stiffness and strength calculations. The fuselage cross section also shows the possibility of added bottom bubbles or fairings, extended downward by the distance ΔR_{fuse}.

The skin and stringers constitute the "shell", which has bending inertias $I_{\text{hshell}}, I_{\text{vshell}}$ about the horizontal and vertical axes. Figure A.3 does not show any hoop-stiffening frames which are typically required, and whose weight is a specified fraction f_{frame} of the skin weight. These typically may be offset from the skin inside of the stringers, and hence are assumed to not contribute to the skin's circumferential tensile strength.

To address the weight and aerodynamic loads of the tail group on the fuselage, the horizontal and vertical tails, the tailcone, and any rear-mounted engines are treated as one lumped mass and aero force at location x_{tail}, shown in Figure A.2.

The bending loads on the shell may require the addition of vertical-bending material concentrated on top and bottom of the fuselage shell (typically as skin doublers or additional stringers). The total added cross sectional area is $A_{\text{hbend}(x)}$, and the associated added bending inertia is $I_{\text{hbend}(x)}$. Corresponding added material on the sides has $A_{\text{vbend}(x)}$ and $I_{\text{vbend}(x)}$. Because the wing box itself will contribute to the fuselage bending strength, these added areas and bending inertias do not match the $\mathcal{M}_{(x)}$ distribution there, but are made linear over the wing box extent, as shown in Figure A.2.
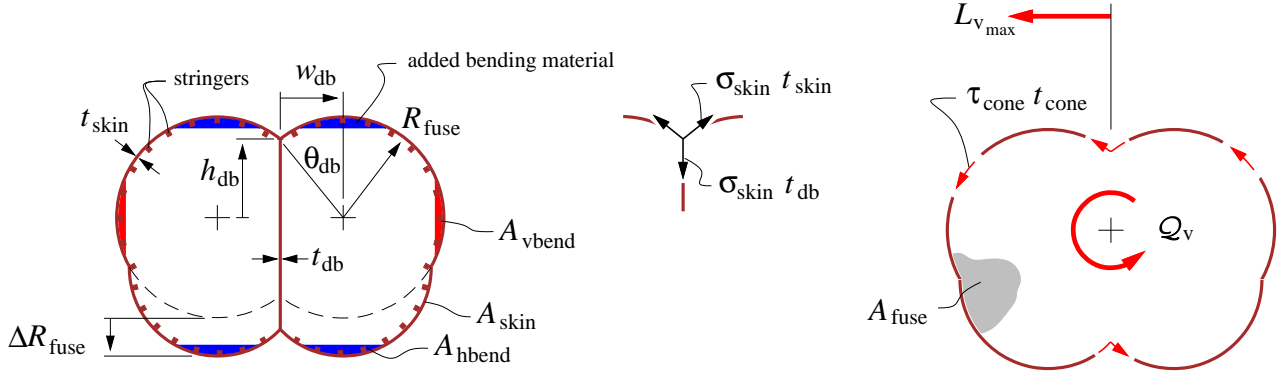
Figure A.3: Fuselage cross-section, shell/web junction tension flows, and torsion shear flow from vertical tail load. An optional bottom fairing extends down by the distance ΔR_{fuse}. Fuselage frames are not shown.

Cross-section relations

The fuselage pressure shell has the following geometric relations and beam quantities.

$$\theta_{\text{db}} = \arcsin(w_{\text{db}}/R_{\text{fuse}}) \tag{A.2}$$

$$h_{\text{db}} = \sqrt{R_{\text{fuse}}^2 - w_{\text{db}}^2} \tag{A.3}$$

$$A_{\text{skin}} = (2\pi + 4\theta_{\text{db}}) R_{\text{fuse}} t_{\text{skin}} + 2\Delta R_{\text{fuse}} t_{\text{skin}} \tag{A.4}$$

$$A_{\text{db}} = (2h_{\text{db}} + \Delta R_{\text{fuse}}) t_{\text{db}} \tag{A.5}$$

$$A_{\text{fuse}} = (\pi + 2\theta_{\text{db}} + \sin 2\theta_{\text{db}}) R_{\text{fuse}}^2 + 2R_{\text{fuse}} \Delta R_{\text{fuse}} \tag{A.6}$$

The skin has some modulus and density $E_{\text{skin}}, \rho_{\text{skin}}$, while the stringers have some possibly different values $E_{\text{bend}}, \rho_{\text{bend}}$. The effective modulus-weighted "shell" thickness t_{shell} can then

be defined as follows, assuming that only the skin and stringers contribute to bending, but not the frames.

$$t_{\text{shell}} = \frac{(Et)_{\text{skin}}}{E_{\text{skin}}} = t_{\text{skin}}\left(1 + r_E \, f_{\text{string}} \frac{\rho_{\text{skin}}}{\rho_{\text{bend}}}\right) \tag{A.7}$$

$$\text{where} \quad r_E = \frac{E_{\text{bend}}}{E_{\text{skin}}} \tag{A.8}$$

This is then convenient for determining the modulus-weighted horizontal-axis and vertical-axis bending inertias. The center web, if any, is assumed to be made of the same material as the skin.

$$
\begin{aligned}
I_{\text{hshell}} &= \frac{(EI)_{\text{hshell}}}{E_{\text{skin}}} \\
&= 4 \int_0^{\pi/2+\theta_{\text{db}}} (R_{\text{fuse}} \sin\theta + \Delta R_{\text{fuse}}/2)^2 \, R_{\text{fuse}} \, t_{\text{shell}} \, d\theta \;+\; \frac{2}{3}(h_{\text{db}} + \Delta R_{\text{fuse}}/2)^3 t_{\text{db}} \\
&= \Big[(\pi + 2\theta_{\text{db}} + \sin 2\theta_{\text{db}}) R_{\text{fuse}}^2 \\
&\qquad + 8\cos\theta_{\text{db}} \, (\Delta R_{\text{fuse}}/2) \, R_{\text{fuse}} \\
&\qquad + (2\pi + 4\theta_{\text{db}}) (\Delta R_{\text{fuse}}/2)^2 \Big] R_{\text{fuse}} \, t_{\text{shell}} \;+\; \frac{2}{3}(h_{\text{db}} + \Delta R_{\text{fuse}}/2)^3 t_{\text{db}} \tag{A.9}
\end{aligned}
$$

$$
\begin{aligned}
I_{\text{vshell}} &= \frac{(EI)_{\text{vshell}}}{E_{\text{skin}}} \\
&= 4 \int_0^{\pi/2+\theta_{\text{db}}} (R_{\text{fuse}} \cos\theta + w_{\text{db}})^2 \, R_{\text{fuse}} \, t_{\text{shell}} \, d\theta \\
&= \Big[(\pi + 2\theta_{\text{db}} - \sin 2\theta_{\text{db}}) R_{\text{fuse}}^2 \\
&\qquad + 8\cos\theta_{\text{db}} \, w_{\text{db}} \, R_{\text{fuse}} \\
&\qquad + (2\pi + 4\theta_{\text{db}}) w_{\text{db}}^2 \Big] R_{\text{fuse}} \, t_{\text{shell}} \tag{A.10}
\end{aligned}
$$

It's useful to note that for the particular case of $w_{\text{db}} = 0$ and $\Delta R_{\text{fuse}} = 0$, the cross-section circles merge into one circle, and the tension and hence the thickness of the center web go to zero, $t_{\text{db}} = 0$. The areas and bending inertias then reduce to those for a single circular cross-section.

$$A_{\text{skin}} = 2\pi R_{\text{fuse}} \, t_{\text{skin}} \qquad (\text{if } w_{\text{db}} = 0, \Delta R_{\text{fuse}} = 0) \tag{A.11}$$

$$S_{\text{skin}} = \pi R_{\text{fuse}}^2 \qquad (\text{if } w_{\text{db}} = 0, \Delta R_{\text{fuse}} = 0) \tag{A.12}$$

$$I_{\text{hshell}} = I_{\text{vshell}} = \pi R_{\text{fuse}}^3 \, t_{\text{shell}} \qquad (\text{if } w_{\text{db}} = 0, \Delta R_{\text{fuse}} = 0) \tag{A.13}$$

Hence, no generality is lost with this double-bubble cross-section model.

Pressure shell loads

The pressurization load from the Δp pressure difference produces the following axial and hoop stresses in the fuselage skin, with the assumption that the stringers share the axial loads, but the frames do not share the hoop loads. This assumes a typical aluminum fuselage structure, where the stringers are contiguous and solidly riveted to the skin, but the frames

are either offset from the skin or have clearance cutouts for the stringers which interrupt the frames' hoop loads.

$$\sigma_x = \frac{\Delta p}{2} \frac{R_{\text{fuse}}}{t_{\text{shell}}} \tag{A.14}$$

$$\sigma_\theta = \Delta p \frac{R_{\text{fuse}}}{t_{\text{skin}}} \tag{A.15}$$

An isotropic (metal) fuselage skin thickness t_{skin} and the web thickness t_{db} will therefore be sized by the larger σ_θ value in order to meet an allowable stress σ_{skin}.

$$t_{\text{skin}} = \frac{\Delta p\, R_{\text{fuse}}}{\sigma_{\text{skin}}} \tag{A.16}$$

$$t_{\text{db}} = 2 \frac{\Delta p\, w_{\text{db}}}{\sigma_{\text{skin}}} \tag{A.17}$$

This particular t_{db} value is obtained from the requirement of equal circumferential stress in the skin and the web, and tension equilibrium at the 3-point web/skin junction.

The volume of the skin material $\mathcal{V}_{\text{skin}}$ is obtained from the cross-sectional skin area, plus the contribution of the ellipsoidal nose endcap and the spherical rear bulkhead. The nose uses Cantrell's approximation for the surface area of an ellipsoid.

$$S_{\text{nose}} \simeq (2\pi + 4\theta_{\text{db}})R_{\text{fuse}}^2 \left[\frac{1}{3} + \frac{2}{3}\left(\frac{l_{\text{nose}}}{R_{\text{fuse}}} \right)^{8/5} \right]^{5/8} \tag{A.18}$$

$$S_{\text{bulk}} \simeq (2\pi + 4\theta_{\text{db}})R_{\text{fuse}}^2 \tag{A.19}$$

$$\mathcal{V}_{\text{cyl}} = A_{\text{skin}}\, l_{\text{shell}} \tag{A.20}$$

$$\mathcal{V}_{\text{nose}} = S_{\text{nose}}\, t_{\text{skin}} \tag{A.21}$$

$$\mathcal{V}_{\text{bulk}} = S_{\text{bulk}}\, t_{\text{skin}} \tag{A.22}$$

$$\mathcal{V}_{\text{db}} = A_{\text{db}}\, l_{\text{shell}} \tag{A.23}$$

$$x\mathcal{V}_{\text{cyl}} = \tfrac{1}{2}(x_{\text{shell}_1} + x_{\text{shell}_2})\, \mathcal{V}_{\text{cyl}} \tag{A.24}$$

$$x\mathcal{V}_{\text{nose}} = \tfrac{1}{2}(x_{\text{nose}} + x_{\text{shell}_1})\, \mathcal{V}_{\text{nose}} \tag{A.25}$$

$$x\mathcal{V}_{\text{bulk}} = (x_{\text{shell}_2} + \tfrac{1}{2}\Delta R_{\text{fuse}})\, \mathcal{V}_{\text{bulk}} \tag{A.26}$$

$$x\mathcal{V}_{\text{db}} = \tfrac{1}{2}(x_{\text{shell}_1} + x_{\text{shell}_2})\, \mathcal{V}_{\text{db}} \tag{A.27}$$

The total fuselage shell weight then follows by specifying a material density ρ_{skin} for the skin and web. The assumed skin-proportional added weights of local reinforcements, stiffeners, and fasteners are represented by the f_{fadd} fraction, and stringers and frames are represented by the $f_{\text{string}}, f_{\text{frame}}$ fractions.

$$W_{\text{skin}} = \rho_{\text{skin}}\, g\, (\mathcal{V}_{\text{cyl}} + \mathcal{V}_{\text{nose}} + \mathcal{V}_{\text{bulk}}) \tag{A.28}$$

$$W_{\text{db}} = \rho_{\text{skin}}\, g\, \mathcal{V}_{\text{db}} \tag{A.29}$$

$$xW_{\text{skin}} = \rho_{\text{skin}}\, g\, (x\mathcal{V}_{\text{cyl}} + x\mathcal{V}_{\text{nose}} + x\mathcal{V}_{\text{bulk}}) \tag{A.30}$$

$$xW_{\text{db}} = \rho_{\text{skin}}\, g\, x\mathcal{V}_{\text{db}} \tag{A.31}$$

$$W_{\text{shell}} = W_{\text{skin}}(1 + f_{\text{string}} + f_{\text{frame}} + f_{\text{fadd}}) + W_{\text{db}} \tag{A.32}$$

$$xW_{\text{shell}} = xW_{\text{skin}}(1 + f_{\text{string}} + f_{\text{frame}} + f_{\text{fadd}}) + xW_{\text{db}} \tag{A.33}$$

Cabin volume and Buoyancy weight

At this point it's convenient to calculate the pressurized cabin volume.

$$\mathcal{V}_{\text{cabin}} = A_{\text{fuse}} (l_{\text{shell}} + 0.67\, l_{\text{nose}} + 0.67\, R_{\text{fuse}}) \tag{A.34}$$

The air in the cabin is pressurized to either the specified minimum cabin pressure p_{cabin}, or the ambient pressure at altitude $p_{0(h)}$, whichever is greater. The resulting negative cabin buoyancy increases the effective instantaneous weight of the aircraft by the added buoyancy weight $W_{\text{buoy}(h)}$ which varies with altitude.

$$\rho_{\text{cabin}(h)} = \frac{1}{RT_{\text{cabin}}} \max\left(p_{\text{cabin}}\, ,\, p_{0(h)}\right) \tag{A.35}$$

$$W_{\text{buoy}} = \left(\rho_{\text{cabin}(h)} - \rho_{0(h)}\right) g\, \mathcal{V}_{\text{cabin}} \tag{A.36}$$

This is then added to the physical weight to give the net effective aircraft weight used for cruise wing sizing and performance calculations.

$$\bar{W} = W + W_{\text{buoy}} \tag{A.37}$$

Windows and Insulation

The window weight is specified by their assumed net weight/length density W'_{window}, together with the cabin length l_{shell}.

$$W_{\text{window}} = W'_{\text{window}}\, l_{\text{shell}} \tag{A.38}$$

$$xW_{\text{window}} = \tfrac{1}{2}(x_{\text{shell}_1} + x_{\text{shell}_2}) W_{\text{window}} \tag{A.39}$$

The W'_{window} value represents the actual window weight, minus the weight of the skin and insulation cutout which is eliminated by the window.

The fuselage insulation and padding weight is specified by its assumed weight/area density W''_{insul}, together with the cabin+endcap shell surface area.

$$W_{\text{insul}} = W''_{\text{insul}} \left[(1.1\pi + 2\theta_{\text{db}}) R_{\text{fuse}}\, l_{\text{shell}} + 0.55\, (S_{\text{nose}} + S_{\text{bulk}}) \right] \tag{A.40}$$

$$xW_{\text{insul}} = \tfrac{1}{2}(x_{\text{shell}_1} + x_{\text{shell}_2}) W_{\text{insul}} \tag{A.41}$$

The 1.1 and 0.55 factors assume that 55% of the fuselage circle is over the cabin, and the remaining 45% is over the cargo hold which has no insulation.

Payload-proportional weights

The APU weight W_{apu} is assumed to be proportional to the payload weight, and is treated as a point weight at some specified location x_{apu}.

$$W_{\text{apu}} = W_{\text{pay}}\, f_{\text{apu}} \tag{A.42}$$

$$xW_{\text{apu}} = x_{\text{apu}}\, W_{\text{apu}} \tag{A.43}$$

The seat weight is also assumed to be proportional to the payload weight, uniformly distributed along the cabin for a single-class aircraft.

$$W_{\text{seat}} = W_{\text{pay}} f_{\text{seat}} \tag{A.44}$$

$$xW_{\text{seat}} = \tfrac{1}{2}(x_{\text{shell}\,1} + x_{\text{shell}\,2})W_{\text{seat}} \tag{A.45}$$

Another payload-proportional weight W_{padd} is used to represent all remaining added weight: flight attendants, food, galleys, toilets, luggage compartments and furnishings, doors, lighting, air conditioning systems, in-flight entertainment systems, etc. These are also assumed to be uniformly distributed on average.

$$W_{\text{padd}} = W_{\text{pay}} f_{\text{padd}} \tag{A.46}$$

$$xW_{\text{padd}} = \tfrac{1}{2}(x_{\text{shell}\,1} + x_{\text{shell}\,2})W_{\text{padd}} \tag{A.47}$$

The proportionality factors $f_{\text{apu}}, f_{\text{seat}}, f_{\text{padd}}$ will depend on generator technology, seat technology, passenger class, and slightly on long-haul versus short-haul aircraft.

Fixed weight

A specified fixed weight contribution W_{fix} is assumed. This represents the pilots, cockpit windows, cockpit seats and control mechanisms, flight instrumentation, navigation and communication equipment, antennas, etc., which are expected to be roughly the same total weight for any transport aircraft. To get the associated weight moment, a specified weight centroid x_{fix} is also specified. Typically this will be located in the nose region.

$$W_{\text{fix}} = \dots \text{ specified} \tag{A.48}$$

$$xW_{\text{fix}} = x_{\text{fix}} W_{\text{fix}} \tag{A.49}$$

Floor

The weight of the transverse floor beams is estimated by assuming the payload weight is distributed uniformly over the floor, producing the shear and bending moment distributions shown in Figure A.4. The weight of the floor itself is typically much smaller than the payload and is neglected. The floor beams are assumed to by sized by some load factor N_{land}, which is typically the emergency landing case and greater than the usual in-flight load factor N_{lift} which sizes most of the airframe. This gives to following total distributed load on the floor.

$$\mathcal{P}_{\text{floor}} = N_{\text{land}}(W_{\text{pay}} + W_{\text{seat}}) \tag{A.50}$$

The floor/wall joints are assumed to be pinned, with the double-bubble fuselage having an additional center floor support. The single-bubble fuselage can of course also have center supports under the floor. The maximum shear and bending moment seen by all the floor beams put together are then readily obtained from simple beam theory.

$$\mathcal{S}_{\text{floor}} = \frac{1}{2}\mathcal{P}_{\text{floor}} \qquad \text{(w/o support)} \tag{A.51}$$

$$\mathcal{S}_{\text{floor}} = \frac{5}{16}\mathcal{P}_{\text{floor}} \qquad \text{(with support)} \tag{A.52}$$
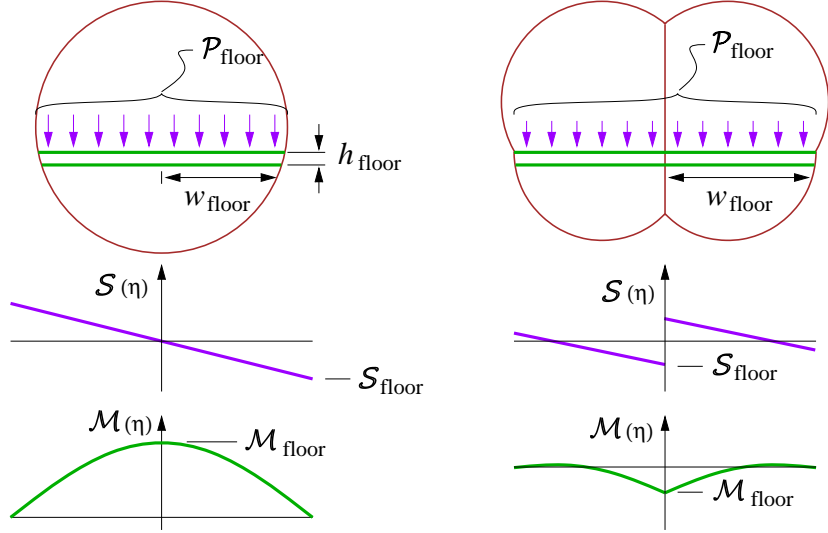
Figure A.4: Distributed floor load $\mathcal{P}_{\text{floor}}$, resulting in maximum shear $\mathcal{S}_{\text{floor}}$ and maximum bending moment $\mathcal{M}_{\text{floor}}$ in all the floor beams, without and with a center support.

$$\mathcal{M}_{\text{floor}} = \frac{1}{4}\,\mathcal{P}_{\text{floor}}\,w_{\text{floor}} \qquad \text{(w/o support)} \tag{A.53}$$

$$\mathcal{M}_{\text{floor}} = \frac{9}{256}\,\mathcal{P}_{\text{floor}}\,w_{\text{floor}} \qquad \text{(with support)} \tag{A.54}$$

$$w_{\text{floor}} \simeq w_{\text{db}} + R_{\text{fuse}} \tag{A.55}$$

Note that $w_{\text{db}}\!=\!0$ for a single-bubble fuselage, so that the expression for the floor half-width w_{floor} above is valid in general.

For a given floor I-beam height h_{floor}, and max allowable cap stress σ_{floor} and shear-web stress τ_{floor}, the beams' total average cross-sectional area and corresponding weight are then determined. The added weight of the floor planking is determined from a specified weight/area density W''_{floor}.

$$A_{\text{floor}} = \frac{2.0\,\mathcal{M}_{\text{floor}}}{\sigma_{\text{floor}}\,h_{\text{floor}}} + \frac{1.5\,\mathcal{S}_{\text{floor}}}{\tau_{\text{floor}}} \tag{A.56}$$

$$\mathcal{V}_{\text{floor}} = 2\,w_{\text{floor}}\,A_{\text{floor}} \tag{A.57}$$

$$l_{\text{floor}} = x_{\text{shell}_2} - x_{\text{shell}_1} + 2R_{\text{fuse}} \tag{A.58}$$

$$W_{\text{floor}} = \rho_{\text{floor}}\,g\,\mathcal{V}_{\text{floor}} + 2\,w_{\text{floor}}\,l_{\text{floor}}\,W''_{\text{floor}} \tag{A.59}$$

$$xW_{\text{floor}} = \tfrac{1}{2}(x_{\text{shell}_1} + x_{\text{shell}_2})W_{\text{floor}} \tag{A.60}$$

Relation (A.56) assumes the beams are uniform in cross-section. Suitable taper of the cross section would reduce the 2.0 and 1.5 coefficients substantially, especially for the center-supported case for which the bending moment rapidly diminishes away from the center.

It's also important to recognize that if clamped ends rather than the assumed pinned end joints are used, and if the center support is present, then the hoop compliance of the fuselage frame cross-section shape will become important. Without doing the much more complicated deformation analysis of the entire fuselage frame + floor cross section, the conservative pinned-end and uniform beam assumptions are therefore deemed appropriate.

Tail cone

The tail cone average wall thickness is assumed to be sized by the torsion moment $\mathcal{Q}_v$ imparted by the vertical tail, defined in terms of its maximum lift $L_{v_{\max}}$, span b_v, and taper ratio λ_v.

$$L_{v_{\max}} = q_{NE}\, S_v\, C_{Lv_{\max}} \tag{A.61}$$

$$\mathcal{Q}_v = \frac{L_{v_{\max}}\, b_v}{3}\frac{1+2\lambda_v}{1+\lambda_v} \tag{A.62}$$

Referring to Figure A.3, this $\mathcal{Q}_v$ produces a shear flow $\tau_{\mathrm{cone}}\, t_{\mathrm{cone}}$ according to the torsion-shell relation

$$\mathcal{Q}_v = 2A_{\mathrm{cone}}\, \tau_{\mathrm{cone}}\, t_{\mathrm{cone}} \tag{A.63}$$

where the cone's enclosed area A_{cone} is assumed to taper linearly with a taper ratio of $\lambda_{\mathrm{cone}}^2$. The cone radius R_{cone} then tapers to a ratio of λ_{cone}, but nonlinearly. The taper extends from $x_{\mathrm{shell}\,2}$ to x_{conend}, the latter being the endpoint of the cone's primary structure, roughly at the horizontal or vertical tail attachment.

$$A_{\mathrm{cone}}(x) = A_{\mathrm{fuse}}\left[1+(\lambda_{\mathrm{cone}}^2-1)\frac{x-x_{\mathrm{shell}\,2}}{x_{\mathrm{conend}}-x_{\mathrm{shell}\,2}}\right] \tag{A.64}$$

$$R_{\mathrm{cone}}(x) = R_{\mathrm{fuse}}\left[1+(\lambda_{\mathrm{cone}}^2-1)\frac{x-x_{\mathrm{shell}\,2}}{x_{\mathrm{conend}}-x_{\mathrm{shell}\,2}}\right]^{1/2} \tag{A.65}$$

Setting $\mathcal{Q}_v$ to the moment imparted by the vertical tail lift gives the cone wall thickness t_{cone} and corresponding material volume and weight.

$$t_{\mathrm{cone}}(x) = \frac{\mathcal{Q}_v}{2\tau_{\mathrm{cone}}A_{\mathrm{cone}}(x)} \tag{A.66}$$

$$\mathcal{V}_{\mathrm{cone}} = \int_{x_{\mathrm{shell}\,2}}^{x_{\mathrm{conend}}} 2(\pi+2\theta_{\mathrm{db}})R_{\mathrm{cone}}\, t_{\mathrm{cone}}\, dx$$

$$= \frac{\mathcal{Q}_v}{\tau_{\mathrm{cone}}}\frac{\pi+2\theta_{\mathrm{db}}}{\pi+2\theta_{\mathrm{db}}+\sin 2\theta_{\mathrm{db}}}\frac{x_{\mathrm{conend}}-x_{\mathrm{shell}\,2}}{R_{\mathrm{fuse}}}\frac{2}{1+\lambda_{\mathrm{cone}}} \tag{A.67}$$

$$W_{\mathrm{cone}} = \rho_{\mathrm{cone}}\, g\, \mathcal{V}_{\mathrm{cone}}(1+f_{\mathrm{string}}+f_{\mathrm{frame}}+f_{\mathrm{fadd}}) \tag{A.68}$$

$$xW_{\mathrm{cone}} = \tfrac{1}{2}(x_{\mathrm{shell}\,2}+x_{\mathrm{conend}})\, W_{\mathrm{cone}} \tag{A.69}$$

A.2.3 Fuselage Bending Loads

In addition to the pressurization and torsion loads, the fuselage also sees bending loads from its distributed weight load plus the tail weight and airloads. In the case where the pressurization-sized shell is not sufficient to withstand this, additional bending material area is assumed to be added at the top and bottom (total of $A_{\mathrm{hbend}(x)}$), and also sides of the shell (total of $A_{\mathrm{vbend}(x)}$), as shown in Figure A.3. If the shell is sufficiently strong, then these areas will be zero.

17

Lumped tail weight and location for fuselage stresses

For simplicity in the fuselage bending stress analysis to be considered next, both the horizontal and vertical tails, the tailcone, and any APU or rear-engine weight loads (if present) are lumped into their summed weight W_{tail}, which is assumed to be located at the corresponding mass centroid location x_{tail}. The tail aero loads are also assumed to act at this point.

$$W_{\text{tail}} \;=\; W_{\text{htail}} + W_{\text{vtail}} + W_{\text{cone}} \;[\,+W_{\text{apu}} + W_{\text{eng}}] \tag{A.70}$$

$$x_{\text{tail}} \;=\; \frac{x_{\text{htail}}W_{\text{htail}} + x_{\text{vtail}}W_{\text{vtail}} + \frac{1}{2}(x_{\text{shell}\,2}+x_{\text{conend}})W_{\text{cone}} \;[\,+x_{\text{apu}}W_{\text{apu}} + x_{\text{eng}}W_{\text{eng}}]}{W_{\text{tail}}} \tag{A.71}$$

For the overall aircraft pitch balance and pitch stability analyses to be presented later, this lumping simplification will not be invoked.

Tail aero loads

An impulsive load on the horizontal or vertical tail will produce a direct static bending load on the aft fuselage. It will also result in an overall angular acceleration of the aircraft, whose distributed inertial-reaction loads will tend to alleviate the tail's static bending loads. These effects are captured by the inertial-relief factor r_{M} evaluated just to the right of the wingbox, which takes on the two different values r_{Mh} and r_{Mv} due to the different wing inertias about the horizontal and vertical axes. Typical values are $r_{\text{Mh}} \simeq 0.4$ and $r_{\text{Mv}} \simeq 0.7$, with the latter applied only over the rear fuselage. The resulting net bending moment distributions are shown in Figure A.5, where the static case is the limit for an infinitely massive wing.

The maximum tail loads are set at a specified never-exceed dynamic pressure q_{NE}, and some assumed max-achievable lift coefficient for each surface.

$$L_{\text{h}_{\max}} \;=\; q_{NE}\, S_{\text{h}}\, C_{Lh_{\max}} \tag{A.72}$$

$$L_{\text{v}_{\max}} \;=\; q_{NE}\, S_{\text{v}}\, C_{Lv_{\max}} \tag{A.73}$$

$$(\mathcal{M}_{\text{h}})_{\text{aero}} \;=\; \begin{cases} r_{\text{Mh}}\, L_{\text{h}_{\max}}\,(x_{\text{tail}} - x) & ,\quad x > x_{\text{wing}} \\ r_{\text{Mh}}\, L_{\text{h}_{\max}}\,(x + x_{\text{tail}} - 2x_{\text{wing}}) & ,\quad x < x_{\text{wing}} \end{cases} \tag{A.74}$$

$$(\mathcal{M}_{\text{v}})_{\text{aero}} \;=\; \begin{cases} r_{\text{Mv}}\, L_{\text{v}_{\max}}\,(x_{\text{tail}} - x) & ,\quad x > x_{\text{wing}} \\ 0.0 & ,\quad x < x_{\text{wing}} \end{cases} \tag{A.75}$$

$$r_{\text{M}} \;=\; 1 - \frac{I_{\text{fuse}}/2}{I_{\text{fuse}}+I_{\text{wing}}} - \frac{m_{\text{fuse}}/4}{m_{\text{fuse}}+m_{\text{wing}}} \tag{A.76}$$

$$r_{\text{Mh}} \;\simeq\; 0.4 \tag{A.77}$$

$$r_{\text{Mv}} \;\simeq\; 0.7 \tag{A.78}$$

Landing gear loads

The maximum vertical load on the landing gear typically occurs in the emergency landing case, and subjects the fuselage to some vertical acceleration $N = N_{\text{land}}$ which is specified. The fuselage distributed mass will then subject the fuselage to a bending load shown in Figure A.2.
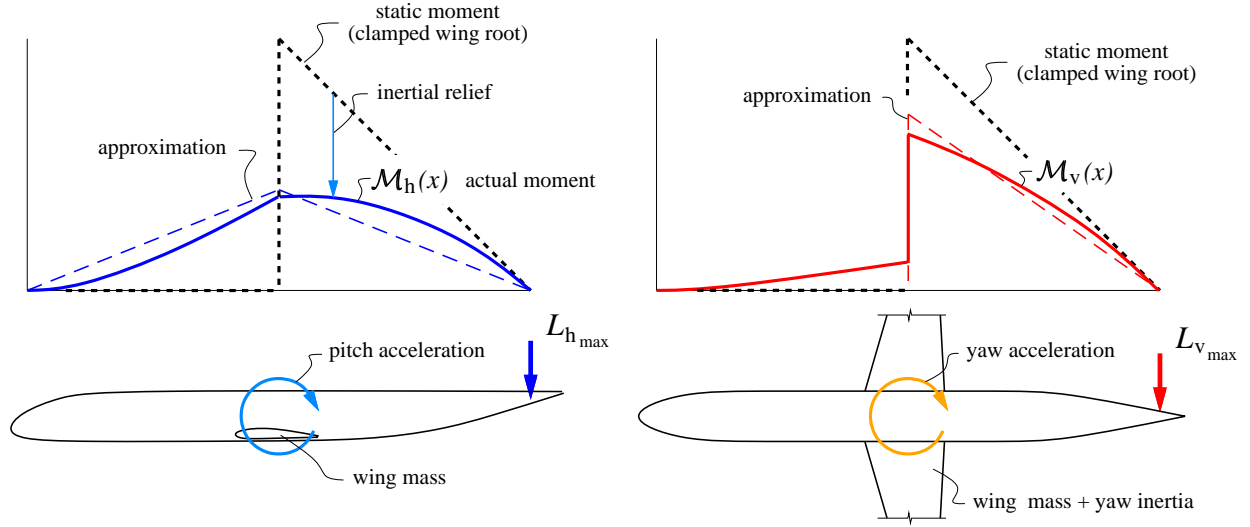
Figure A.5: Fuselage bending moments due to unbalanced horizontal and vertical tail aero loads. The static bending moment (dashed lines) is partly relieved by reaction loads from the overall angular acceleration.

Distributed and point weight loads

The fuselage is loaded by the payload weight W_{pay}, plus its own component weights W_{padd}, $W_{\text{shell}} \ldots$ etc. which are all assumed to be uniformly distributed over the fuselage shell length l_{shell}. The overall tail weight W_{tail} is assumed to be a point load at x_{tail}. With all weights scaled up by a load factor N, plus the impulsive horizontal-tail aero load moment (A.74), gives the following quadratic+linear horizontal-axis fuselage bending moment distribution, also sketched in Figure A.2.

$$
\begin{aligned}
\mathcal{M}_{\text{h}(x)} \;=\; & N \frac{W_{\text{pay}} + W_{\text{padd}} + W_{\text{shell}} + W_{\text{window}} + W_{\text{insul}} + W_{\text{floor}} + W_{\text{seat}}}{2\, l_{\text{shell}}} (x_{\text{shell}\,2} - x)^2 \\
& + \; (NW_{\text{tail}} + r_{\text{Mh}} L_{\text{h}})\, (x_{\text{tail}} - x)
\end{aligned}
\tag{A.79}
$$

Expression (A.79) has been constructed to represent the bending moment over the rear fuselage. Since the wing's inertial-reaction pitching moments are small compared to those of the tail and fuselage, the horizontal-axis bending moment is assumed to be roughly symmetric about the wing's center of lift at x_{wing}, as sketched in Figure A.2, so that (A.79) if reflected about x_{wing} also gives the bending moment over the front fuselage. For the same reason, the fixed weight W_{fix} is assumed to be concentrated near the aircraft nose, and hence it does not impose either a distributed load or a point load on the rear fuselage, and hence does not appear in (A.79).

Added horizontal-axis bending material

The total bending moment $\mathcal{M}_{\text{h}(x)}$ defined by (A.79) is used to size the added horizontal-axis bending area $A_{\text{hbend}(x)}$. Two loading scenarios are considered:

1. Maximum load factor at V_{NE}

$$N = N_{\text{lift}} \tag{A.80}$$

$$L_{\text{h}} = L_{\text{h}_{\text{max}}} \tag{A.81}$$

2. Emergency landing impact

$$N = N_{\text{land}} \tag{A.82}$$

$$L_{\text{h}} = 0 \tag{A.83}$$

The scenario which gives the larger added structural weight will be selected.

The maximum axial stress, which is related to the sum of the bending and pressurization strains, is limited everywhere to some maximum allowable value σ_{bend}.

$$E_{\text{bend}} \epsilon_x(x) = E_{\text{bend}} \left(\epsilon_{\text{bend}}(x) + \epsilon_{\text{press}} \right) \leq \sigma_{\text{bend}} \tag{A.84}$$

$$r_E \left(\frac{\mathcal{M}_{\text{h}}(x)\, h_{\text{fuse}}}{I_{\text{hshell}} + r_E\, I_{\text{hbend}}(x)} + \frac{\Delta p}{2} \frac{R_{\text{fuse}}}{t_{\text{shell}}} \right) \leq \sigma_{\text{bend}} \tag{A.85}$$

$$\text{where} \qquad h_{\text{fuse}} = R_{\text{fuse}} + \tfrac{1}{2} \Delta R_{\text{fuse}} \tag{A.86}$$

Relation (A.85) can then be solved for the required $I_{\text{hbend}(x)}$ and the associated $A_{\text{hbend}(x)}$.

$$I_{\text{hbend}}(x) = \max \left(\frac{\mathcal{M}(x)\, h_{\text{fuse}}}{\sigma_{\text{Mh}}} - \frac{I_{\text{hshell}}}{r_E} \, , \, 0 \right) \tag{A.87}$$

$$\text{where} \qquad \sigma_{\text{Mh}} = \sigma_{\text{bend}} - r_E \frac{\Delta p}{2} \frac{R_{\text{fuse}}}{t_{\text{shell}}} \tag{A.88}$$

$$A_{\text{hbend}}(x) = \frac{I_{\text{hbend}}(x)}{h_{\text{fuse}}^2} = A_2 (x_{\text{shell}_2} - x)^2 + A_1 (x_{\text{tail}} - x) + A_0 \tag{A.89}$$

$$\text{where} \qquad A_2 = \frac{N(W_{\text{pay}} + W_{\text{padd}} + W_{\text{shell}} + W_{\text{window}} + W_{\text{insul}} + W_{\text{floor}} + W_{\text{seat}})}{2\, l_{\text{shell}}\, h_{\text{fuse}}\, \sigma_{\text{Mh}}} \tag{A.90}$$

$$A_1 = \frac{N W_{\text{tail}} + r_{\text{Mh}} L_{\text{h}}}{h_{\text{fuse}}\, \sigma_{\text{Mh}}} \tag{A.91}$$

$$A_0 = -\frac{I_{\text{hshell}}}{r_E\, h_{\text{fuse}}^2} \tag{A.92}$$

The volume and weight of the added bending material is defined by integration of A_{hbend}, from the wing box to the location $x = x_{\text{hbend}}$ where $A_{\text{hbend}} = 0$ in the quadratic definition (A.89). If this quadratic has no real solution, then the inequality (A.79) holds for $\mathcal{M}_{\text{h}(x)} = 0$ everywhere, and no added bending material is needed.

Two separate integration limits are used for the front and back fuselage, to account for the shifted wing box for a swept wing. The integral for $\mathcal{V}_{\text{hbend}_f}$ for the front fuselage is actually computed over the back, by exploiting the assumed symmetry of $\mathcal{M}_{\text{h}(x)}$ and $A_{\text{hbend}(x)}$ about $x = x_{\text{wing}}$. The wing box offset Δx_{wing} is computed later in the wing-sizing section, so here it is taken from the previous iteration.

$$x_f = x_{\text{wing}} + \Delta x_{\text{wing}} + \tfrac{1}{2} c_o \bar{w} \tag{A.93}$$

$$x_b = x_{\text{wing}} - \Delta x_{\text{wing}} + \tfrac{1}{2}c_o\bar{w} \tag{A.94}$$

$$\mathcal{V}_{\text{hbend}_f} = \int_{x_f}^{x_{\text{hbend}}} A_{\text{hbend}(x)}\, dx$$

$$= A_2 \frac{1}{3}\left[(x_{\text{shell}_2} - x_f)^3 - (x_{\text{shell}_2} - x_{\text{hbend}})^3\right]$$

$$+ A_1 \frac{1}{2}\left[(x_{\text{tail}} - x_f)^2 - (x_{\text{tail}} - x_{\text{hbend}})^2\right]$$

$$+ A_0\left(x_{\text{hbend}} - x_f\right) \tag{A.95}$$

$$\mathcal{V}_{\text{hbend}_b} = \int_{x_b}^{x_{\text{hbend}}} A_{\text{hbend}(x)}\, dx$$

$$= A_2 \frac{1}{3}\left[(x_{\text{shell}_2} - x_b)^3 - (x_{\text{shell}_2} - x_{\text{hbend}})^3\right]$$

$$+ A_1 \frac{1}{2}\left[(x_{\text{tail}} - x_b)^2 - (x_{\text{tail}} - x_{\text{hbend}})^2\right]$$

$$+ A_0\left(x_{\text{hbend}} - x_b\right) \tag{A.96}$$

$$\mathcal{V}_{\text{hbend}_c} = \frac{1}{2}\left[A_{\text{hbend}(x_b)} + A_{\text{hbend}(x_f)}\right]c_o\bar{w} \tag{A.97}$$

$$\mathcal{V}_{\text{hbend}} = \mathcal{V}_{\text{hbend}_f} + \mathcal{V}_{\text{hbend}_c} + \mathcal{V}_{\text{hbend}_b} \tag{A.98}$$

$$W_{\text{hbend}} = \rho_{\text{bend}}\, g\, \mathcal{V}_{\text{hbend}} \tag{A.99}$$

$$xW_{\text{hbend}} = x_{\text{wing}}W_{\text{hbend}} \tag{A.100}$$

Added vertical-axis bending material

The vertical-axis bending moment on the rear fuselage is entirely due to the airload on the vertical tail (A.75), reduced by the r_{Mv} factor to account for inertial relief.

$$\mathcal{M}_{\text{v}(x)} = r_{\text{Mv}}\, L_{\text{v}_{\max}}\left(x_{\text{tail}} - x\right) \tag{A.101}$$

Since the wing is assumed to react the local $\mathcal{M}_{\text{v}}$ via its large yaw inertia, as sketched in Figure A.5, the moment distribution (A.101) is imposed only on the rear fuselage. The required bending inertia $I_{\text{vbend}(x)}$ and area $A_{\text{vbend}(x)}$ are then sized to keep the axial stress constant. The defining relations follow the ones for the horizontal-axis case above.

$$E_{\text{bend}}\epsilon_{x}(x) = r_E\left(\frac{\mathcal{M}_{\text{v}(x)}\, w_{\text{fuse}}}{I_{\text{vshell}} + r_E\, I_{\text{vbend}(x)}} + \frac{\Delta p}{2}\frac{R_{\text{fuse}}}{t_{\text{shell}}}\right) \leq \sigma_{\text{bend}} \tag{A.102}$$

$$\text{where} \qquad w_{\text{fuse}} = R_{\text{fuse}} + w_{\text{db}} \tag{A.103}$$

$$I_{\text{vbend}(x)} = \max\left(\frac{\mathcal{M}_{\text{v}(x)}\, w_{\text{fuse}}}{\sigma_{\text{Mv}}} - \frac{I_{\text{vshell}}}{r_E}\ ,\ 0\right) \tag{A.104}$$

$$\text{where} \qquad \sigma_{\text{Mv}} = \sigma_{\text{bend}} - r_E\frac{\Delta p}{2}\frac{R_{\text{fuse}}}{t_{\text{shell}}} \tag{A.105}$$

$$A_{\text{vbend}(x)} = \frac{I_{\text{vbend}(x)}}{w_{\text{fuse}}^2} = B_1(x_{\text{tail}} - x) + B_0 \tag{A.106}$$

$$\text{where} \qquad B_1 = \frac{r_{\text{Mv}}L_{\text{v}}}{w_{\text{fuse}}\,\sigma_{\text{Mv}}} \tag{A.107}$$

21

$$B_0 \;\; = \;\; -\frac{I_{\text{vshell}}}{r_E \, w_{\text{fuse}}^2} \tag{A.108}$$

The volume and weight of the added bending material is defined by integration of $A_{\text{vbend}(x)}$ over the rear fuselage, from the rear of the wing box x_b, up to the point $x = x_{\text{vbend}}$ where $A_{\text{vbend}} = 0$ in definition (A.106).

$$
\begin{aligned}
\mathcal{V}_{\text{vbend}_b} \;\; &= \;\; \int_{x_b}^{x_{\text{vbend}}} A_{\text{vbend}(x)} \, dx \\
&= \;\; B_1 \frac{1}{2} \left[(x_{\text{tail}} - x_b)^2 - (x_{\text{tail}} - x_{\text{vbend}})^2 \right] \; + \; B_0 \, (x_{\text{vbend}} - x_b) \tag{A.109}
\end{aligned}
$$

$$\mathcal{V}_{\text{vbend}_c} \;\; = \;\; \frac{1}{2} A_{\text{vbend}(x_b)} \, c_o \bar{w} \tag{A.110}$$

$$\mathcal{V}_{\text{vbend}} \;\; = \;\; \mathcal{V}_{\text{vbend}_c} + \mathcal{V}_{\text{vbend}_b} \tag{A.111}$$

$$W_{\text{vbend}} \;\; = \;\; \rho_{\text{bend}} \, g \mathcal{V}_{\text{vbend}} \tag{A.112}$$

$$xW_{\text{vbend}} \;\; = \;\; \tfrac{1}{3}(2x_{\text{wing}} + x_{\text{vbend}}) W_{\text{vbend}} \tag{A.113}$$

For simplicity, the $W_{\text{hbend}}, W_{\text{vbend}}$ weights' contributions to $\mathcal{M}_h$ are excluded from (A.79) and the subsequent calculations. A practical reason is that the added material does not have a simple distribution, and hence would greatly complicate the $\mathcal{M}_{h(x)}$ function, thus preventing the analytic integration of the added material's weight. Fortunately, the added bending material is localized close to the wing centroid and hence its contribution to the overall bending moment is very small in any case, so neglecting its weight on the loading is well justified at this level of approximation.

A.2.4 Total Fuselage Weight

The total fuselage weight includes the shell with stiffeners, tailcone, floor beams, fixed weight, payload-proportional equipment and material, seats, and the added horizontal and vertical-axis bending material.

$$
\begin{aligned}
W_{\text{fuse}} \;\; = \;\; & W_{\text{fix}} \; + \; W_{\text{apu}} \; + \; W_{\text{padd}} \; + \; W_{\text{seat}} \\
& + \; W_{\text{shell}} \; + \; W_{\text{cone}} \; + \; W_{\text{window}} \; + \; W_{\text{insul}} \; + \; W_{\text{floor}} \\
& + \; W_{\text{hbend}} \; + \; W_{\text{vbend}} \tag{A.114}
\end{aligned}
$$

$$
\begin{aligned}
xW_{\text{fuse}} \;\; = \;\; & xW_{\text{fix}} + xW_{\text{apu}} + xW_{\text{padd}} + xW_{\text{seat}} \\
& + \; xW_{\text{shell}} + xW_{\text{cone}} + xW_{\text{window}} + xW_{\text{insul}} + xW_{\text{floor}} \\
& + \; xW_{\text{hbend}} + xW_{\text{vbend}} \tag{A.115}
\end{aligned}
$$

A.2.5 Wing or Tail Planform

The surface geometry relations derived below correspond to the wing. Most of these apply equally to the tails if the wing parameters are simply replaced with the tail counterparts. The exceptions which pertail to only the wing will be indicated with "(Wing only)" in the subsection title.

Chord distribution

The wing or tail surface is assumed to have a two-piece linear planform with constant sweep Λ, shown in Figure A.6. The inner and outer surface planforms are defined in terms of the center chord c_o and the inner and outer taper ratios.

$$\lambda_s = c_s/c_o \tag{A.116}$$
$$\lambda_t = c_t/c_o \tag{A.117}$$

Similarly, the spanwise dimensions are defined in terms of the span b and the normalized spanwise coordinate η.

$$\eta = 2y/b \tag{A.118}$$
$$\eta_o = b_o/b \tag{A.119}$$
$$\eta_s = b_s/b \tag{A.120}$$

For generality, the wing center box width b_o is assumed to be different from the fuselage width to allow possibly strongly non-circular fuselage cross-sections. It will also be different for the tail surfaces. A planform break inner span b_s is defined, where possibly also a strut or engine is attached. Setting $b_s\!=\!b_o$ and $c_s\!=\!c_o$ will recover a single-taper surface.
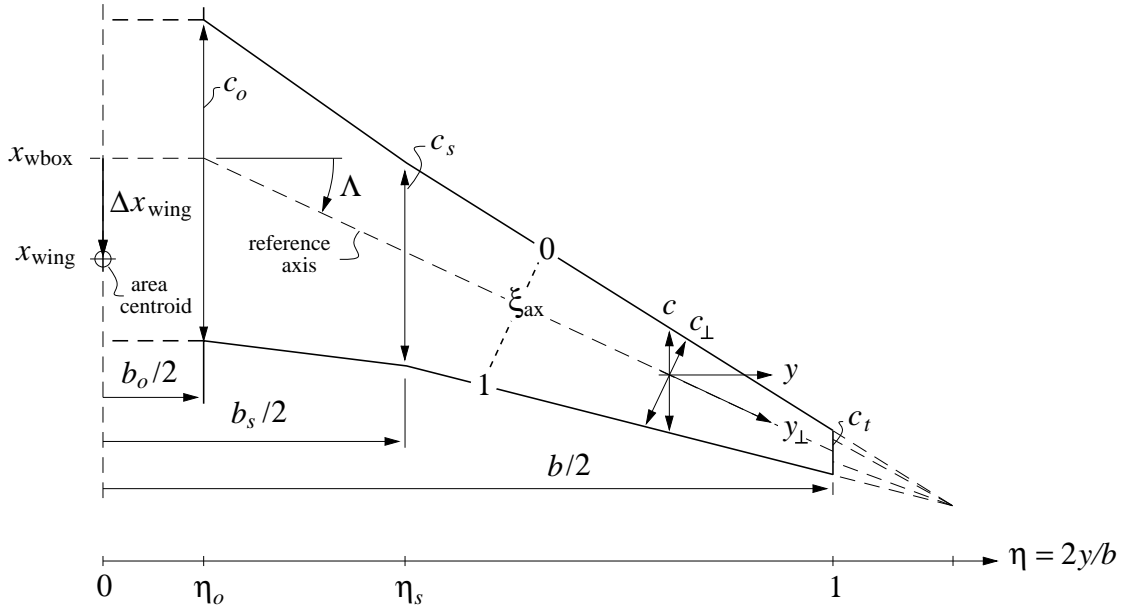
Figure A.6: Piecewise-linear wing or tail surface planform, with break at η_s.

It's convenient to define the piecewise-linear normalized chord function $C_{(\eta)}$.

$$\frac{c(\eta)}{c_o} \equiv C_{(\eta\,;\,\eta_o,\eta_s,\lambda_s,\lambda_t)} = \begin{cases} 1 & ,\ \ 0 < \eta < \eta_o \\[2mm] 1 + (\lambda_s\!-\!1)\dfrac{\eta-\eta_o}{\eta_s-\eta_o} & ,\ \ \eta_o < \eta < \eta_s \\[2mm] \lambda_s + (\lambda_t\!-\!\lambda_s)\dfrac{\eta-\eta_s}{1-\eta_s} & ,\ \ \eta_s < \eta < 1 \end{cases} \tag{A.121}$$

The following integrals will be useful for area, volume, shear, and moment calculations.

$$\int_0^{\eta_o} C \, d\eta = \eta_o \tag{A.122}$$

$$\int_{\eta_o}^{\eta_s} C \, d\eta = \frac{1}{2}(1+\lambda_s)(\eta_s-\eta_o) \tag{A.123}$$

$$\int_{\eta_s}^1 C \, d\eta = \frac{1}{2}(\lambda_s+\lambda_t)(1-\eta_s) \tag{A.124}$$

$$\int_0^{\eta_o} C^2 \, d\eta = \eta_o \tag{A.125}$$

$$\int_{\eta_o}^{\eta_s} C^2 \, d\eta = \frac{1}{3}(1+\lambda_s+\lambda_s^2)(\eta_s-\eta_o) \tag{A.126}$$

$$\int_{\eta_s}^1 C^2 \, d\eta = \frac{1}{3}(\lambda_s^2+\lambda_s\lambda_t+\lambda_t^2)(1-\eta_s) \tag{A.127}$$

$$\int_{\eta_o}^{\eta_s} C \, (\eta-\eta_o) \, d\eta = \frac{1}{6}(1+2\lambda_s)(\eta_s-\eta_o)^2 \tag{A.128}$$

$$\int_{\eta_s}^1 C \, (\eta-\eta_s) \, d\eta = \frac{1}{6}(\lambda_s+2\lambda_t)(1-\eta_s)^2 \tag{A.129}$$

$$\int_{\eta_o}^{\eta_s} C^2 \, (\eta-\eta_o) \, d\eta = \frac{1}{12}(1+2\lambda_s+3\lambda_s^2)(\eta_s-\eta_o)^2 \tag{A.130}$$

$$\int_{\eta_s}^1 C^2 \, (\eta-\eta_s) \, d\eta = \frac{1}{12}(\lambda_s^2+2\lambda_s\lambda_t+3\lambda_t^2)(1-\eta_s)^2 \tag{A.131}$$

Surface area and aspect ratio

The surface area S is defined as the exposed surface area plus the fuselage carryover area.

$$S = 2\int_0^{b/2} c \, dy = c_o \, b \, K_c \tag{A.132}$$

where
$$K_c = \int_0^1 C \, d\eta = \eta_o + \tfrac{1}{2}(1+\lambda_s)(\eta_s-\eta_o) + \tfrac{1}{2}(\lambda_s+\lambda_t)(1-\eta_s) \tag{A.133}$$

The aspect ratio is then defined in the usual way. This will also allow relating the root chord to the span and the taper ratios.

$$AR = \frac{b^2}{S} \tag{A.134}$$

It is also useful to define the wing's mean aerodynamic chord c_{ma} and area-centroid offset Δx_{wing} from the center axis.

$$\frac{c_{\mathrm{ma}}}{c_o} = \frac{2}{S}\int_0^{b/2} c^2 \, dy = \frac{K_{cc}}{K_c} \tag{A.135}$$

$$\Delta x_{\mathrm{wing}} = \frac{2}{S}\int_{b_o/2}^{b/2} c \, (y-y_o) \tan\Lambda \, dy = \frac{K_{cx}}{K_c} b \, \tan\Lambda \tag{A.136}$$

$$x_{\mathrm{wing}} = x_{\mathrm{wbox}} + \Delta x_{\mathrm{wing}} \tag{A.137}$$

where $K_{cc} = \displaystyle\int_0^1 C^2 \, d\eta$

24

$$= \eta_o + \frac{1}{3}(1+\lambda_s+\lambda_s^2)(\eta_s-\eta_o) + \frac{1}{3}(\lambda_s^2+\lambda_s\lambda_t+\lambda_t^2)(1-\eta_s) \tag{A.138}$$

$$K_{cx} = \int_{\eta_o}^{1} C\,(\eta-\eta_o)\,d\eta$$

$$= \frac{1}{12}(1+2\lambda_s)(\eta_s-\eta_o)^2 + \frac{1}{12}(\lambda_s+2\lambda_t)(1-\eta_s)^2 + \frac{1}{4}(\lambda_s+\lambda_t)(1-\eta_s)(\eta_s-\eta_o) \tag{A.139}$$

The wing area centroid is used in the fuselage bending load calculations as described earlier.

Reference quantities

The aircraft reference quantities are chosen to be simply the values for the wing.

$$b_{\text{ref}} = (b)_{\text{wing}} \tag{A.140}$$
$$S_{\text{ref}} = (S)_{\text{wing}} \tag{A.141}$$
$$AR_{\text{ref}} = (AR)_{\text{wing}} \tag{A.142}$$

For normalizing pitching moments the mean aerodynamic chord is traditionally used.

$$c_{\text{ref}} = c_{MA} \tag{A.143}$$

$$c_{MA} \equiv \frac{2}{S_{\text{ref}}} \int_0^{b/2} c^2\,dy = \frac{c_o^2\,b}{S_{\text{ref}}} \int_0^1 C^2\,d\eta$$

$$= \frac{c_o^2\,b}{S_{\text{ref}}} \left[\eta_o + \frac{1}{3}(1+\lambda_s+\lambda_s^2)(\eta_s-\eta_o) + \frac{1}{3}(\lambda_s^2+\lambda_s\lambda_t+\lambda_t^2)(1-\eta_s) \right] \tag{A.144}$$

A.2.6 Surface Airloads

Lift distribution

The surface lift distribution $\tilde{p}$ is defined in terms of a baseline piecewise-linear distribution $p_{(\eta)}$ defined like the chord planform, but with its own taper ratios γ_s and γ_t. These are actually defined using local section c_ℓ factors $r_{c_{\ell s}}$ and $r_{c_{\ell t}}$.

$$\gamma_s = r_{c_{\ell s}}\lambda_s \tag{A.145}$$
$$\gamma_t = r_{c_{\ell t}}\lambda_t \tag{A.146}$$

$$\frac{p_{(\eta)}}{p_o} \equiv P_{(\eta\,;\,\eta_o,\eta_s,\gamma_s,\gamma_t)} = \begin{cases} 1 & ,\quad 0 < \eta < \eta_o \\[2mm] 1 + (\gamma_s-1)\dfrac{\eta-\eta_o}{\eta_s-\eta_o} & ,\quad \eta_o < \eta < \eta_s \\[2mm] \gamma_s + (\gamma_t-\gamma_s)\dfrac{\eta-\eta_s}{1-\eta_s} & ,\quad \eta_s < \eta < 1 \end{cases} \tag{A.147}$$

To get the actual aerodynamic load $\tilde{p}$, lift corrections ΔL_o and ΔL_t are applied to account for the fuselage carryover and tip lift rolloff, as sketched in Figure A.7. The detailed shapes of these modifications are not specified, but instead only their integrated loads are defined by the following integral relation.

$$\frac{L_{\text{wing}}}{2} = \int_0^{b/2} \tilde{p}\,dy = \int_0^{b/2} p\,dy + \Delta L_o + \Delta L_t \tag{A.148}$$
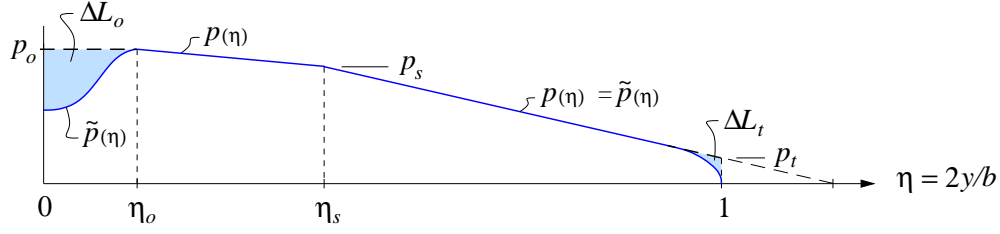
Figure A.7: Piecewise-linear aerodynamic load $\tilde{p}_{(\eta)}$, with modifications at center and tip.

The corrections are specified in terms of the center load magnitude p_o and the f_{L_o}, f_{L_t} adjustment factors.

$$\Delta L_o \;\;=\;\; f_{L_o}\, p_o\, \frac{b_o}{2} \;\;=\;\; f_{L_o}\, p_o\, \frac{b}{2}\, \eta_o \tag{A.149}$$

$$\Delta L_t \;\;=\;\; f_{L_t}\, p_t\, c_t \;\;=\;\; f_{L_t}\, p_o\, c_o\, \gamma_t\, \lambda_t \tag{A.150}$$

$$f_{L_o} \;\;\simeq\;\; -0.5 \tag{A.151}$$

$$f_{L_t} \;\;\simeq\;\; -0.05 \tag{A.152}$$

Lift load magnitude (Wing only)

The wing's p_o center loading magnitude is determined by requiring that the aerodynamic loading integrated over the whole span is equal to the total weight times the load factor, minus the tail lift.

$$2 \int_0^{b/2} \tilde{p}_{(\eta)}\, dy \;\;=\;\; p_o\, b \int_0^1 P_{(\eta)}\, d\eta \;+\; 2\Delta L_o \;+\; 2\Delta L_t \;\;=\;\; NW - (L_{\mathrm{htail}})_N \tag{A.153}$$

For structural sizing calculations $N = N_{\mathrm{lift}}$ is chosen, and the appropriate value of $(L_{\mathrm{htail}})_N$ is the worst-case (most negative) tail lift expected in the critical sizing case. One possible choice is the trimmed tail load at dive speed, where N_{lift} is most likely to occur.

The wing area (A.132) and aspect ratio (A.134) definitions allow the root chord and the tip lift drop (A.150) to be expressed as

$$c_o \;\;=\;\; b\, K_o \tag{A.154}$$

$$\Delta L_t \;\;=\;\; f_{L_t}\, p_o\, b\, K_o\, \gamma_t\, \lambda_t \tag{A.155}$$

$$\text{where} \qquad K_o \;\;=\;\; \frac{1}{K_c\, AR} \tag{A.156}$$

so that (A.153) can be evaluated to the following. The $P_{(\eta)}$ integrals have the form as for $C_{(\eta)}$, given by (A.122)–(A.131), but with the λ's replaced by γ's.

$$p_o\, b\, K_p \;\;=\;\; NW - (L_{\mathrm{htail}})_N \tag{A.157}$$

$$\text{where} \qquad K_p \;\;=\;\; \eta_o + \tfrac{1}{2}(1+\gamma_s)(\eta_s-\eta_o) + \tfrac{1}{2}(\gamma_s+\gamma_t)(1-\eta_s)$$

$$+\;\; f_{L_o}\eta_o + 2 f_{L_t} K_o \gamma_t \lambda_t \tag{A.158}$$

The root and planform-break loadings can then be explicitly determined.

$$p_o = \frac{NW - (L_{\text{htail}})_N}{K_p\, b} \tag{A.159}$$

$$p_s = p_o\, \gamma_s \tag{A.160}$$

$$p_t = p_o\, \gamma_t \tag{A.161}$$

Surface pitching moment

The surface's reference axis is at some specified chordwise fractional location ξ_{ax}, as shown in Figure A.6. The profile pitching moment acts along the span-axis coordinate $y_\perp$, and scales with the normal-plane chord $c_\perp$. These are shown in Figure A.6, and related to the spanwise and streamwise quantities via the sweep angle.

$$y_\perp = y/\cos\Lambda \tag{A.162}$$

$$c_\perp = c\,\cos\Lambda \tag{A.163}$$

$$V_\perp = V_\infty\,\cos\Lambda \tag{A.164}$$

The airfoil's pitching moment contribution shown in Figure A.8 is

$$dM_{y_\perp} = \frac{1}{2}\rho V_\perp^2\, c_\perp^2\, c_m\, dy_\perp \tag{A.165}$$

$$c_m(\eta) = \begin{cases} c_{m_o} & , \quad 0 < \eta < \eta_o \\[2mm] c_{m_o} + (c_{m_s} - c_{m_o})\dfrac{\eta - \eta_o}{\eta_s - \eta_o} & , \quad \eta_o < \eta < \eta_s \\[2mm] c_{m_s} + (c_{m_t} - c_{m_s})\dfrac{\eta - \eta_s}{1 - \eta_s} & , \quad \eta_s < \eta < 1 \end{cases} \tag{A.166}$$

and including the contribution of the lift load $\tilde{p}$ with its moment arm gives the following overall wing pitching moment ΔM_{wing} increment about the axis center location.

$$d\Delta M_{\text{wing}} = \tilde{p}\left[c_\perp\left(\xi_{\text{ax}} - \tfrac{1}{4}\right)\cos\Lambda - (y - y_o)\tan\Lambda\right] dy + dM_{y_\perp}\cos\Lambda \tag{A.167}$$

Integrating this along the whole span then gives the total surface pitching moment about its root axis.

$$\begin{aligned} \Delta M_{\text{wing}} = &\; (p_o\, b_o + 2\Delta L_o)\, c_o\left(\xi_{\text{ax}} - \tfrac{1}{4}\right) \\[2mm] &+\; \cos^2\Lambda\, b \int_{\eta_o}^{1} p_{(\eta)}\, c_{(\eta)}\left(\xi_{\text{ax}} - \tfrac{1}{4}\right) d\eta \\[2mm] &-\; \frac{b}{2}\tan\Lambda\, b \int_{\eta_o}^{1} p_{(\eta)}(\eta - \eta_o)\, d\eta \\[2mm] &+\; 2\Delta L_t\left[c_o \lambda_t\left(\xi_{\text{ax}} - \tfrac{1}{4}\right)\cos^2\Lambda - \frac{b}{2}(1 - \eta_o)\tan\Lambda\right] \\[2mm] &+\; \frac{1}{2}\rho V_\infty^2\,\cos^4\Lambda\, b \int_{\eta_o}^{1} c_{m(\eta)}\, c_{(\eta)}^2\, d\eta \end{aligned} \tag{A.168}$$

$$\Delta M_{\text{wing}} = p_o\, b\, c_o\, \eta_o\,(1 + f_{Lo})\left(\xi_{\text{ax}} - \tfrac{1}{4}\right)$$

$$+ \; p_o \, b \, c_o \left(\xi_{\text{ax}} - \tfrac{1}{4}\right) \cos^2\!\Lambda \; \frac{1}{3} \left[\left(1 + \tfrac{1}{2}\left(\lambda_s + \gamma_s\right) + \lambda_s\gamma_s\right)\left(\eta_s - \eta_o\right) \right.$$
$$\left. + \left(\lambda_s\gamma_s + \tfrac{1}{2}\left(\lambda_s\gamma_t + \gamma_s\lambda_t\right) + \lambda_t\gamma_t\right)\left(1 - \eta_s\right) \right]$$
$$- \; p_o \, b \, c_o \, \frac{\tan\Lambda}{K_o} \frac{1}{12} \left[\left(1 + 2\gamma_s\right)\left(\eta_s - \eta_o\right)^2 + \left(\gamma_s + 2\gamma_t\right)\left(1 - \eta_s\right)^2 + 3\left(\gamma_s + \gamma_t\right)\left(\eta_s - \eta_o\right)\left(1 - \eta_s\right) \right]$$
$$+ \; 2\, p_o \, b \, c_o \, f_{L_t} \, \lambda_t \, \gamma_t \left[K_o \lambda_t \left(\xi_{\text{ax}} - \tfrac{1}{4}\right) \cos^2\!\Lambda - \tfrac{1}{2}(1 - \eta_o)\tan\Lambda \right]$$
$$+ \; \frac{1}{2}\rho V_\infty^2 \, S \, c_o \, \frac{\cos^4\!\Lambda}{K_c} \frac{1}{12} \left[\left(c_{m_o}(3 + 2\lambda_s + \lambda_s^2) + c_{m_s}(3\lambda_s^2 + 2\lambda_s + 1)\right)\left(\eta_s - \eta_o\right) \right.$$
$$\left. + \left(c_{m_s}(3\lambda_s^2 + 2\lambda_s\lambda_t + \lambda_t^2) + c_{m_t}(3\lambda_t^2 + 2\lambda_s\lambda_t + \lambda_s^2)\right)\left(1 - \eta_s\right) \right] \qquad \text{(A.169)}$$

By using the relation

$$p_o \, b \;=\; \frac{1}{2}\rho V_\infty^2 \, S \, \frac{1}{K_p}\left(C_L - \frac{S_\text{h}}{S}C_{L_\text{h}}\right) \qquad\qquad \text{(A.170)}$$

equation (A.169) gives the equivalent pitching moment coefficient constant and C_L derivative.

$$\Delta C_{M_\text{wing}} \;\equiv\; \frac{\Delta M_\text{wing}}{\frac{1}{2}\rho V_\infty^2 S c_o} \;=\; \Delta C_{M_0} + \frac{dC_M}{dC_L}\left(C_L - \frac{S_\text{h}}{S}C_{L_\text{h}}\right) \qquad\qquad \text{(A.171)}$$

$$\frac{dC_M}{dC_L} \;=\; \frac{1}{K_p}\left\{ \eta_o\left(1 + f_{L_o}\right)\left(\xi_{\text{ax}} - \tfrac{1}{4}\right) \right.$$
$$+ \left(\xi_{\text{ax}} - \tfrac{1}{4}\right)\cos^2\!\Lambda \; \frac{1}{3}\left[\left(1 + \tfrac{1}{2}\left(\lambda_s + \gamma_s\right) + \lambda_s\gamma_s\right)\left(\eta_s - \eta_o\right)\right.$$
$$\left. + \left(\lambda_s\gamma_s + \tfrac{1}{2}\left(\lambda_s\gamma_t + \gamma_s\lambda_t\right) + \lambda_t\gamma_t\right)\left(1 - \eta_s\right)\right]$$
$$- \frac{\tan\Lambda}{K_o}\frac{1}{12}\left[\left(1 + 2\gamma_s\right)\left(\eta_s - \eta_o\right)^2 + \left(\gamma_s + 2\gamma_t\right)\left(1 - \eta_s\right)^2\right.$$
$$\left. + 3\left(\gamma_s + \gamma_t\right)\left(\eta_s - \eta_o\right)\left(1 - \eta_s\right)\right]$$
$$\left. + 2\, f_{L_t}\,\lambda_t\,\gamma_t\left[K_o\lambda_t\left(\xi_{\text{ax}} - \tfrac{1}{4}\right)\cos^2\!\Lambda - \tfrac{1}{2}(1 - \eta_o)\tan\Lambda\right] \right\} \qquad \text{(A.172)}$$

$$\Delta C_{M_0} \;=\; \frac{\cos^4\!\Lambda}{K_c}\frac{1}{12}\left[\left(c_{m_o}(3 + 2\lambda_s + \lambda_s^2) + c_{m_s}(3\lambda_s^2 + 2\lambda_s + 1)\right)\left(\eta_s - \eta_o\right)\right.$$
$$\left. + \left(c_{m_s}(3\lambda_s^2 + 2\lambda_s\lambda_t + \lambda_t^2) + c_{m_t}(3\lambda_t^2 + 2\lambda_s\lambda_t + \lambda_s^2)\right)\left(1 - \eta_s\right)\right] \qquad \text{(A.173)}$$

A.2.7   Wing or Tail Structural Loads

Figure A.9 shows the airload $\tilde{p}$ again, partly offset by weight load distributions of the structure and fuel, producing shear and bending moment distributions.

Shear and bending moment magnitudes

The $\mathcal{S}_s$, $\mathcal{M}_s$ magnitudes at η_s are set by integration of the assumed $p_{(\eta)}$ defined by (A.147), with the tip lift drop ΔL_t is included as a point load at the tip station. The weight loading
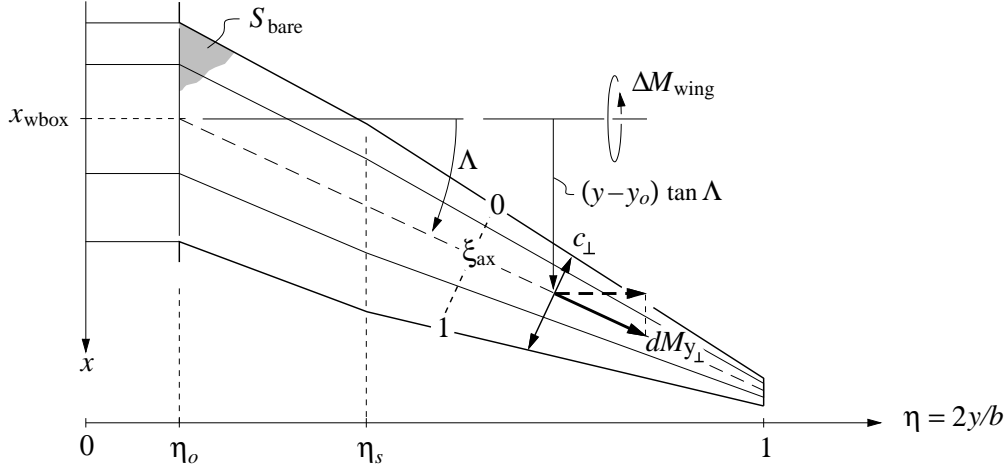
Figure A.8: Wing pitching moment quantities.

$w_{(\eta)}$ is also included via its overall outer panel weight W_{out} and weight moment $\Delta y W_{\text{out}}$, which are typically taken from a previous weight iteration.

$$
\begin{aligned}
\mathcal{S}_s &= \frac{b}{2} \int_{\eta_s}^{1} p_{(\eta)} \, d\eta \; + \; \Delta L_t \; - \; N W_{\text{out}} \\
&= \frac{p_o \, b}{4} (\gamma_s + \gamma_t)(1 - \eta_s) \; + \; \Delta L_t \; - \; N W_{\text{out}}
\end{aligned}
\tag{A.174}
$$

$$
\begin{aligned}
\mathcal{M}_s &= \frac{b^2}{4} \int_{\eta_s}^{1} p_{(\eta)} (\eta - \eta_s) \, d\eta \; + \; \Delta L_t \frac{b}{2}(1 - \eta_s) \; - \; N \Delta y W_{\text{out}} \\
&= \frac{p_o \, b^2}{24} (\gamma_s + 2\gamma_t)(1 - \eta_s)^2 \; + \; \Delta L_t \frac{b}{2}(1 - \eta_s) \; - \; N \Delta y W_{\text{out}}
\end{aligned}
\tag{A.175}
$$

Similarly, the $\mathcal{S}_o$ and $\mathcal{M}_o$ magnitudes at η_o are obtained by integrating the inner loading $p_{(\eta)}$, and adding the contributions of the strut load vertical component $\mathcal{R}$ and the spar compression component $\mathcal{P}$. The latter is applied at the strut attachment point, at a normal-offset distance n_s, as shown in Figure A.9.

$$
\begin{aligned}
\mathcal{S}_o &= \mathcal{S}_s \; - \; \mathcal{R} \; + \; \frac{b}{2} \int_{\eta_o}^{\eta_s} p_{(\eta)} \, d\eta \; - \; N W_{\text{inn}} \\
&= \mathcal{S}_s \; - \; \mathcal{R} \; + \; \frac{p_o \, b}{4} (1 + \gamma_s)(\eta_s - \eta_o) \; - \; N W_{\text{inn}}
\end{aligned}
\tag{A.176}
$$

$$
\begin{aligned}
\mathcal{M}_o &= \mathcal{M}_s - \mathcal{P} n_s + (\mathcal{S}_s - \mathcal{R})\frac{b}{2}(\eta_s - \eta_o) + \frac{b^2}{4} \int_{\eta_o}^{\eta_s} p_{(\eta)} (\eta - \eta_o) \, d\eta \; - \; N \Delta y W_{\text{inn}} \\
&= \mathcal{M}_s - \mathcal{P} n_s + (\mathcal{S}_s - \mathcal{R})\frac{b}{2}(\eta_s - \eta_o) + \frac{p_o \, b^2}{24}(1 + 2\gamma_s)(\eta_s - \eta_o)^2 \; - \; N \Delta y W_{\text{inn}}
\end{aligned}
\tag{A.177}
$$

Outer surface shear and bending moment distributions

Rather than obtain the exact $\mathcal{S}_{(\eta)}$ and $\mathcal{M}_{(\eta)}$ distributions by integration of the assumed $p_{(\eta)}$, $\mathcal{S}_s$ and $\mathcal{M}_s$ are simply scaled with the appropriate power of the local chord.

$$
\mathcal{S}_{(\eta)} \;=\; \mathcal{S}_s \left(\frac{c}{c_s} \right)^2 \quad , \qquad (\eta_s \le \eta \le 1)
\tag{A.178}
$$

29
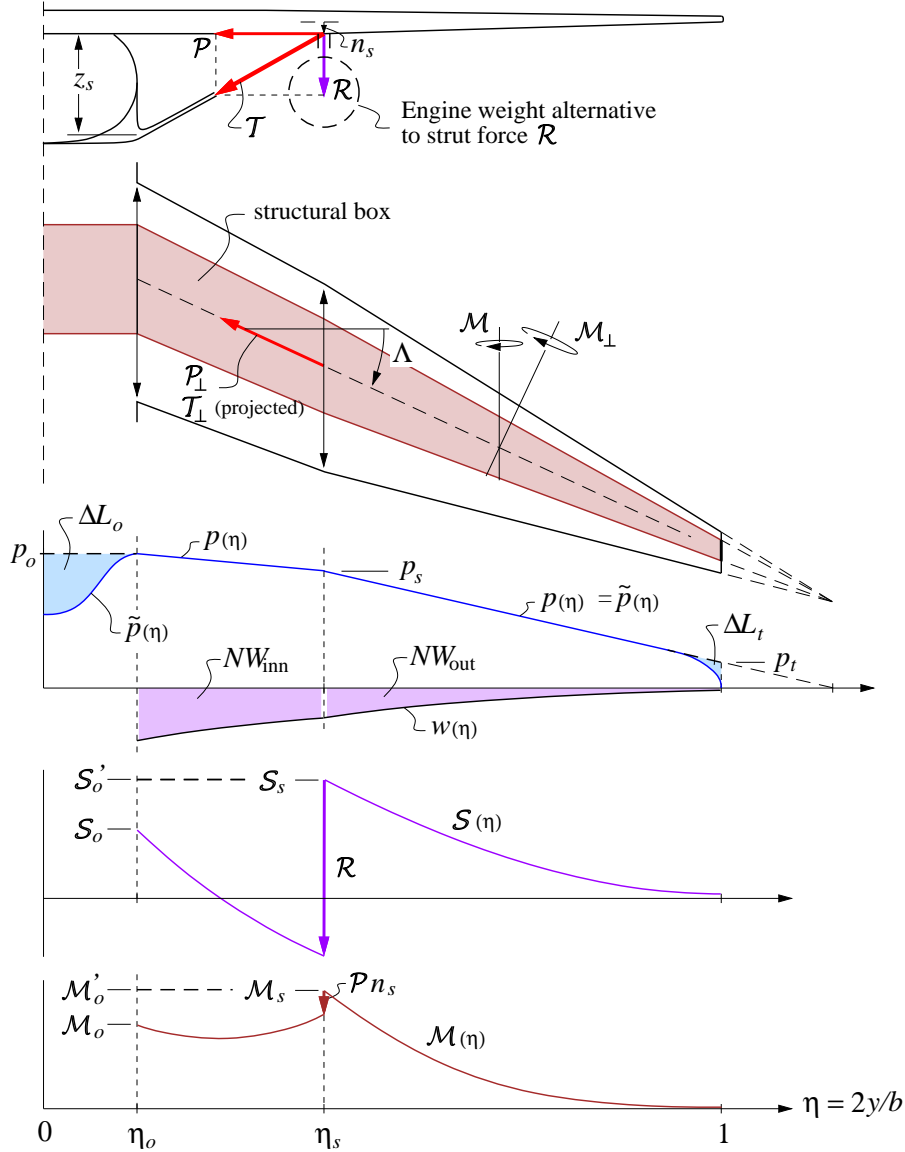
Figure A.9: Aerodynamic load $\tilde{p}_{(\eta)}$ and weight load $w_{(\eta)}$, with resulting shear and bending moments. An optional strut modifies the shear and bending moment as indicated.

$$\mathcal{M}_{(\eta)} \;=\; \mathcal{M}_s \left(\frac{c}{c_s}\right)^3 \quad , \qquad (\eta_s \leq \eta \leq 1) \tag{A.179}$$

These approximations are exact in the sharp-taper limit $\lambda_t, \gamma_t \to 0$, and are quite accurate for the small λ_t values typical of transport aircraft. Their main error is to slightly overpredict the loads near the tip where minimum-gauge constraints are most likely be needed anyway, so the approximation is deemed to be justified. Their great benefit is that they give a self-similar structural cross section for the entire cantilevered surface portion, and thus give simple explicit relations for the cross-section dimensions and the surface weight.

Strut or engine loads

The vertical load $\mathcal{R}$ applied at location η_s can represent either a strut load, or an engine weight. The two cases are described separately below.

Inner surface shear and moment — strut load case

In principle, both the strut anchor position η_s and the vertical strut load $\mathcal{R}$ can be optimized so as to achieve some best overall aircraft performance objective. A complication here is that multiple load conditions would need to be considered during the optimization, since a strut-braced wing optimized for a straight pullup case may not be able to withstand significant downloads, or may be too flexible in torsion and be susceptible to flutter. To avoid these great complications, it is assumed here that the strut is prestressed so as to give equal bending moments at the ends of the inner panel in level flight. The particular $\mathcal{R}$ which is then required in level flight is determined from (A.177).

$$\mathcal{M}_o = \mathcal{M}_s - \mathcal{P} n_s \qquad \text{(assumed)} \qquad \text{(A.180)}$$

$$\mathcal{R} = \frac{p_o b}{12}(1+2\gamma_s)(\eta_s-\eta_o) + \mathcal{S}_s \qquad \text{(A.181)}$$

Referring to Figure A.9, this required $\mathcal{R}$ then gives the projected strut tension $\mathcal{T}$ and the inner-wing projected compression $\mathcal{P}$ loads from the strut front-view geometry.

$$\ell_s = \sqrt{z_s^2 + \frac{b^2}{4}(\eta_s-\eta_o)^2} \qquad \text{(A.182)}$$

$$\mathcal{T} = \mathcal{R}\frac{\ell_s}{z_s} \qquad \text{(A.183)}$$

$$\mathcal{P} = \mathcal{R}\frac{b/2}{z_s}(\eta_s-\eta_o) \qquad \text{(A.184)}$$

The applied vertical load (A.181) implicitly contains the strut's own weight, although this is immaterial in the present formulation. The associated strut tension force (A.183) which will be used to size the strut cross-section will still correctly give the maximum strut tension at the wing strut-attach location.

Although the inner shear and moment distributions can be obtained by integrating the inner loading $p_{(\eta)}$ and including the contribution of the strut tension, these inner $\mathcal{S}_{(\eta)}$ and $\mathcal{M}_{(\eta)}$ are not appropriate for sizing the inner wing structure at each spanwise location, since buckling, torsional stiffness, etc. typically come into play here. Instead, the inner wing structure will be sized to match the $\mathcal{S}_s$ and $\mathcal{M}_s$ values.

Inner surface shear and moment — engine load case

For the case of an engine attached at location η_s, the vertical load $\mathcal{R}$ is simply the engine weight times the load factor N. The new inner wing compression load is zero in this case.

$$\mathcal{R} = N W_{\text{eng}}/n_{\text{eng}} \qquad \text{(A.185)}$$

$$\mathcal{T} = 0 \qquad \text{(A.186)}$$

$$\mathcal{P} = 0 \qquad \text{(A.187)}$$

31

The wing root shear and bending moment $\mathcal{S}_o$ and $\mathcal{M}_o$ are then obtained immediately from (A.176) and (A.177). Unlike in the strut case, these root loads will in general be greater than $\mathcal{S}_s$ and $\mathcal{M}_s$, so the inner wing panel structural elements need to be sized accordingly.

A.2.8 Wing or Tail Stresses

Normal-plane quantities

The wing and tail surface stress and weight analyses are performed in the cross-sectional plane, normal to the spanwise axis $y_\perp$ running along the wing box sketched in Figures A.6 and A.9. Together with the normal-plane coordinate and chord relations (A.162) and (A.163), the shear and bending moment are related to the corresponding airplane-axes quantities and to the sweep angle Λ as follows.

$$\mathcal{S}_\perp = \mathcal{S} \tag{A.188}$$
$$\mathcal{M}_\perp = \mathcal{M}/\cos\Lambda \tag{A.189}$$

Wing or tail section

The assumed wing or tail airfoil and structural box cross-section is shown in Figure A.10. The box is assumed to be the only structurally-significant element, with the slats, flaps, and spoilers (if any), represented only by added weight. It is convenient to define all dimensions as ratios with the local normal-plane chord $c_\perp$.

$$\bar{h} = \frac{h_{\mathrm{wbox}}}{c_\perp} \tag{A.190}$$
$$\bar{w} = \frac{w_{\mathrm{wbox}}}{c_\perp} \tag{A.191}$$
$$\bar{t}_{\mathrm{cap}} = \frac{t_{\mathrm{cap}}}{c_\perp} \tag{A.192}$$
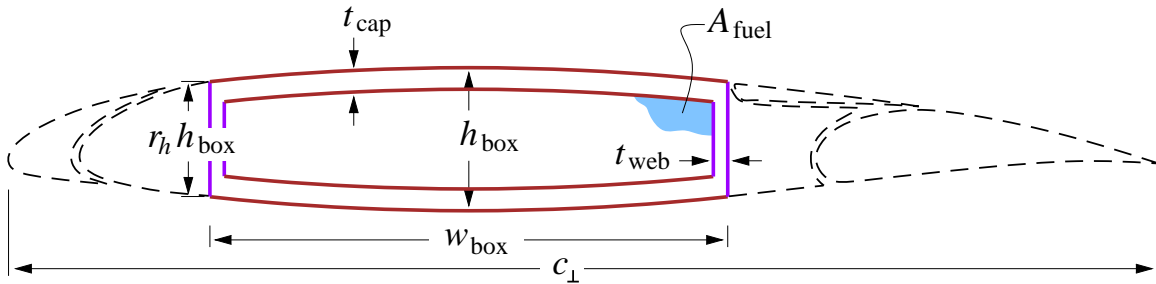$$\bar{t}_{\mathrm{web}} = \frac{t_{\mathrm{web}}}{c_\perp} \tag{A.193}$$

Figure A.10: Wing or tail airfoil and structure cross-section, shown perpendicular to spar axis. Leading edges, fairings, slats, flaps, and spoilers contribute to weight but not to the primary structure.

The maximum height h_{wbox} at the box center corresponds to the airfoil thickness, so that $\bar{h}$ is the usual "t/c" airfoil thickness ratio. The height is assumed to taper off quadratically to a fraction r_h at the webs, so that the local height $h_{(\xi)}$ is

$$h_{(\xi)} \;=\; h_{\mathrm{wbox}}\left[\,1 - (1-r_h)\xi^2\,\right] \tag{A.194}$$

where $\xi = -1\ldots 1$ runs chordwise over the sparbox extent. Typical metal wings and airfoils have $\bar{w} \simeq 0.5$, $r_h \simeq 0.75$, although these are left as input parameters. For evaluating areas and approximating the bending inertia, it's useful to define the simple average and r.m.s. average normalized box heights.

$$\bar{h}_{\mathrm{avg}} \;=\; \frac{1}{c_\perp}\int_0^1 h_{(\xi)}\,d\xi \;=\; \bar{h}\left[\,1 - \frac{1}{3}(1-r_h)\,\right] \tag{A.195}$$

$$\bar{h}_{\mathrm{rms}}^2 \;=\; \frac{1}{c_\perp^2}\int_0^1 h^2{}_{(\xi)}\,d\xi \;=\; \bar{h}^2\left[\,1 - \frac{2}{3}(1-r_h) + \frac{1}{5}(1-r_h)^2\,\right] \tag{A.196}$$

The areas and the bending and torsion inertias, all normalized by the normal chord, can now be determined.

$$\bar{A}_{\mathrm{fuel}} \;=\; \frac{A_{\mathrm{fuel}}}{c_\perp^2} \;=\; (\bar{w} - 2\bar{t}_{\mathrm{web}})(\bar{h}_{\mathrm{avg}} - 2\bar{t}_{\mathrm{cap}}) \tag{A.197}$$

$$\bar{A}_{\mathrm{cap}} \;=\; \frac{A_{\mathrm{cap}}}{c_\perp^2} \;=\; 2\,\bar{t}_{\mathrm{cap}}\bar{w} \tag{A.198}$$

$$\bar{A}_{\mathrm{web}} \;=\; \frac{A_{\mathrm{web}}}{c_\perp^2} \;=\; 2\,\bar{t}_{\mathrm{web}}\,r_h\,\bar{h} \tag{A.199}$$

$$\bar{I}_{\mathrm{cap}} \;\simeq\; \frac{I_{\mathrm{cap}}}{c_\perp^4} \;=\; \frac{\bar{w}}{12}\left[\,\bar{h}_{\mathrm{rms}}^3 - (\bar{h}_{\mathrm{rms}} - 2\bar{t}_{\mathrm{cap}})^3\,\right] \tag{A.200}$$

$$\bar{I}_{\mathrm{web}} \;=\; \frac{I_{\mathrm{web}}}{c_\perp^4} \;=\; \frac{\bar{t}_{\mathrm{web}}\,r_h^3\,\bar{h}^3}{6} \;\ll\; \bar{I}_{\mathrm{cap}} \qquad \text{(typically)} \tag{A.201}$$

$$G\bar{J} \;=\; \frac{4(\bar{w} - \bar{t}_{\mathrm{web}})^2(\bar{h}_{\mathrm{avg}} - \bar{t}_{\mathrm{cap}})^2}{2\dfrac{r_h\bar{h} - \bar{t}_{\mathrm{cap}}}{G_{\mathrm{web}}\bar{t}_{\mathrm{web}}} + 2\dfrac{\bar{w} - \bar{t}_{\mathrm{web}}}{G_{\mathrm{cap}}\bar{t}_{\mathrm{cap}}}} \tag{A.202}$$

Outboard surface stresses

The wing or tail surface outboard of the strut-attach location η_s is a simple cantilever, whose local shear and bending stresses can be obtained explicitly.

$$\tau_{\mathrm{web}} \;=\; \frac{\mathcal{S}_\perp}{A_{\mathrm{web}}} \;=\; \frac{\mathcal{S}_\perp}{c_\perp^2}\frac{1}{2\,\bar{t}_{\mathrm{web}_s}\bar{h}} \tag{A.203}$$

$$\sigma_{\mathrm{cap}} \;=\; \frac{\mathcal{M}_\perp h_{\mathrm{wbox}}/2}{I_{\mathrm{cap}} + r_E I_{\mathrm{web}}} \;\simeq\; \frac{\mathcal{M}_\perp h_{\mathrm{wbox}}/2}{I_{\mathrm{cap}}} \;=\; \frac{\mathcal{M}_\perp}{c_\perp^3}\frac{6\bar{h}}{\bar{w}}\frac{1}{\bar{h}_{\mathrm{rms}}^3 - (\bar{h}_{\mathrm{rms}} - 2\bar{t}_{\mathrm{cap}_s})^3} \tag{A.204}$$

$$r_E \;=\; \frac{E_{\mathrm{web}}}{E_{\mathrm{cap}}} \tag{A.205}$$

With the assumed triangular chord distribution (A.121), and the simplified shear and bending moment distributions (A.178) and (A.179), the shear and bending stresses become

$$\tau_{\text{web}} = \frac{\mathcal{S}_s}{c_s^2} \frac{1}{2\,\bar{t}_{\text{web}_s}\,r_h\,\bar{\bar{h}}} \frac{1}{\cos^2 \Lambda} \tag{A.206}$$

$$\sigma_{\text{cap}} = \frac{\mathcal{M}_s}{c_s^3} \frac{6\bar{h}}{\bar{w}} \frac{1}{\bar{h}_{\text{rms}}^3 - (\bar{h}_{\text{rms}} - 2\bar{t}_{\text{cap}_s})^3} \frac{1}{\cos^4 \Lambda} \tag{A.207}$$

which are spanwise constant across the outer wing. This great simplification was the major motivator behind assuming the simple triangular planform and loading and the chord-scaled shear and moment (A.178), (A.179) for the outer wing. The optimally-sized wing sections at all spanwise locations then become geometrically self-similar, and only one convenient characteristic cross-section, e.g. at the strut-attach location η_s, needs to be sized to fully define the outer wing's structural and weight characteristics.

For a wing or tail surface without a strut, the outer surface constitutes the entire surface. In this case, the strut and inner-surface sizing below is omitted.

Inboard surface — strut case

The inboard surface structure is defined by its two end locations η_o and η_s, with linear material-gauge variation in between. The shear webs of the inner surface are assumed to be dominated by torsional requirements rather than bending-related shear requirements. Hence the inner panel is sized for the shear distribution shown dashed in Figure A.9, defined by the strut-attach value $\mathcal{S}_s$.

$$\mathcal{S}_o' = \mathcal{S}_s \tag{A.208}$$

$$\tau_{\text{web}} = \frac{\mathcal{S}_o'}{c_o^2} \frac{1}{2\,\bar{t}_{\text{web}_o}\,r_h\,\bar{\bar{h}}} \frac{1}{\cos^2 \Lambda} \tag{A.209}$$

Similarly, the inner panel bending stiffness must not only withstand the normal-flight bending loads, but also landing downloads and buckling loads from the strut compression. Hence, the sparcaps are sized to the linear bending moment shown dashed in Figure A.9, and defined by the end values $\mathcal{M}_s$ and $\mathcal{M}_o'$.

With the strut assumed to be attached to the bottom sparcap at $n_s = h/2$, the strut's compression load $\mathcal{P}$ cannot influence the compression stress on the top sparcap. An equivalent alternative view is that the offset-load bending moment reduction $-\mathcal{P}n_s$ is cancelled by $\mathcal{P}$'s own added compression stress. In any case, $\mathcal{P}$ does not explicitly enter into the sparcap sizing, provided $\mathcal{M}$ is positive everywhere on the inner panel, which is a reasonable assumption for a structurally-efficient wing. Hence, the strut-attach outer moment $\mathcal{M}_s$ is used for sizing the bending structure of the inner panel.

$$\mathcal{M}_o' = \mathcal{M}_s \tag{A.210}$$

$$\sigma_{\text{cap}} = \frac{\mathcal{M}_o'}{c_o^3} \frac{6\bar{h}}{\bar{w}} \frac{1}{\bar{h}_{\text{rms}}^3 - (\bar{h}_{\text{rms}} - 2\bar{t}_{\text{cap}_o})^3} \frac{1}{\cos^4 \Lambda} \tag{A.211}$$

Inboard surface — engine case

In the case of an engine mounted at η_s, the root shear is simply offset by the single-engine weight, as shown in Figure A.11.
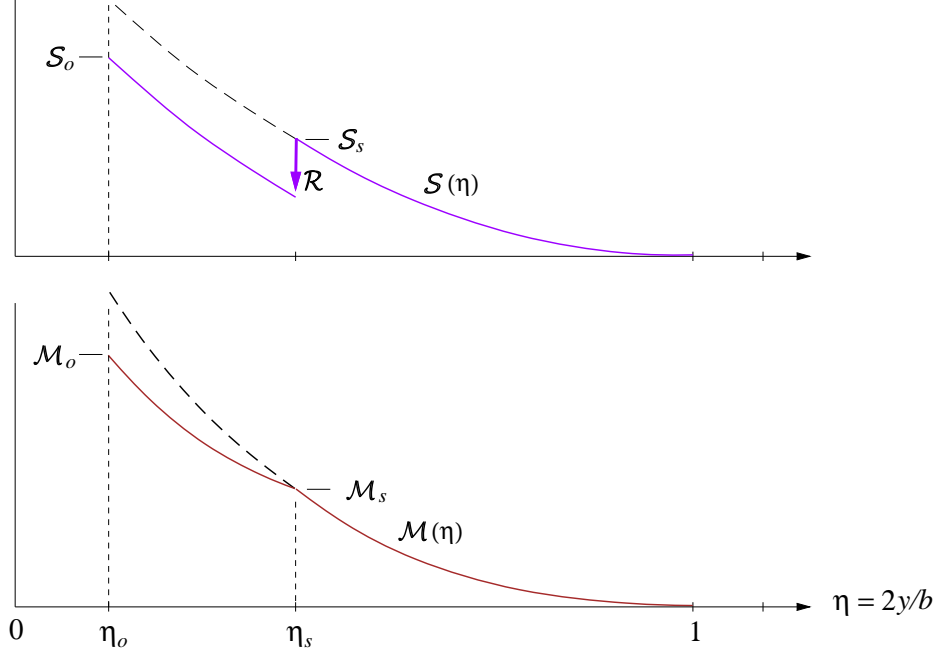
Figure A.11: Surface loads modified by load $\mathcal{R}$ equal to engine weight attached at η_s.

$$\mathcal{R} = NW_{\text{eng}}/n_{\text{eng}} \tag{A.212}$$

$$\mathcal{P} = 0 \tag{A.213}$$

The root shear and moment $\mathcal{S}_o$ and $\mathcal{M}_o$ are then given immediately by (A.176) and (A.177). The root web and cap stresses are then obtained with the same relations (A.206) and (A.207) used for station η_s.

$$\tau_{\text{web}} = \frac{\mathcal{S}_o}{c_o^2} \frac{1}{2\,\bar{t}_{\text{web}_o}\, r_h\, \bar{h}} \frac{1}{\cos^2 \Lambda} \tag{A.214}$$

$$\sigma_{\text{cap}} = \frac{\mathcal{M}_o}{c_o^3} \frac{6\bar{h}}{\bar{w}} \frac{1}{\bar{h}_{\text{rms}}^3 - (\bar{h}_{\text{rms}} - 2\bar{t}_{\text{cap}_o})^3} \frac{1}{\cos^4 \Lambda} \tag{A.215}$$

The $r_{\tau_{\text{web}}}$ and $r_{\sigma_{\text{cap}}}$ factors are estimated or known max/average stress ratios, and account for the fact that the material in a realistic structure is never all at the same stress, due to approximate detailed design or analysis, or from manufacturing or cost considerations.

Strut

The full strut length $\ell_{s_\perp}$ and full tension $\mathcal{T}_\perp$ are determined from the strut geometry.

$$\ell_{s_\perp} = \sqrt{z_s^2 + \frac{b^2}{4} \frac{(\eta_s - \eta_o)^2}{\cos^2 \Lambda}} \tag{A.216}$$

$$\mathcal{T}_{\perp} = \mathcal{T}\frac{\ell_{s_{\perp}}}{\ell_s} \tag{A.217}$$

The strut stress is then simply related to $\mathcal{T}_{\perp}$ and the strut cross-sectional area A_{strut}.

$$\sigma_{\text{strut}} = \frac{\mathcal{T}_{\perp}}{A_{\text{strut}}} \tag{A.218}$$

A.2.9   Surface Weights

Surface material volumes and volume moments

The surface structural weight is obtained directly from the total volume of the caps and webs, and the corresponding material densities. The volume $\mathcal{V}$ of any element of the swept surface is computed using the element's normalized cross sectional area $\bar{A}$, and the local streamwise chord $c_{(\eta)}$. The volume x-moment offsets $\Delta x\mathcal{V}$ from the center box are also computed for mass-centroid calculations. The volume y-moment offsets $\Delta y\mathcal{V}$ from y_o or y_s are computed for their contributions to the structural shear bending moment (A.174) and (A.175).

$$dy_{\perp} = \frac{dy}{\cos\Lambda} = \frac{b}{2}\frac{d\eta}{\cos\Lambda} \tag{A.219}$$

$$A = \bar{A}c_{\perp}^2 = \bar{A}c^2\cos^2\Lambda \tag{A.220}$$

$$\mathcal{V} = \int A\,dy_{\perp} = \frac{b}{2}\int \bar{A}c^2\cos\Lambda\,d\eta \tag{A.221}$$

$$\Delta x\mathcal{V} = \int A\,(x-x_{\text{wbox}})\,dy_{\perp} = \frac{b^2}{4}\int \bar{A}c^2\,(\eta-\eta_o)\sin\Lambda\,d\eta \tag{A.222}$$

$$\Delta y\mathcal{V} = \int A\,(y-y_o)\,dy_{\perp} = \frac{b^2}{4}\int \bar{A}c^2\,(\eta-\eta_o)\cos\Lambda\,d\eta \tag{A.223}$$

Using the assumed three-panel chord distribution (A.121), the unit-area ($\bar{A}{=}1$) volume and volume moments evaluate to the following for each of the three panels of one wing half.

$$\mathcal{V}_{\text{cen}} = \frac{b}{2}\int_0^{\eta_o} c^2\,d\eta = c_o^2\frac{b}{2}\eta_o \tag{A.224}$$

$$\mathcal{V}_{\text{inn}} = \frac{b}{2}\int_{\eta_o}^{\eta_s} c^2\cos\Lambda\,d\eta = c_o^2\frac{b}{6}(1+\lambda_s+\lambda_s^2)(\eta_s-\eta_o)\cos\Lambda \tag{A.225}$$

$$\mathcal{V}_{\text{out}} = \frac{b}{2}\int_{\eta_s}^1 c^2\cos\Lambda\,d\eta = c_o^2\frac{b}{6}(\lambda_s^2+\lambda_s\lambda_t+\lambda_t^2)(1-\eta_s)\cos\Lambda \tag{A.226}$$

$$\Delta x\mathcal{V}_{\text{inn}} = \frac{b^2}{4}\int_{\eta_o}^{\eta_s} c^2\,(\eta-\eta_o)\sin\Lambda\,d\eta = c_o^2\frac{b^2}{48}(1+2\lambda_s+3\lambda_s^2)(\eta_s-\eta_o)^2\sin\Lambda \tag{A.227}$$

$$\Delta x\mathcal{V}_{\text{out}} = \frac{b^2}{4}\int_{\eta_s}^1 c^2\,(\eta-\eta_o)\sin\Lambda\,d\eta = c_o^2\frac{b^2}{48}(\lambda_s^2+2\lambda_s\lambda_t+3\lambda_t^2)(1-\eta_s)^2\sin\Lambda$$

$$\qquad\qquad + c_o^2\frac{b^2}{12}(\lambda_s^2+\lambda_s\lambda_t+\lambda_t^2)(\eta_s-\eta_o)(1-\eta_s)\sin\Lambda \tag{A.228}$$

$$\Delta y\mathcal{V}_{\text{inn}} = \frac{b^2}{4}\int_{\eta_o}^{\eta_s} c^2\,(\eta-\eta_o)\sin\Lambda\,d\eta = c_o^2\frac{b^2}{48}(1+2\lambda_s+3\lambda_s^2)(\eta_s-\eta_o)^2\cos\Lambda \tag{A.229}$$

$$\Delta y\mathcal{V}_{\text{out}} = \frac{b^2}{4}\int_{\eta_s}^1 c^2\,(\eta-\eta_s)\sin\Lambda\,d\eta = c_o^2\frac{b^2}{48}(\lambda_s^2+2\lambda_s\lambda_t+3\lambda_t^2)(1-\eta_s)^2\cos\Lambda \tag{A.230}$$

Surface weights and weight moments

For the structural sizing calculations it's necessary to determine the contributions of the structure and fuel separately for the inner and outer panels. These are calculated by applying the material densities and actual area ratios to the unit-area volumes calculated previously.

$$\bar{A}_{\text{cap}_{\text{inn}}} = \frac{\bar{A}_{\text{cap}_o} + \bar{A}_{\text{cap}_s}\lambda_s^2}{1 + \lambda_s^2} \tag{A.231}$$

$$\bar{A}_{\text{web}_{\text{inn}}} = \frac{\bar{A}_{\text{web}_o} + \bar{A}_{\text{web}_s}\lambda_s^2}{1 + \lambda_s^2} \tag{A.232}$$

$$W_{\text{scen}} = \left[\rho_{\text{cap}}\,\bar{A}_{\text{cap}_o} + \rho_{\text{web}}\,\bar{A}_{\text{web}_o}\right] g\,\mathcal{V}_{\text{cen}} \tag{A.233}$$

$$W_{\text{sinn}} = \left[\rho_{\text{cap}}\,\bar{A}_{\text{cap}_{\text{inn}}} + \rho_{\text{web}}\,\bar{A}_{\text{web}_{\text{inn}}}\right] g\,\mathcal{V}_{\text{inn}} \tag{A.234}$$

$$\Delta x W_{\text{sinn}} = \left[\rho_{\text{cap}}\,\bar{A}_{\text{cap}_{\text{inn}}} + \rho_{\text{web}}\,\bar{A}_{\text{web}_{\text{inn}}}\right] g\,\Delta x \mathcal{V}_{\text{inn}} \tag{A.235}$$

$$\Delta y W_{\text{sinn}} = \left[\rho_{\text{cap}}\,\bar{A}_{\text{cap}_{\text{inn}}} + \rho_{\text{web}}\,\bar{A}_{\text{web}_{\text{inn}}}\right] g\,\Delta y \mathcal{V}_{\text{inn}} \tag{A.236}$$

$$W_{\text{sout}} = \left[\rho_{\text{cap}}\,\bar{A}_{\text{cap}_s} + \rho_{\text{web}}\,\bar{A}_{\text{web}_s}\right] g\,\mathcal{V}_{\text{out}} \tag{A.237}$$

$$\Delta x W_{\text{sout}} = \left[\rho_{\text{cap}}\,\bar{A}_{\text{cap}_s} + \rho_{\text{web}}\,\bar{A}_{\text{web}_s}\right] g\,\Delta x \mathcal{V}_{\text{out}} \tag{A.238}$$

$$\Delta y W_{\text{sout}} = \left[\rho_{\text{cap}}\,\bar{A}_{\text{cap}_s} + \rho_{\text{web}}\,\bar{A}_{\text{web}_s}\right] g\,\Delta y \mathcal{V}_{\text{out}} \tag{A.239}$$

$$W_{\text{fcen}} = \rho_{\text{fuel}}\,\bar{A}_{\text{fuel}_o}\,g\,\mathcal{V}_{\text{inn}} \tag{A.240}$$

$$\bar{A}_{\text{fuel}_{\text{inn}}} = \frac{\bar{A}_{\text{fuel}_o} + \bar{A}_{\text{fuel}_s}\lambda_s^2}{1 + \lambda_s^2} \tag{A.241}$$

$$W_{\text{finn}} = \rho_{\text{fuel}}\,\bar{A}_{\text{fuel}_{\text{inn}}}\,g\,\mathcal{V}_{\text{inn}} \tag{A.242}$$

$$\Delta x W_{\text{finn}} = \rho_{\text{fuel}}\,\bar{A}_{\text{fuel}_{\text{inn}}}\,g\,\Delta x \mathcal{V}_{\text{inn}} \tag{A.243}$$

$$\Delta y W_{\text{finn}} = \rho_{\text{fuel}}\,\bar{A}_{\text{fuel}_{\text{inn}}}\,g\,\Delta y \mathcal{V}_{\text{inn}} \tag{A.244}$$

$$W_{\text{fout}} = \rho_{\text{fuel}}\,\bar{A}_{\text{fuel}_s}\,g\,\mathcal{V}_{\text{out}} \tag{A.245}$$

$$\Delta x W_{\text{fout}} = \rho_{\text{fuel}}\,\bar{A}_{\text{fuel}_s}\,g\,\Delta x \mathcal{V}_{\text{out}} \tag{A.246}$$

$$\Delta y W_{\text{fout}} = \rho_{\text{fuel}}\,\bar{A}_{\text{fuel}_s}\,g\,\Delta y \mathcal{V}_{\text{out}} \tag{A.247}$$

Assuming chord^2-weighted average areas $\bar{A}_{\text{inn}}$ over the inner panel is deemed to be adequate for approximating the material and fuel volumes, since $\bar{A}_o$ and $\bar{A}_s$ will be very similar for any reasonable wing/strut configuration, and in fact are equal for the small taper ratio cantilevered wing case like for the outer panel.

The total structural wing weight and x-moment is obtained by summing the weights for all the panels for the two wing halves, with added wing weight accounted for by the f_{wadd} fraction components.

$$f_{\text{wadd}} = f_{\text{flap}} + f_{\text{slat}} + f_{\text{aile}} + f_{\text{lete}} + f_{\text{ribs}} + f_{\text{spoi}} + f_{\text{watt}} \tag{A.248}$$

$$W_{\text{wing}} = 2\left(W_{\text{scen}} + W_{\text{sinn}} + W_{\text{sout}}\right)\left(1 + f_{\text{wadd}}\right) \tag{A.249}$$

$$\Delta x W_{\text{wing}} = 2\left(\Delta x W_{\text{sinn}} + \Delta x W_{\text{sout}}\right)\left(1 + f_{\text{wadd}}\right) \tag{A.250}$$

The maximum (volume-limited) wing fuel weight and x-moment is computed the same way.

$$W_{\text{fmax}} = 2\left(W_{\text{fcen}} + W_{\text{finn}} + W_{\text{fout}}\right) \tag{A.251}$$

$$\Delta x W_{\text{fmax}} = 2\left(\Delta x W_{\text{finn}} + \Delta x W_{\text{fout}}\right) \tag{A.252}$$

This can be modified if only some of the wingbox volume is chosen to hold fuel.

Total panel weights

The wing structural shear and bending moment relations (A.174) – (A.177) require the weights and weight y-moments of the individual wing panels. These are assembled by summing the structure's and maximum fuel's weight contributions derived previously, with the latter simply scaled by the max-fuel usage fraction r_{fmax}.

$$r_{\text{fmax}} = \frac{W_{\text{fuel}}}{W_{\text{fmax}}} \tag{A.253}$$

$$W_{\text{inn}} = W_{\text{sinn}}(1 + f_{\text{wadd}}) + r_{\text{fmax}} W_{\text{finn}} \tag{A.254}$$

$$W_{\text{out}} = W_{\text{sout}}(1 + f_{\text{wadd}}) + r_{\text{fmax}} W_{\text{fout}} \tag{A.255}$$

$$\Delta y W_{\text{inn}} = \Delta y W_{\text{sinn}}(1 + f_{\text{wadd}}) + r_{\text{fmax}} \Delta y W_{\text{finn}} \tag{A.256}$$

$$\Delta y W_{\text{out}} = \Delta y W_{\text{sout}}(1 + f_{\text{wadd}}) + r_{\text{fmax}} \Delta y W_{\text{fout}} \tag{A.257}$$

Using a single r_{fmax} value assumes the partial fuel load is uniformly distributed percentage-wise in all the available volume. Of course, r_{fmax} could be varied between the panels to reflect other fuel distributions.

Strut weight

The weight of the strut is computed directly from its cross-sectional area and total length for the two sides.

$$W_{\text{strut}} = \rho_{\text{strut}}\, g A_{\text{strut}}\, 2\ell_{s_\perp} \tag{A.258}$$

$$\Delta x W_{\text{strut}} = \frac{b}{4}\left(\eta_s - \eta_o\right)\tan\Lambda\, W_{\text{strut}} \tag{A.259}$$

Wingbox component weights

The overall sparcap and web weights for the entire wing can also be determined, although these are merely informative and are not needed for any other calculations.

$$W_{\text{cap}} = 2\rho_{\text{cap}}\, g\left[\bar{A}_{\text{cap}_o}\mathcal{V}_{\text{cen}} + \tfrac{1}{2}\left(\bar{A}_{\text{cap}_o} + \bar{A}_{\text{cap}_s}\right)\mathcal{V}_{\text{inn}} + \bar{A}_{\text{cap}_s}\mathcal{V}_{\text{out}}\right] \tag{A.260}$$

$$W_{\text{web}} = 2\rho_{\text{web}}\, g\left[\bar{A}_{\text{web}_o}\mathcal{V}_{\text{cen}} + \tfrac{1}{2}\left(\bar{A}_{\text{web}_o} + \bar{A}_{\text{web}_s}\right)\mathcal{V}_{\text{inn}} + \bar{A}_{\text{web}_s}\mathcal{V}_{\text{out}}\right] \tag{A.261}$$

Tail surface weight

All the wing wing stress and weight analyses above apply equally to the vertical and horizontal tail surfaces, with the appropriate span and load definitions. It is assumed that no strut is used, so that

$$c_{s_\mathrm{h}} = c_{o_\mathrm{h}} \tag{A.262}$$
$$b_{s_\mathrm{h}} = b_{o_\mathrm{h}} \tag{A.263}$$

and likewise for the vertical tail. The main difference is the derivation of the root loading magnitude p_o, which is set by the maximum design loads at q_{NE}, defined by (A.72) and (A.74). Specifically, we have

$$p_{o_\mathrm{h}} = \frac{L_{\mathrm{h_{max}}}}{b_\mathrm{h}} \frac{2}{1+\lambda_\mathrm{h}} \tag{A.264}$$

where the $(\ )_\mathrm{h}$ subscript denotes the horizontal tail/ The same relation is used for the vertical tail. Gravity and inertial loads are neglected here, since for tails they are typically much smaller than the airloads at q_{NE}. Of course, they could be included as was done for the wing. With the tail p_o values defined, the structural-box sizing and weight estimation proceeds using the same relations as for the wing, starting with $\mathcal{S}_o$. The vertical tail is treated by assuming its mirror image exists, so that the b value in (A.174) and (A.175) is actually twice the actual vertical tail span. No other adjustments need to be made. The net result is the overall horizontal and vertical tail weights, and tail weight moments.

$$\rightarrow \quad W_{\mathrm{htail}} \tag{A.265}$$
$$\rightarrow \quad W_{\mathrm{vtail}} \tag{A.266}$$
$$\rightarrow \quad \Delta x W_{\mathrm{htail}} \tag{A.267}$$
$$\rightarrow \quad \Delta x W_{\mathrm{vtail}} \tag{A.268}$$

A.2.10   Engine System Weight

The bare engine weight W_{ebare} is calculated using an assumed dependence on the engine design core mass flow $\dot{m}_\mathrm{D}$, overall design pressure ratio OPR_D, and the design bypass ratio BPR_D. The model's constants have been calibrated with listed weights for existing turbofans. The added weight W_{eadd}, specified via the empirical fraction f_{eadd}, accounts for the fuel system and miscellaneous related equipment.

$$W_{\mathrm{ebare}} = n_{\mathrm{eng}} W_{e_1}(\dot{m}_\mathrm{D}, OPR_\mathrm{D}, BPR_\mathrm{D}) \tag{A.269}$$
$$W_{\mathrm{eadd}} = W_{\mathrm{ebare}} f_{\mathrm{eadd}} \tag{A.270}$$

The nacelle plus thrust reverser weight is calculated using an assumed dependence on the engine fan diameter d_f and the nacelle surface area, the latter being specified by the empirical area ratio r_{Snace} relative to the fan area.

$$S_{\mathrm{nace}_1} = r_{\mathrm{Snace}} \frac{\pi}{4} d_\mathrm{f}^2 \tag{A.271}$$
$$W_{\mathrm{nace}} = n_{\mathrm{eng}} W_{n_1}(d_\mathrm{f}, S_{\mathrm{nace}_1}) \tag{A.272}$$

The pylon weight W_{pylon}, specified via the empirical fraction f_{pylon}, accounts for the pylon and other mounting structure.

$$W_{\text{ebare}} = n_{\text{eng}} W_{e_1}(\dot{m}_{\text{D}}, OPR_{\text{D}}, BPR_{\text{D}}) \tag{A.273}$$

$$W_{\text{pylon}} = (W_{\text{ebare}} + W_{\text{eadd}} + W_{\text{nace}}) f_{\text{pylon}} \tag{A.274}$$

The total engine system weight and weight moment is then defined as follows. The engine weight fraction is also defined, and is used in the overall weight iteration procedure.

$$W_{\text{eng}} = W_{\text{ebare}} + W_{\text{eadd}} + W_{\text{nace}} + W_{\text{pylon}} \tag{A.275}$$

$$xW_{\text{eng}} = x_{\text{eng}} W_{\text{eng}} \tag{A.276}$$

$$f_{\text{eng}} = \frac{W_{\text{eng}}}{W_{\text{MTO}}} \tag{A.277}$$

A.2.11   Moments and Balance

Weight moment and aerodynamic moment calculations are used to size the horizontal tail to meet stability or trim-limit requirements, to determine allowable CG limits, and to determine the required pitch-trim tail lift.

Overall weight moment

The overall flying weight is summed as follows. Partial payload and partial fuel are specified with the arbitrary r_{pay} and r_{fuel} ratios relative to maximum design values.

$$
\begin{aligned}
W = \ & r_{\text{pay}} W_{\text{pay}} + r_{\text{fuel}} W_{\text{fuel}} \\
& + W_{\text{fuse}} + W_{\text{wing}} + W_{\text{strut}} + W_{\text{htail}} + W_{\text{vtail}} \\
& + W_{\text{eng}} + W_{\text{hpesys}} + W_{\text{lgnose}} + W_{\text{lgmain}}
\end{aligned}
\tag{A.278}
$$

The partial passenger payload distribution in the cabin is specified by the parameter ξ_{pay} which can take on any value $0 \ldots 1$. Specific instances are

$$
\xi_{\text{pay}} = \begin{cases} 0.0 & , \quad \text{passengers packed towards the front} \\ 0.5 & , \quad \text{passengers centered in cabin} \\ 1.0 & , \quad \text{passengers packed towards the back} \end{cases}
\tag{A.279}
$$

This then determines the passenger payload weight centroid x_{pay}.

$$x_{\text{cabin}} = \tfrac{1}{2}(x_{\text{shell}\,1} + x_{\text{shell}\,2}) \tag{A.280}$$

$$l_{\text{cabin}} = x_{\text{shell}\,2} - x_{\text{shell}\,1} \tag{A.281}$$

$$x_{\text{pay}} = x_{\text{cabin}} + l_{\text{cabin}} \left(\xi_{\text{pay}} - \tfrac{1}{2}\right)(1 - r_{\text{pay}}) \tag{A.282}$$

Note that with a full passenger load, $r_{\text{pay}} = 1$, the mass centroid is always at the center point x_{cabin}, regardless of ξ_{pay}. The overall aircraft weight moment is then computed as follows.

$$xW = r_{\text{pay}}\, x_{\text{pay}} W_{\text{pay}}$$

$$
\begin{aligned}
&+& & r_{\text{fuel}}\left(x_{\text{wbox}}W_{\text{fuel}} + \Delta x W_{\text{fuel}}\right) \\
&+& & x W_{\text{fuse}} \\
&+& & x_{\text{wbox}}W_{\text{wing}} + \Delta x W_{\text{wing}} \\
&+& & x_{\text{wbox}}W_{\text{strut}} + \Delta x W_{\text{strut}} \\
&+& & x_{\text{htail}}W_{\text{htail}} + \Delta x W_{\text{htail}} \\
&+& & x_{\text{vtail}}W_{\text{vtail}} + \Delta x W_{\text{vtail}} \\
&+& & x W_{\text{eng}} \\
&+& & x_{\text{hpesys}}W_{\text{hpesys}} \\
&+& & x_{\text{lgnose}}W_{\text{lgnose}} \\
&+& & x_{\text{lgmain}}W_{\text{lgmain}} \quad\quad\quad\quad\quad\quad\quad\quad\quad (A.283)
\end{aligned}
$$

The aircraft CG location then follows.

$$
x_{CG} \;=\; \frac{x W}{W} \tag{A.284}
$$

Overall aerodynamic moment

The overall aerodynamic pitching moment about the origin comes from the wing, the horizontal tail, and the fuselage. For simplicity, the wing root chord c_o is used as the reference moment arm rather than the more traditional m.a.c.

$$
\begin{aligned}
C_M \equiv \frac{M}{\frac{1}{2}\rho V_\infty^2 S c_o} \;=\;\; & C_{Mw_0} + \left(C_{Mw_1} - \frac{x_{\text{wbox}}}{c_o}\right)\left(C_L - \frac{S_h}{S}C_{L_h}\right) \\
& + \frac{S_h\, c_{oh}}{S\, c_o} C_{Mh_0} + \left(\frac{c_{oh}}{c_o} C_{Mh_1} - \frac{x_{\text{hbox}}}{c_o}\right)\frac{S_h}{S} C_{L_h} \\
& + \frac{CMV_{f_1}}{S c_o}\left(C_L - C_{L_{Mf0}}\right)
\end{aligned} \tag{A.285}
$$

and CMV_{f_1} and $C_{L_{Mf0}}$ give the fuselage's pitching moment volume dependence on aicraft C_L.

$$
\frac{M_{\text{fuse}}}{\frac{1}{2}\rho V_\infty^2} \;\equiv\; CMV_f \;=\; CMV_{f_1}\left(C_L - C_{L_{Mf0}}\right) \tag{A.286}
$$

From slender body theory, a fuselage of volume $\mathcal{V}_f$ isolated from the wing has

$$
CMV_f \;\simeq\; 2\mathcal{V}_f\left(\alpha - \alpha_{Mf0}\right) \tag{A.287}
$$

$$
CMV_{f_1} \;\simeq\; \frac{2\mathcal{V}_f}{dC_L/d\alpha} \tag{A.288}
$$

but this will typically be considerably modified by the interaction with the wing. Ragardless, the aircraft center of pressure (or lift centroid) is given as follows.

$$
x_{CP} \;=\; -\frac{c_o\, C_M}{C_L} \tag{A.289}
$$

41

Neutral point

The neutral point is estimated by first translating the aerodynamic pitching moment (A.285) to some arbitrary reference x location.

$$C_M(x) = C_M + \frac{x}{c_o} C_L \qquad (A.290)$$

The neutral point is the x location which makes (A.290) stationary with respect to C_L, or

$$\frac{\partial C_M(x_{NP})}{\partial C_L} = \frac{\partial C_M}{\partial C_L} + \frac{x_{NP}}{c_o} = 0 \qquad (A.291)$$

$$x_{NP} = -c_o \frac{\partial C_M}{\partial C_L} \qquad (A.292)$$

$$\text{where} \quad c_o \frac{\partial C_M}{\partial C_L} = (c_o C_{Mw_1} - x_{\text{wbox}})\left(1 - \frac{S_h}{S} \frac{\partial C_{L_h}}{\partial C_L}\right)$$

$$+ (c_{oh} C_{Mh_1} - x_{\text{hbox}}) \frac{S_h}{S} \frac{\partial C_{L_h}}{\partial C_L}$$

$$+ \frac{CMV_{f_1}}{S} \qquad (A.293)$$

Pitch trim requirement

Every operating point must meet the requirement of pitch trim, which is equivalent to the centers of weight and pressure cooinciding. This is enforced by requiring that the following total-moment residual is zero.

$$\mathcal{R}_M(x_{\text{wbox}}, S_h, C_{Lh}, C_L, r_{\text{fuel}}, r_{\text{pay}}, \xi_{\text{pay}}) \equiv x_{CG} - x_{CP} = \frac{xW}{W} + \frac{c_o C_M}{C_L} = 0 \text{ (A.294)}$$

The argument list of the residual indicates the variables which have the strongest influence on pitch trim.

Pitch stability requirement

An aircraft must also have some minimum amount of static pitch stability, which means that the rearmost center of gravity must be ahead of the neutral point by the static margin fraction f_{SM} of the mean aerodynamic chord. This is met when the following stability residual is zero.

$$\mathcal{R}_S(x_{\text{wbox}}, S_h, r_{\text{fuel}}, r_{\text{pay}}, \xi_{\text{pay}}) \equiv x_{CG} - x_{NP} + f_{SM} c_{MA} = 0 \qquad (A.295)$$

The argument list indicates the variables which have the strongest influence on pitch stability.

A.2.12 Tail Sizing

The tail areas can be sized by a number of alternative requirements. The most common approaches are outlined here.

Specified tail volumes

This is the simplest approach. The stability margin or damping requirements are assumed to be quantified by the horizontal and vertical tail volumes,

$$l_{\mathrm{h}} = x_{\mathrm{htail}} - x_{\mathrm{wing}} \tag{A.296}$$

$$l_{\mathrm{v}} = x_{\mathrm{vtail}} - x_{\mathrm{wing}} \tag{A.297}$$

$$V_{\mathrm{h}} = \frac{S_{\mathrm{h}}}{S} \frac{l_{\mathrm{h}}}{c_{\mathrm{mac}}} \tag{A.298}$$

$$V_{\mathrm{v}} = \frac{S_{\mathrm{v}}}{S} \frac{l_{\mathrm{v}}}{b} \tag{A.299}$$

which when specified give the necessary S_{h} or S_{v}. Defining the tail arms from the center of wing centroid rather than from the CG or the wing's aerodynamic center is reasonable for these rather simple sizing relations.

Design-case: Horizontal tail sizing and wing positioning

For the design case, both S_{h} and x_{wbox} are determined so as to drive the pitch trim and stability residuals (A.294) and (A.295) to zero simultaneously. Their remaining arguments are set for the appropriate worst-case situations:

$$\mathcal{R}_M = \mathcal{R}_M(x_{\mathrm{wbox}}, S_{\mathrm{h}} \, ; \, (C_{L\mathrm{h}})_{\min}, (C_L)_{\max}, (r_{\mathrm{fuel}})_{\mathrm{fwd}}, (r_{\mathrm{pay}})_{\mathrm{fwd}}, 0) = 0 \tag{A.300}$$

$$\mathcal{R}_S = \mathcal{R}_S(x_{\mathrm{wbox}}, S_{\mathrm{h}} \, ; \, (r_{\mathrm{fuel}})_{\mathrm{aft}}, (r_{\mathrm{pay}})_{\mathrm{aft}}, 1) = 0 \tag{A.301}$$

Specifically, for pitch trim the most-forward CG and most-negative flaps-down wing airfoil c_m, at maximum flight C_L are assumed. For stability the most-aft CG is assumed. The r_{pay} values which give the extreme forward and aft CG locations are obtained by solving the extremizing relation

$$\frac{\partial \mathcal{R}_M}{\partial r_{\mathrm{pay}}} = 0 \tag{A.302}$$

which is a quadratic for r_{pay}. It is solved twice, with $\xi_{\mathrm{pay}} = 0$ chosen to give $(r_{\mathrm{pay}})_{\mathrm{fwd}}$, and then $\xi_{\mathrm{pay}} = 1$ chosen to give $(r_{\mathrm{pay}})_{\mathrm{aft}}$. Zero fuel, or $r_{\mathrm{fuel}} = 0$ is assumed for both cases, as this typically gives the most extreme CG locations together with the worst-case payload distributions.

The two residuals (A.300) and (A.301) are simultaneously driven to zero by varying the wing position x_{wbox} and the horizontal tail area S_{h}, by solving the 2×2 Newton system. The four Jacobian elements are readily calculated.

$$\begin{bmatrix} \dfrac{\partial \mathcal{R}_M}{\partial S_{\mathrm{h}}} & \dfrac{\partial \mathcal{R}_M}{\partial x_{\mathrm{wbox}}} \\[2ex] \dfrac{\partial \mathcal{R}_S}{\partial S_{\mathrm{h}}} & \dfrac{\partial \mathcal{R}_S}{\partial x_{\mathrm{wbox}}} \end{bmatrix} \begin{Bmatrix} \delta S_{\mathrm{h}} \\[2ex] \delta x_{\mathrm{wbox}} \end{Bmatrix} = - \begin{Bmatrix} \mathcal{R}_M \\[2ex] \mathcal{R}_S \end{Bmatrix} \tag{A.303}$$

Off-design case: Tail lift setting

For off-design calculations where the wing location and horizontal tail area is set, pitch trim is achieved by adjusting C_{L_h}. The pitch-trim residual (A.294) is therefore driven to zero with a Newton step on C_{L_h}.

$$\frac{\partial \mathcal{R}_M}{\partial C_{L_h}} = \frac{1}{C_L}\left[-(c_o C_{M_1} - x_{\text{wbox}})\frac{S_h}{S} + (c_{oh} C_{Mh_1} - x_{\text{hbox}})\frac{S_h}{S}\right] \tag{A.304}$$

$$(C_{L_h})_{\text{new}} = C_{L_h} - \frac{\mathcal{R}_M}{\partial \mathcal{R}_M / \partial C_{L_h}} \tag{A.305}$$

Vertical tail sizing via engine-out yaw power

An alternative to the specified vertical tail volume (A.299) is to size the vertical tail so that it can achieve yaw trim with one engine out. The requirement is

$$q_{\min} C_{L_{v_{\text{yaw}}}} S_v\, l_v = (F_{\text{eng}} + q_{\min} C_{D\text{eng}} A_{\text{eng}})\, y_{\text{eng}} \tag{A.306}$$

where $q_{\min}$ is the minimum takeoff dynamic pressure, $C_{L_{v_{\text{yaw}}}}$ is the maximum lift coefficient of the vertical tail with some yaw control margin, F_{eng} is the thrust of one engine, $C_{D\text{eng}}$ is the drag coefficient of a windmilling engine with reference area A_{eng}, and y_{eng} is the lateral distance of the outermost engine from the centerline.

A.2.13   Dissipation (Drag) Calculation

Power-based formulation

The performance calculations used here are based on the power balance and dissipation analysis of Drela [12]. In brief, the usual streamwise force balance equation in constant-velocity flight is replaced with the power balance relation

$$F'V_\infty = D'V_\infty + W\dot{h} \tag{A.307}$$

where $\dot{h}$ is the climb rate, F' is an effective thrust, and D' is an effective drag. These two effective forces are actually defined in terms of the net propulsive power and the net dissipation and vortex kinetic energy loss rate.

$$F'V_\infty \equiv P_{K_{\text{inl}}} + P_V + P_{K_{\text{out}}} - \Phi_{\text{jet}} \tag{A.308}$$

$$D'V_\infty \equiv \Phi_{\text{surf}} + \Phi_{\text{wake}} + \dot{E}_{\text{vortex}} \tag{A.309}$$

The advantage of this power-balance approach is that it naturally handles the presence of boundary layer ingestion (BLI) without the ambiguities or complications which arise with a force-balance approach. If no BLI is present then the two approaches become entirely equivalent, and F', D' become the conventional thrust and drag F, D. The BLI accounting is described in more detail in the separate document "Power Accounting with Boundary Layer Ingestion". Only the relevant results will be used here.

The disspation and power loss terms in the above power equations are used to define the following convenient coefficients.

$$C'_{D_p} \equiv \frac{\Phi_{\text{surf}} + \Phi_{\text{wake}}}{\frac{1}{2}\rho V_\infty^3 S} \tag{A.310}$$

$$C'_{D_i} \equiv \frac{\dot{E}_{\text{vortex}}}{\frac{1}{2}\rho V_\infty^3 S} = C_{D_i} \tag{A.311}$$

$$C'_D \equiv \frac{D' V_\infty}{\frac{1}{2}\rho V_\infty^3 S} = C'_{D_p} + C_{D_i} \tag{A.312}$$

As with "F'" and "D", the "C_D" notation is used as a reminder that if there is no BLI, the above definitions reduce to the conventional drag coefficients and the primes can be simply dropped in that case.

In the following subsections, the various contributions to the overall power-loss coefficient C'_D will be computed. Most of these rely on traditional drag models and terminology, hence the "Drag" label will be used in the sections titles, mostly out of habit. As a useful indicator, the prime $()'$ will be retained only for those contributions which are potentially influenced by BLI. Unprimed contributions will thus also correspond to the conventional drag coefficients.

Fuselage Profile Drag

The fuselage profile drag is determined by an pseudo-axisymmetric viscous/inviscid calculation method, which is described in the separate document "Simplified Viscous/Inviscid Calculation for Nearly-Axisymmetric Bodies". This gives reliable viscous flow and fuselage drag predictions for any reasonable fuselage shape, without the need to rely on effective wetted area or fineness-ratio correlations.

The method requires the geometry to be specified in the form of a cross-sectional area distribution $A_{(x)}$ and also a perimeter distribution $b_{0(x)}$, shown in Figure A.12. For a round cross-section these are of course related, but to allow treating more general fuselage cross-sections, they are assumed to be specified separately. The cross section sizes and shapes can vary along the body, provided the variation is reasonably smooth.
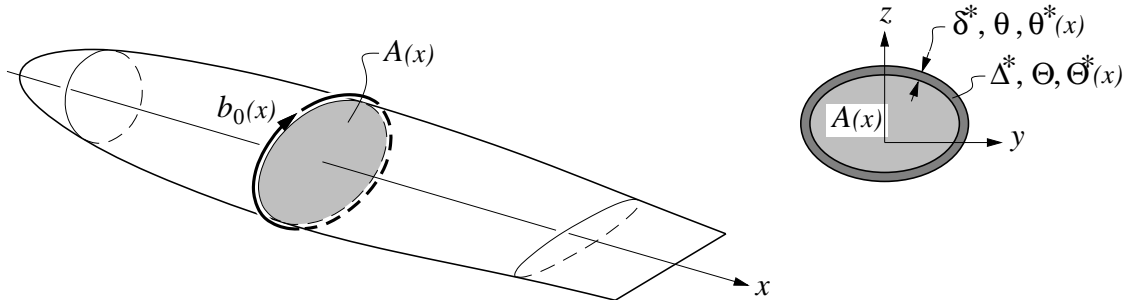

Figure A.12: Fuselage defined by cross-sectional area $A_{(x)}$ and perimeter $b_{0(x)}$ distributions. Viscous calculation produces displacement, momentum, and kinetic energy areas $\Delta^*, \Theta, \Theta^*_{(x)}$.

The cross-sectional area over the center cylindrical portion is A_{fuse}, which has already been defined by (A.6). This also defines the radius of the equivalent round cylinder.

$$R_{\text{cyl}} = \sqrt{\frac{A_{\text{fuse}}}{\pi}} \qquad (A.313)$$

The equivalent radii over the tapering nose and radius are then defined via the following convenient functions.

$$R_{(x)} = \begin{cases} R_{\text{cyl}} \left[1 - \left(\dfrac{x_{\text{blend}_1} - x}{x_{\text{blend}_1} - x_{\text{nose}}} \right)^a \right]^{1/a} & , \quad x_{\text{nose}} < x < x_{\text{blend}_1} \\[2ex] R_{\text{cyl}} & , \quad x_{\text{blend}_1} < x < x_{\text{blend}_2} \\[2ex] R_{\text{cyl}} \left[1 - \left(\dfrac{x - x_{\text{blend}_2}}{x_{\text{end}} - x_{\text{blend}_2}} \right)^b \right] & , \quad x_{\text{blend}_2} < x < x_{\text{tail}} \end{cases} \qquad (A.314)$$

$$a \simeq 1.6 \qquad (A.315)$$
$$b \simeq 2.0 \qquad (A.316)$$

The x_{blend_1} and x_{blend_2} locations are the nose and tailcone blend points, and do not necessarily have to be exactly the same as the x_{shell_1} and x_{shell_2} locations which define the loaded pressure shell. Likewise, x_{end} is the aerodynamic endpoint of the tailcone, and is distinct from its structural endpoint x_{conend}. The a and b constant values above give reasonable typical fuselage shapes.

If the fuselage is nearly round, the necessary area and perimeter distributions follow immediately.

$$A_{(x)} = \pi R_{(x)}^2 \qquad (A.317)$$
$$b_{0(x)} = 2\pi R_{(x)} \qquad (A.318)$$

This would be suitably modified for non-circular cross-sections.

With this geometry definition, the viscous/inviscid calculation procedure provides the momentum and kinetic energy area distributions along the body and wake,

$$\{\Theta_{(s)}, \Theta^*_{(s)}\} = f_{\text{f}_{\text{excr}}} \mathcal{F}(M_\infty, Re_\ell \,;\, A_{(x)}, b_{0(x)}) \qquad (A.319)$$

where $\mathcal{F}$ denotes the overall viscous/inviscid calculation procedure, and $f_{\text{f}_{\text{excr}}} \geq 1$ is an empirical factor to allow for fuselage excrescence drag sources.

Specific values of interest are the far-downstream momentum area Θ_{wake} at the wake endpoint, and the kinetic energy area Θ_{TE} at the body endpoint or trailing edge.

$$\Theta_{\text{wake}} = \Theta(s_{\text{wake}}) \qquad (A.320)$$
$$\Theta^*_{TE} = \Theta^*(s_{TE}) \qquad (A.321)$$

The fuselage surface + wake dissipated power in the absence of BLI is then evaluated as follows, consistent with the usual wake momentum defect relations.

$$C_{D_{\text{fuse}}} \equiv \frac{\Phi_{\text{fuse}}}{\frac{1}{2}\rho V_\infty^3 S} = \frac{\Phi_{\text{surf}} + \Phi_{\text{wake}}}{\frac{1}{2}\rho V_\infty^3 S} \qquad \text{(without BLI)} \qquad (A.322)$$

$$C_{D_{\text{fuse}}} = \frac{D_{\text{fuse}}}{\frac{1}{2}\rho V^2 S} = \frac{2\Theta_{\text{wake}}}{S} \qquad \text{(without BLI)} \qquad (A.323)$$

If BLI is present at or near the trailing edge, the upstream boundary layer and corresponding surface dissipation Φ_{surf} will be mostly unaffected. But the viscous fluid flowing into the wake is now reduced by the ingestion fraction f_{BLI_f}, so that the wake dissipation Φ_{wake} will be reduced by the same fraction. This then gives the following overall fuselage dissipation coefficient for the BLI case.

$$C'_{D_{\text{fuse}}} \ \equiv \ \frac{\Phi_{\text{fuse}}}{\frac{1}{2}\rho V_\infty^3 S} \ = \ \frac{\Phi_{\text{surf}} + \Phi_{\text{wake}}(1 - f_{\text{BLI}_f})}{\frac{1}{2}\rho V_\infty^3 S} \qquad \text{(with BLI)} \quad \text{(A.324)}$$

$$C'_{D_{\text{fuse}}} \ = \ C_{\Phi_{\text{surf}}} + C_{\Phi_{\text{wake}}}(1 - f_{\text{BLI}_f}) \ = \ C_{D_{\text{fuse}}} - C_{\Phi_{\text{wake}}} f_{\text{BLI}_f} \qquad \text{(with BLI)} \ \text{(A.325)}$$

$$\text{where} \quad C_{\Phi_{\text{surf}}} \ = \ \frac{\Theta_{TE}^*}{S} \qquad\qquad\qquad\qquad\qquad\qquad\qquad\qquad \text{(A.326)}$$

$$C_{\Phi_{\text{wake}}} \ = \ \frac{2\Theta_{\text{wake}}}{S} - \frac{\Theta_{TE}^*}{S} \qquad\qquad\qquad\qquad\qquad\qquad \text{(A.327)}$$

Wing Profile Drag

The power dissipated in the wing's surface and wake for the non-ingesting case defines the wing's profile drag coefficient.

$$C_{D_{\text{wing}}} \ \equiv \ \frac{\Phi_{\text{wing}}}{\frac{1}{2}\rho V_\infty^3 S} \ = \ \frac{\Phi_{\text{surf}} + \Phi_{\text{wake}}}{\frac{1}{2}\rho V_\infty^3 S} \qquad\qquad \text{(without BLI)} \qquad \text{(A.328)}$$

Any ingestion of the wing boundary layer is captured by the ingestion fraction f_{BLI_w}, in the same manner as for the fuselage.

$$C'_{D_{\text{wing}}} \ \equiv \ \frac{\Phi_{\text{wing}}}{\frac{1}{2}\rho V_\infty^3 S} \ = \ \frac{\Phi_{\text{surf}} + \Phi_{\text{wake}}(1 - f_{\text{BLI}_w})}{\frac{1}{2}\rho V_\infty^3 S} \qquad \text{(with BLI)} \qquad \text{(A.329)}$$

$$C'_{D_{\text{wing}}} \ = \ C_{D_{\text{wing}}} - C_{\Phi_{\text{wake}}} f_{\text{BLI}_w} \qquad \text{(with BLI)} \qquad\qquad\qquad \text{(A.330)}$$

$$\text{where} \quad C_{\Phi_{\text{wake}}} \ \simeq \ r_{\Phi_{\text{wake}}} C_{D_{\text{wing}}} \qquad\qquad\qquad\qquad\qquad\qquad \text{(A.331)}$$

$$r_{\Phi_{\text{wake}}} \ \simeq \ 0.15 \qquad\qquad\qquad\qquad\qquad\qquad\qquad\qquad \text{(A.332)}$$

The wake dissipation is assumed here to be $r_{\Phi_{\text{wake}}} = 15\%$ of the total airfoil dissipation, which is typical of optimized modern transonic airfoils.

The actual calculation of $C_{D_{\text{wing}}}$ is via the drag using infinite swept wing theory, which also gives the lift in term of the perpendicular-plane velocity $V_\perp$ and lift coefficient $c_{\ell_\perp}$. Figure A.13 shows the relations. These quantities are related to the local loading via

$$V_\perp \ = \ V_\infty \cos\Lambda \qquad\qquad\qquad\qquad\qquad\qquad\qquad \text{(A.333)}$$

$$dL \ = \ \tilde{p}\, dy \ = \ \tfrac{1}{2}\rho V_\perp^2\, c_\perp\, c_{\ell_\perp}\, dy_\perp \qquad\qquad\qquad \text{(A.334)}$$

$$p_o\, P_{(\eta)} \ = \ \tfrac{1}{2}\rho V_\infty^2\, c_o\, C_{(\eta)}\, c_{\ell_\perp}{(\eta)}\, \cos^2\Lambda \qquad\qquad \text{(A.335)}$$

excluding the wing center and extreme tip where the lift adjustements ΔL_o and ΔL_t are located. The loading scale p_o in level flight is obtained from (A.159) with $N = 1$ as follows.

$$W \ = \ L \ = \ \tfrac{1}{2}\rho V_\infty^2\, S\, C_L \qquad\qquad\qquad\qquad\qquad \text{(A.336)}$$

$$L_{\text{htail}} \ = \ \tfrac{1}{2}\rho V_\infty^2\, S_{\text{h}}\, C_{L_{\text{h}}} \qquad\qquad\qquad\qquad\qquad \text{(A.337)}$$

$$p_o \ = \ \frac{1}{K_p\, b}\, (L - L_{\text{htail}}) \qquad\qquad\qquad\qquad\qquad \text{(A.338)}$$

Using (A.338) to substitute for p_o in (A.335) and rearranging gives an explicit expression for the local section lift coefficient.

$$C_{L_{\text{htail}}} = \frac{S_{\text{h}}}{S} C_{L_{\text{h}}} \tag{A.339}$$

$$c_{\ell_\perp}(\eta) = \frac{C_L - C_{L_{\text{htail}}}}{\cos^2 \Lambda} \frac{S}{K_p \, b \, c_o} \frac{P_{(\eta)}}{C_{(\eta)}} \tag{A.340}$$
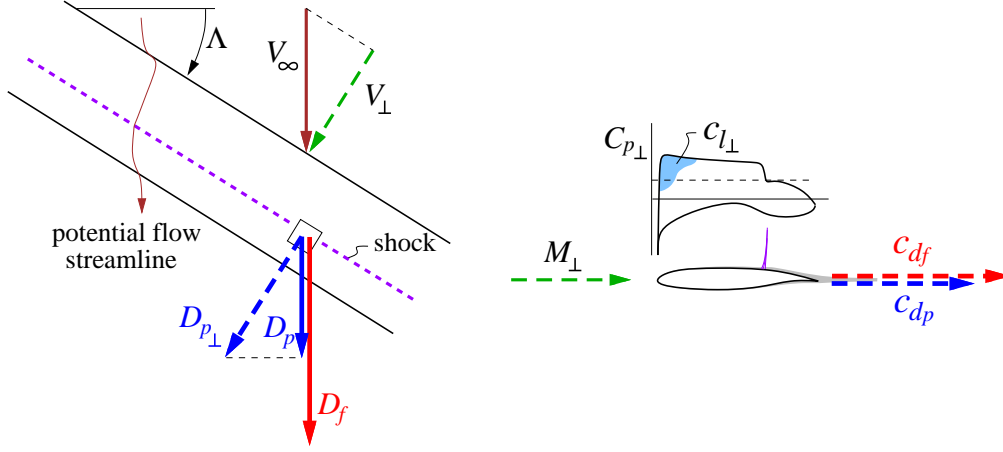

Figure A.13: Friction and pressure drag forces on infinite swept wing

Using this $c_{\ell_\perp}$ and also $M_\perp$, the perpendicular-plane friction and pressure drag coefficients are then obtained from a 2D airfoil drag database having the form

$$c_{d_f} = f_{\text{wexcr}} \, \bar{c}_{d_f}(c_{\ell_\perp}, M_\perp, \tfrac{t}{c}) \left(\frac{Re_c}{Re_{\text{ref}}} \right)^{a_{Re}} \tag{A.341}$$

$$c_{d_p} = f_{\text{wexcr}} \, \bar{c}_{d_p}(c_{\ell_\perp}, M_\perp, \tfrac{t}{c}) \left(\frac{Re_c}{Re_{\text{ref}}} \right)^{a_{Re}} \tag{A.342}$$

$$\text{where} \qquad M_\perp = M_\infty \cos \Lambda \tag{A.343}$$

$$\frac{t}{c} = \bar{h} \tag{A.344}$$

$$Re_c = \frac{\rho_\infty V_\infty c}{\mu_\infty} \tag{A.345}$$

$$a_{Re} \simeq -0.15 \tag{A.346}$$

and $f_{\text{wexcr}} \geq 1$ is an empirical specified factor to account for wing excrescence drag sources, and Re_{ref} is a reference Reynolds number at which the database functions $\bar{c}_{d_f}, \bar{c}_{d_p}$ were computed. The chord Reynolds number Re_c could of course be treated as an additional parameter in the database, but at a considerable increase in the size of the database and the computational effort needed to construct it. The value of the Re-scaling exponent $a_{Re} \simeq -0.15$ is appropriate for fully-turbulent flow.

Note that the database includes the airfoil thickness/chord ratio $\frac{t}{c} = \bar{h}$, which is crucial for obtaining a realistic wing thickness/sweep/C_L/Mach tradeoff. The thickness dependence is determined by viscous MSES [18] calculations on a number of transonic airfoils or varying thickness, such as the ones shown in Figure A.14. Each airfoil has been designed independently for a well-behaved transonic drag rise, so that the database returns c_{d_f} and c_{d_p} values

representative of the best transonic airfoil technology. A piecewise-linear airfoil thickness distribution is assumed, defined by the three values $\bar{h}_o, \bar{h}_s, \bar{h}_t$.

$$\bar{h}(\eta) = \begin{cases} \bar{h}_o & , \quad 0 < \eta < \eta_o \\ \bar{h}_o + (\bar{h}_s - \bar{h}_o)\dfrac{\eta - \eta_o}{\eta_s - \eta_o} & , \quad \eta_o < \eta < \eta_s \\ \bar{h}_s + (\bar{h}_t - \bar{h}_s)\dfrac{\eta - \eta_s}{1 - \eta_s} & , \quad \eta_o < \eta < \eta_s \end{cases} \qquad (A.347)$$

On typical transport wings most of the thickness/chord variation occurs inboard, so in that case, only $\bar{h}_o$ and $\bar{h}_s$ would be considered as design variables, and $\bar{h}_t = \bar{h}_s$ would be assumed.

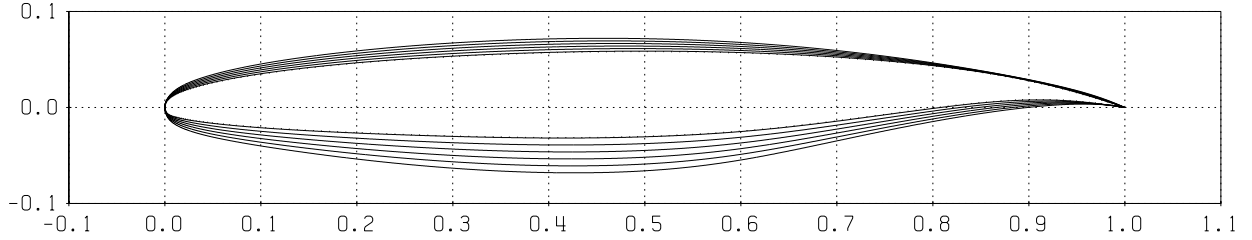|	NC090	NC100	NC110	NC120	NC130	NC140
area =	0.06210	0.06836	0.07464	0.08093	0.08723	0.09355
thick. =	0.09001	0.10000	0.11000	0.12000	0.13000	0.13999
camber =	0.02142	0.02036	0.01930	0.01826	0.01722	0.01620
r_{LE} =	0.01457	0.01489	0.01522	0.01556	0.01590	0.01632
$\Delta\theta_{TE}$ =	11.78°	11.74°	11.71°	11.68°	11.64°	11.62°

Figure A.14: Airfoil family used to generate airfoil-performance database.

The 2D profile drag coefficients are applied to the swept wing using infinite swept-wing theory, illustrated in Figure A.13. This treatment is exact for laminar flow on untapered wings, and quite accurate for turbulent flow. The friction drag is assumed to scale with freestream dynamic pressure and to act mostly along the freestream flow direction, while the pressure drag from the shock and viscous diplacement is assumed to scale with the wing-normal dynamic pressure and to act normal to the wing-spanwise axis. The total local streamwise drag element is then given as follows.

$$\begin{aligned} dD_{\text{wing}} &= dD_f + dD_p = dD_f + dD_{p_\perp}\cos\Lambda \\ &= \tfrac{1}{2}\rho V_\infty^2\, c\, c_d\, dy \end{aligned} \qquad (A.348)$$

$$c_d = c_{d_f} + c_{d_p}\cos^3\Lambda \qquad \text{(infinite swept wing)} \qquad (A.349)$$

However, this relation is not realistic near the fuselage. Here the potential flow is forced parallel to the freestream direction which causes the wing shock to become locally unswept, as shown in Figure A.15. Also, the full streamwise dynamic pressure (as opposed to the wing-normal dynamic pressure) acts at the trailing edge where most of the displacement-effect pressure drag occurs. Hence, the sweep correction is dropped off towards the fuselage via the heuristic "unsweep" function $f_{\text{Suns}}(\eta)$.

$$c_d(\eta) = \left\{ c_{d_f} + c_{d_p}\left[f_{\text{Suns}} + (1 - f_{\text{Suns}})\cos^2\Lambda \right]\cos\Lambda \right\} \qquad \text{(actual swept wing)} \quad (A.350)$$

$$f_{\text{Suns}}(\eta) = \exp\!\left(-\frac{1}{k_{\text{Suns}}}\frac{y - y_o}{c}\right) = \exp\!\left(-\frac{1}{k_{\text{Suns}}}\frac{\eta - \eta_o}{C(\eta)}\frac{b}{2c_o}\right) \qquad (A.351)$$

$$k_{\text{Suns}} \simeq 0.5 \qquad (A.352)$$

49

The k_{Suns} decay constant controls the area of the wing most influenced by the shock unsweep correction, as shown in Figure A.15.
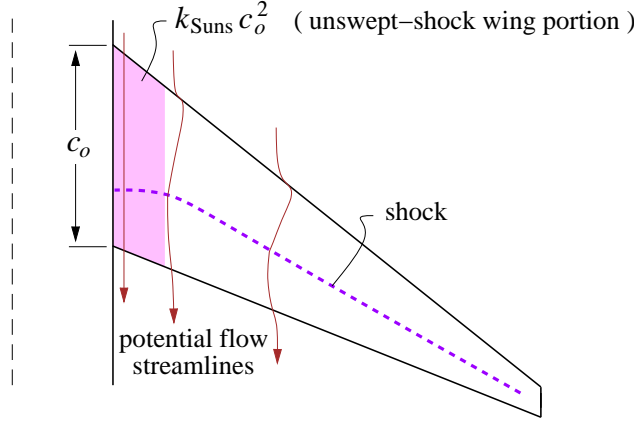

Figure A.15: Wing shock unsweeps near the fuselage, roughly over the area $k_{\text{uns}}c_o^2$.

The overall wing profile drag is then obtained by numerical integration of (A.348), using (A.350) for the $c_{d(\eta)}$ function and (A.121) for the chord $c_{(\eta)}$ function.

$$C_{D_{\text{wing}}} \equiv \frac{D_{\text{wing}}}{\frac{1}{2}\rho V_\infty^2 S} = \frac{bc_o}{S}\int_{\eta_o}^{1} c_{d(\eta)}\, C_{(\eta)}\, d\eta \qquad (A.353)$$

Tail Profile Drag

The viscous dissipation of the tail surfaces is computed using the same relations as for the wing, giving the equivalent tail drag coefficients $C_{D_{\text{htail}}}$ and $C_{D_{\text{vtail}}}$. No BLI is assumed, but could be included in the same manner as for the wing. Because tail surfaces typically do not have significant shock waves, the shock-unsweep correction (A.350) is inappropriate. Instead, the 2D friction and pressure drag coefficients c_{d_f} and c_{d_p} are specified directly and are used in the infinite-wing relation (A.349), and are assumed constant over the surface so that numerical spanwise integration is unnecessary.

$$C_{D_{\text{htail}}} = c_{d_{f\text{h}}} + c_{d_{p\text{h}}}\cos^3\Lambda_{\text{h}} \qquad (A.354)$$
$$C_{D_{\text{vtail}}} = c_{d_{f\text{v}}} + c_{d_{p\text{v}}}\cos^3\Lambda_{\text{v}} \qquad (A.355)$$

Strut Profile Drag

In the absence of any BLI on the strut, its dissipation is fully captured by its conventional drag coefficient, scaled by the local mean-cube-average velocity ratio $r_{V_{\text{strut}}}$ to allow for the fact that a strut is typically in the decreased flow velocity below a lifting wing. Simple sweep corrections are also used as for the wing.

$$c_{\text{strut}} = \sqrt{\frac{A_{\text{strut}}}{k_A\,\overline{h}_{\text{strut}}}} \quad , \qquad k_A \simeq 0.65 \qquad (A.356)$$
$$S_{\text{strut}} = 2c_{\text{strut}}\,\ell_{s_\perp} \qquad (A.357)$$

50

$$\cos \Lambda_s \quad = \quad \frac{\ell_s}{\ell_{s_\perp}} \tag{A.358}$$

$$C_{D_\text{strut}} \quad = \quad \frac{S_\text{strut}}{S} \left(c_{d_{f\text{s}}} + c_{d_{p\text{s}}} \cos^3\Lambda_\text{s} \right) r_{V_\text{strut}}^3 \tag{A.359}$$

Picking a strut thickness/chord ratio $\bar{h}_\text{strut} \simeq 0.15\ldots0.20$ typically gives the minimum overall drag for a given strut cross-sectional area A_strut. The k_A area factor of 0.65 is typical of most symmetric airfoils.

Engine Nacelle Profile Drag

The nacelle viscous dissipation accounts for the external nacelle flow only, since the internal flow is represented by the engine diffuser and nozzle losses. The external wetted area and corresponding area fraction is determined as an assumed fraction r_Snace of the engine fan area.

$$S_\text{nace} \quad = \quad n_\text{eng}\, r_\text{Snace}\, \frac{\pi}{4}\, d_\text{fan}^2 \tag{A.360}$$

$$f_\text{Snace} \quad = \quad \frac{S_\text{nace}}{S} \tag{A.361}$$

The skin friction coefficient can also be calculated based on the nacelle-length Reynolds number and a standard turbulent skin-friction law, with an excrescence factor $f_{n_\text{excr}} \geq 1$ included as for the fuselage and wing.

$$\ell_\text{nace} \quad = \quad 0.15\, r_\text{Snace}\, d_\text{fan} \tag{A.362}$$

$$Re_\text{nace} \quad = \quad \frac{\rho_\infty V_\infty \ell_\text{nace}}{\mu_\infty} \tag{A.363}$$

$$C_{f_\text{nace}} \quad = \quad f_{n_\text{excr}}\, C_{f_\text{turb}}(Re_\text{nace}) \tag{A.364}$$

The nacelle is assumed to be immersed in the potential nearfield of a nearby wing or fuselage, with a local effective freestream V_nace which differs somewhat from the true freestream V_∞, and is specified via the ratio V_nace/V_∞. Depending on the flight condition and engine power, the fan-face Mach number M_2 will in general differ considerably from the corresponding local M'_∞. The nacelle is therefore effectively a loaded ring airfoil, which can be represented by a ring vortex sheet whose resulting external nacelle-surface velocity is approximately

$$V_{n_{LE}} \quad \simeq \quad 2V_\text{nace} - V_2 \tag{A.365}$$

$$\frac{V_\text{nace}}{V_\infty} \quad = \quad r_{V_\text{nace}} \tag{A.366}$$

$$\frac{V_{n_{LE}}}{V_\infty} \quad = \quad 2\frac{V_\text{nace}}{V_\infty} - \frac{V_2}{V_\infty} \quad \simeq \quad \max\!\left(2r_{V_\text{nace}} - \frac{M_2}{M_\infty}\,,\ 0 \right) \tag{A.367}$$

at the lip, as sketched in Figure A.16. Limiting $V_{n_{LE}}$ above zero avoids unrealistic results for low airspeed, high-power operation situations.

Assuming a linear acceleration or deceleration from $V_{n_{LE}}$ to V_nace at the nacelle nozzle gives the following mean-cube velocity ratio on the nacelle surface.

$$r_{V_\text{nsurf}}^3 \quad \equiv \quad \frac{1}{V_\infty^3} \int_0^1 \left[V_\text{nace} + (V_{n_{LE}} - V_\text{nace})\,(1-\xi) \right]^3 d\xi \tag{A.368}$$
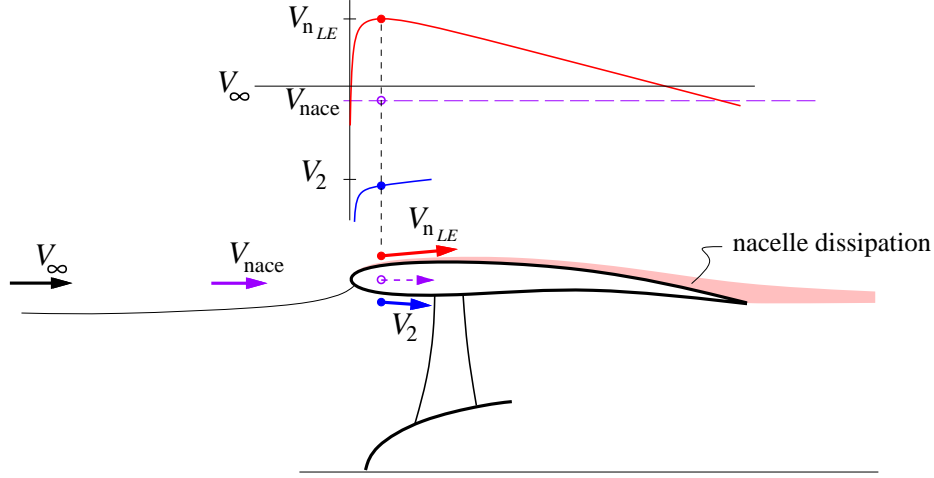
Figure A.16: Velocity distribution on inside and outside of engine nacelle. Outside velocity determines nacelle dissipation and implied nacelle drag. The $V_{n_{LE}} > V_2$ case shown is for a typical cruise condition, while $V_{n_{LE}} < V_2$ will occur at low speeds and high power.

$$= \frac{1}{4} \left[\frac{V_{n_{LE}}}{V_\infty} + r_{V_{\text{nace}}} \right] \left[\left(\frac{V_{n_{LE}}}{V_\infty} \right)^2 + r_{V_{\text{nace}}}^2 \right] \tag{A.369}$$

The nacelle-surface dissipation, expressed as the equivalent nacelle drag coefficient, is now estimated using a turbulent wetted-area skin-friction coefficient, weighted by the mean-cube velocity ratio.

$$C_{D_{\text{nace}}} = f_{\text{Snace}} \, C_{f_{\text{nace}}} \, r_{V_{\text{nsurf}}}^3 \tag{A.370}$$

Induced Drag

The induced drag is calculated using a discrete vortex Trefftz-Plane analysis. The circulation of the wing wake immediately behind the trailing edge is

$$\Gamma_{\text{wing}}(\eta) = \frac{\tilde{p}(\eta)}{\rho V_\infty} \simeq \frac{p(\eta)}{\rho V_\infty} \sqrt{1 - \eta^{k_t}} \tag{A.371}$$

$$k_t \simeq 16 \tag{A.372}$$

where the approximation realistically represents the tip lift rolloff for typical taper ratios, and is consistent with the assumed $f_{L_t} \simeq -0.05$ value for the tip lift loss factor. This circulation is convected into the wake along streamlines which will typically constrict behind the fuselage by continuity. Figure A.17 shows two possible aft fuselage taper shapes, giving two different wake constrictions.

An annular streamtube at the wing contracts to another annular streamtube in the wake with the same cross-sectional area. The y and y' locations on the wing and wake which are connected by a streamline are therefore related by the correspondence function.

$$y'_{(y)} = \sqrt{y^2 - y_o^2 + y_o'^2} \tag{A.373}$$
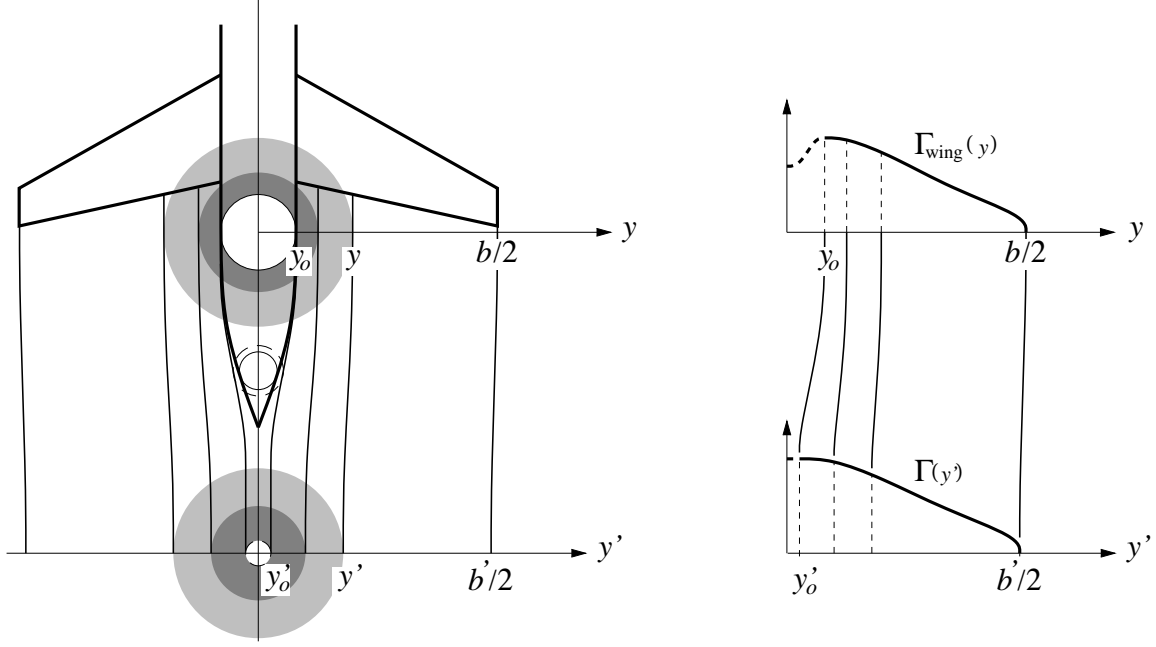
Figure A.17: Wake streamline contraction due to fuselage thickness, carrying wing circulation into the wake. Two shaded streamtubes are shown. Wake center radius y'_o is nonzero due to the fuselage viscous wake displacement area.

The Trefftz Plane circulation $\Gamma_{(y')}$ is then given by the coordinate shift. The mapping function $y'_{(y)}$ is not defined for $y < y_o$, so the circulation there is simply set from the y_o value.

$$\Gamma_{\text{wake}}(y') = \begin{cases} \Gamma_{\text{wing}}(y(y')) & , \quad y > y_o \\ \Gamma_{\text{wing}}(y_o) \end{cases} \tag{A.374}$$

The Trefftz Plane analysis uses point vortices. The circulation (A.374) is evaluated at the midpoints of n intervals along the wake trace, spaced more or less evenly in the Glauert angle to give a cosine distribution in physical space. The wake's vertical z positions are simply taken directly from the wing.

$$\theta_{i+1/2} = \frac{\pi}{2} \frac{i - 1/2}{n} \quad , \quad i = 1 \dots n \tag{A.375}$$

$$y_{i+1/2} = \frac{b}{2} \cos \theta_{i+1/2} \tag{A.376}$$

$$y'_{i+1/2} = \sqrt{y_{i+1/2}^2 - y_o^2 + y_o'^2} \tag{A.377}$$

$$z'_{i+1/2} = z_{i+1/2} \tag{A.378}$$

$$\Gamma_{i+1/2} = \Gamma_{\text{wing}}(y_{i+1/2}) \tag{A.379}$$

The locations of $n + 1$ trailing vortices are computed similarly.

$$\theta_i = \frac{\pi}{2} \frac{i - 1}{n} \quad , \quad i = 1 \dots n+1 \tag{A.380}$$

$$y_i = \frac{b}{2} \cos \theta_i \tag{A.381}$$

53

$$y_i' = \sqrt{y_i^2 - y_o^2 + y_o'^2} \qquad (A.382)$$

$$z_i' = z_i \qquad (A.383)$$

The circulations of these trailing vortices are the differences of the adjacent bound circulations, with the circulation beyond the tips effectively zero.

$$\bar{\Gamma}_i = \begin{cases} -\Gamma_{i-1/2} & , \quad i = 1 \qquad \text{(left tip)} \\ \Gamma_{i+1/2} - \Gamma_{i-1/2} & , \quad i = 2 \ldots n \\ \Gamma_{i+1/2} & , \quad i = n+1 \qquad \text{(right tip)} \end{cases} \qquad (A.384)$$

The above definitions are also applied to the horizontal tail, with its discrete points simply appended to the list and n increased accordingly.
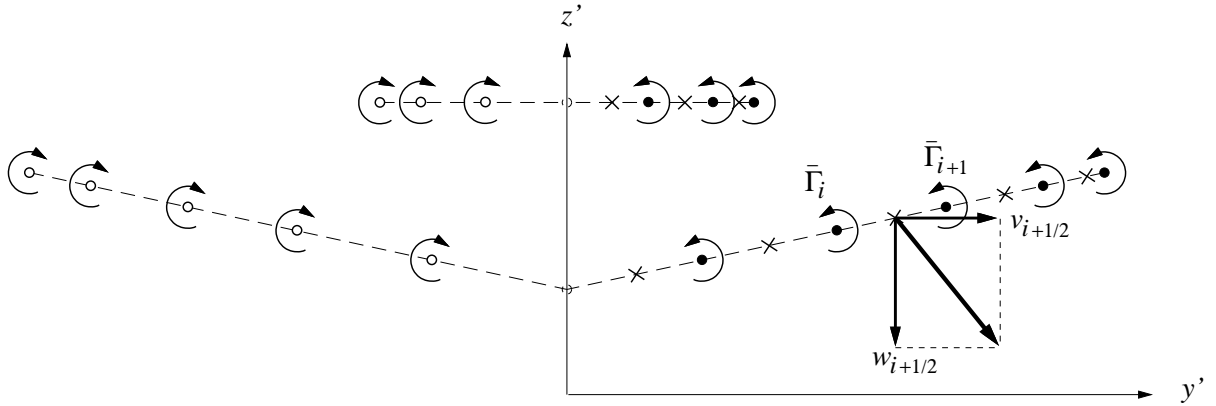
Figure A.18: Trefftz Plane vortices $i, i+1 \ldots$ and collocation points $i+1/2$ used for velocity, impulse, and kinetic energy calculations. Left/right symmetry is exploited.

The Trefftz plane calculation proceeds by first calculating the y-z wake velocity components at the $y_{i+1/2}', z_{i+1/2}'$ interval midpoints, induced by all the trailing vortices and their left-side images.

$$v_{i+1/2} = \sum_{j=1}^{n+1} \frac{\bar{\Gamma}_j}{2\pi} \left[\frac{-(z_{i+1/2}' - z_j')}{(y_{i+1/2}' - y_j')^2 + (z_{i+1/2}' - z_j')^2} - \frac{-(z_{i+1/2}' - z_j')}{(y_{i+1/2}' + y_j')^2 + (z_{i+1/2}' - z_j')^2} \right] \qquad (A.385)$$

$$w_{i+1/2} = \sum_{j=1}^{n+1} \frac{\bar{\Gamma}_j}{2\pi} \left[\frac{y_{i+1/2}' - y_j'}{(y_{i+1/2}' - y_j')^2 + (z_{i+1/2}' - z_j')^2} - \frac{y_{i+1/2}' + y_j'}{(y_{i+1/2}' + y_j')^2 + (z_{i+1/2}' - z_j')^2} \right] \qquad (A.386)$$

The overall lift and induced drag are then computed using the Trefftz Plane vertical impulse and kinetic energy. The sums are doubled to account for the left side image.

$$C_{L_{TP}} = \frac{2}{\frac{1}{2}\rho V_\infty^2 S} \sum_{i=1}^{n} \rho V_\infty \Gamma_{i+1/2} (y_{i+1}' - y_i') \qquad (A.387)$$

$$C_{D_{TP}} = \frac{2}{\frac{1}{2}\rho V_\infty^2 S} \sum_{i=1}^{n} -\frac{\rho}{2} \Gamma_{i+1/2} \left[w_{i+1/2} (y_{i+1}' - y_i') - v_{i+1/2} (z_{i+1}' - z_i') \right] \qquad (A.388)$$

To minimize any modeling and numerical errors incurred in the wake contraction model and the point-vortex summations, the final induced drag value is scaled by the square of the

surface-integral and Trefftz-Plane drag values.

$$C_{D_i} = C_{D_{TP}} \left(\frac{C_L}{C_{L_{TP}}} \right)^2 \tag{A.389}$$

This is equivalent to using the Trefftz Plane analysis to calculate the span efficiency rather than the actual induced drag coefficient.

Total Drag

The total effective aircraft dissipation coefficient is obtained by summing all the contributions.

$$C_D' = C_{D_i} + C_{D_{\text{fuse}}}' + C_{D_{\text{wing}}}' + C_{D_{\text{htail}}} + C_{D_{\text{vtail}}} + C_{D_{\text{strut}}} + C_{D_{\text{nace}}} \tag{A.390}$$

A.2.14 Engine Performance Model and Sizing

Engine model summary

The extensive details of the engine calculations are given in the separate documents "Turbofan Sizing and Analysis with Variable $c_{p(T)}$" and "Film Cooling Flow Loss Model". The treatment of the inlet kinetic energy defect K_{inl} is described in the document "Power Accounting with Boundary Layer Ingestion". In brief, K_{inl} reduces the fan inlet total pressure, and also adds to the net effective thrust by the amount K_{inl}/V_∞, which in engine parlance can be interpreted as a reduction in inlet "ram drag".

The engine model can be run in one of three modes:

1) Design sizing mode. The net thrust F_e' and combustor exit temperature T_{t4} are specified along with a number of other component and operating parameters, and the engine flow areas $A_2, A_5 \ldots$ are computed.

2) Off-design analysis mode. The areas and T_{t4} are prescribed, and thrust F_e' is computed.

3) Off-design analysis mode. The areas and F_e' are prescribed, and T_{t4} is computed.

For all three modes, the specific fuel consumption $TSFC'$ and all other engine operating parameters which are not specified are also computed.

$$\{A_2, A_{5\ldots}; \, TSFC'\ldots\} = \mathcal{F}_{\text{eng}_1}(F_e', T_{t4}, OPR_{\text{D}}, BPR_{\text{D}\ldots}; \, M_\infty, p_\infty, T_\infty, K_{\text{inl}\ldots}) \tag{A.391}$$

$$\{F_e'; \, TSFC', OPR, BPR\ldots\} = \mathcal{F}_{\text{eng}_2}(T_{t4}, A_2, A_{5\ldots}; \, M_\infty, p_\infty, T_\infty, K_{\text{inl}\ldots}) \tag{A.392}$$

$$\{T_{t4}; \, TSFC', OPR, BPR\ldots\} = \mathcal{F}_{\text{eng}_3}(F_e', A_2, A_{5\ldots}; \, M_\infty, p_\infty, T_\infty, K_{\text{inl}\ldots}) \tag{A.393}$$

$$\text{where} \qquad TSFC' \equiv \frac{F_e'}{\dot{m}_{\text{fuel}} \, g} \tag{A.394}$$

$$K_{\text{inl}} \equiv \left(\tfrac{1}{2} \rho_e V_e^3 \Theta^* \right)_{\text{inl}} = \frac{f_{\text{BLI}_\text{f}}}{n_{\text{eng}}} \left(\tfrac{1}{2} \rho_e V_e^3 \Theta^* \right)_{TE} \tag{A.395}$$

In these calculations, the fan inlet total pressure p_{t2} is reduced as a result of the BLI. A reasonable estimate is

$$p_{t2} = p_{t\infty} - \frac{K_{\text{inl}}}{\dot{\mathcal{V}}_{\text{inl}}} \tag{A.396}$$

$$\dot{\mathcal{V}}_{\text{inl}} = \iint_{\text{inl}} V \, dA \tag{A.397}$$

where $\dot{\mathcal{V}}_{\text{inl}}$ is the fan face volume flow.

Engine Sizing

In the design mode 1), the specified thrust is obtained is determined from the start-of-cruise weight W_c, lift/drag ratio, and the slight cruise-climb angle γ_{CR}.

$$F_{\text{D}}' = r_{B_c} W_c \left(\frac{C_D'}{C_L} + \gamma_{\text{CR}} \right)_c \tag{A.398}$$

$$F_{e_{\text{D}}}' = \frac{F_{\text{D}}'}{n_{\text{eng}}} \tag{A.399}$$

The engine calculations determine the specific thrust

$$F_{\text{sp}_{\text{D}}} \equiv \frac{F_{e_{\text{D}}}'}{a_\infty \dot{m}_{\text{core}}(1+BPR_{\text{D}})} \tag{A.400}$$

which then determines the core mass flow $\dot{m}_{\text{core}}$ and the associated fan flow area A_2 and fan diameter d_{f}.

$$A_2 = \frac{\dot{m}_{\text{core}}(1+BPR_{\text{D}})}{\rho_2 u_2} = \frac{1}{F_{\text{sp}_{\text{D}}}} \frac{F_{e_{\text{D}}}'}{\gamma p_\infty} \frac{1}{M_{2_{\text{D}}}} \left(\frac{1+\frac{\gamma-1}{2}M_{2_{\text{D}}}^2}{1+\frac{\gamma-1}{2}M_\infty^2} \right)^{\frac{\gamma+1}{2(\gamma-1)}} \tag{A.401}$$

$$d_{\text{f}} = \sqrt{\frac{4A_2}{\pi(1-HTR_{\text{f}}^2)}} \tag{A.402}$$

Similar calculations are used for the other component and nozzle areas.

A.2.15   Mission Performance and Fuel Burn Analysis

Mission profiles

The altitude, weight, and thrust profiles versus range are schematically shown in Figure A.19.

At any profile point these are related via the following normal force and axial force relations.

$$W \sin\gamma = F' - D' - \frac{W}{g}\frac{dV}{dt} \tag{A.403}$$

$$W \cos\gamma = L \tag{A.404}$$
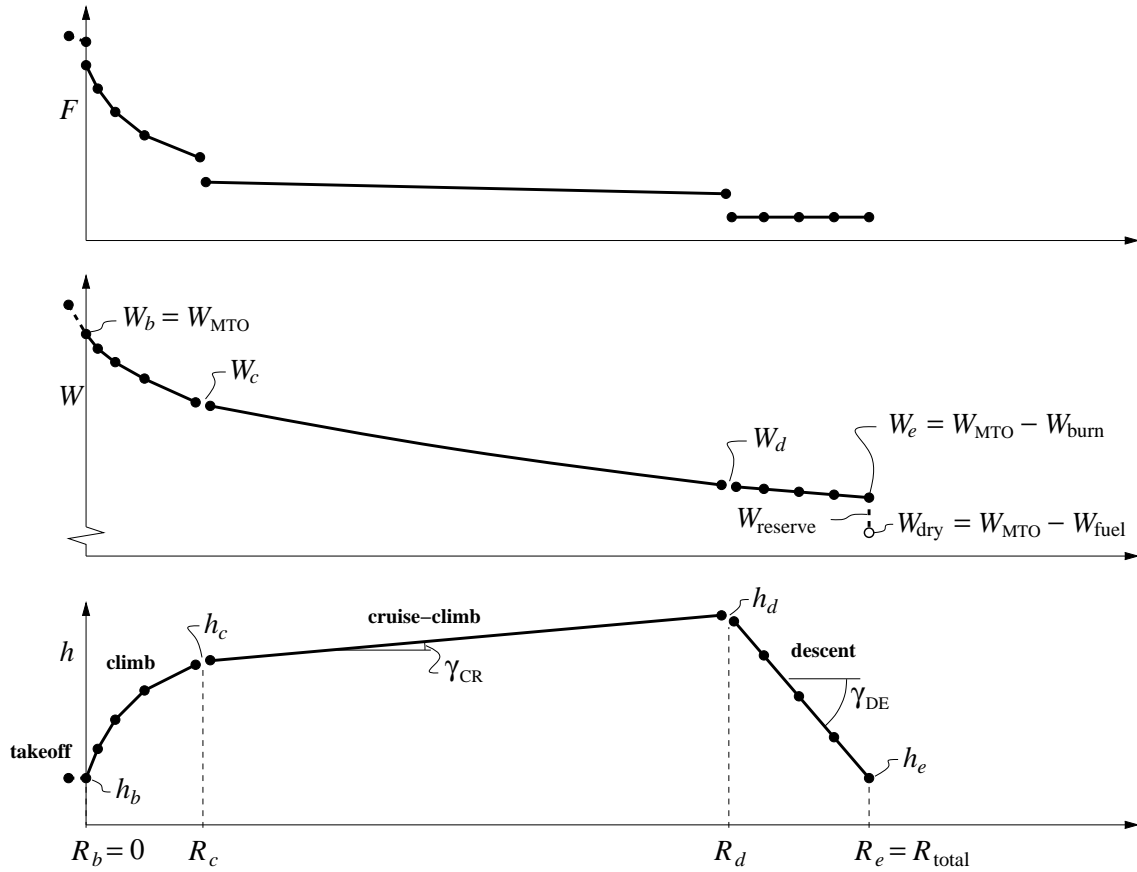
Figure A.19: Design-mission profiles of altitude, weight, thrust, versus range.

Equation (A.403) is merely a recast form of the power-balance equation (A.307), with the added last acceleration term. The subscript has also been dropped from V_∞ for convenience.

The flight speed at any profile point is obtained from a specified C_L and ambient density using equation (A.404).

$$V = \sqrt{\frac{2W\cos\gamma}{\rho\,S\,C_L}} \tag{A.405}$$

Some iteration is required with the thrust/drag relations below to determine the climb angle γ needed in (A.405).

Dividing (A.403) by (A.404), and using the kinematic ground-speed relation

$$\frac{dR}{dt} = V\cos\gamma \tag{A.406}$$

together with the fuel-burn to thrust relation

$$\frac{dW}{dt} = -\dot{m}_{\text{fuel}}g = -F'\,TSFC' \tag{A.407}$$

gives an expression for the climb angle γ or the equivalent climb gradient dh/dR, and also the weight-loss gradient dW/dR.

$$\tan\gamma = \frac{dh}{dR} = \frac{F'}{W}\frac{1}{\cos\gamma} - \frac{D'}{L} - \frac{1}{2g}\frac{d(V^2)}{dR} \tag{A.408}$$

$$\frac{dW}{dR} = -F' \frac{TSFC'}{V \cos \gamma} \tag{A.409}$$

These will be suitably integrated over the mission segments to obtain the altitude and weight profiles $h(R)$ and $W(R)$.

The instantaneous climb or descent angle γ in the above expressions can be computed by combining (A.403) and (A.404), and solving for the resulting quadratic equation for $\sin \gamma$.

$$\phi = \frac{F'}{W} - \frac{\dot{V}}{g} \tag{A.410}$$

$$\epsilon = \frac{C'_D}{C_L} \tag{A.411}$$

$$\sin \gamma = \frac{\phi - \epsilon \sqrt{1 - \phi^2 + \epsilon^2}}{1 + \epsilon^2} \tag{A.412}$$

The $\dot{V}$ acceleration term in the excess thrust-to-weight ratio ϕ can be neglected for most transport aircraft. The corresponding integrated $d(V^2)$ differential in (A.408) is also typically small, but there's little reason to exclude it in calculations.

Mission profile integration

The fuel weight required for a given mission range is determined by integration of the trajectory equations (A.408) and (A.409), which are first put in the following equivalent differential forms.

$$dR = \left(dh + \frac{d(V^2)}{2g} \right) \left(\frac{F'}{W} \frac{1}{\cos \gamma} - \frac{C'_D}{C_L} \right)^{-1} \tag{A.413}$$

$$d(\ln W) = -\frac{F'}{W} \frac{TSFC'}{V \cos \gamma} dR \tag{A.414}$$

The various terms are then approximated with 2-point finite differences or averages, and marched forward using a predictor/corrector scheme, over the climb, cruise, and descent segments of the mission. The details will be given in the Calculation Procedures section.

The following segment endpoint values are inputs to the integration, and are either specified externally, or obtained from the weight-sizing calculations:

W_b takeoff weight
C_L lift coefficient for all points
M_{CR} cruise Mach number
h_b takeoff altitude
h_c start-of-cruise altitude
h_e landing altitude

Climb distance

The climb-segment range R_c is computed by integrating equations (A.413) and (A.414) from the takeoff range $R_b = 0$, over the prescribed climb altitude change $h_b \ldots h_c$. The start-of-climb weight W_c is also computed in the process.

Cruise and descent angles, distances

Before the cruise and descent segments are integrated, it is first necessary to determine the end-of-cruise range R_d and altitude h_d.

The first step is to calculate the slight cruise-climb angle γ_{CR}, so as to preserve a constant flight Mach number M and flight C_L as the aircraft loses weight from fuel burn. These are related to the current weight W at any point in the cruise by the lift equation.

$$\frac{1}{2}\rho V^2 \;=\; \frac{\gamma}{2}pM^2 \;=\; \frac{W}{SC_L} \tag{A.415}$$

This assumes that $\cos\gamma \simeq 1$ which is appropriate for the extremely small climb angles ocurring during a typical cruise-climb segment. With M and C_L held at their prescribed cruise values, this then gives the atmospheric pressure as a function of weight.

$$p \;=\; \frac{2}{\gamma M^2\, S\, C_L}\, W \tag{A.416}$$

$$\frac{dp}{dW} \;=\; \frac{p}{W} \tag{A.417}$$

The very small change in W_{buoy} over the cruise-climb is neglected here. Using the atmospheric hydrostatic pressure gradient $dp/dh = -\rho g$, and the fuel-burn weight gradient (A.409), equation (A.417) is used to explicitly obtain the small climb angle during the cruise.

$$\gamma \;\simeq\; \tan\gamma \;=\; \frac{dh}{dR} \;=\; \frac{dh}{dp}\frac{dp}{dW}\frac{dW}{dR} \tag{A.418}$$

$$=\; \left[-\frac{1}{\rho g}\right]\left[\frac{p}{W}\right]\left[-W\frac{TSFC'}{V}\left(\frac{C_D'}{C_L}+\gamma\right)\right] \tag{A.419}$$

$$\gamma_{\mathrm{CR}} \;=\; \left(\frac{C_D'}{C_L}\frac{p\,TSFC'}{\rho g V - p\,TSFC'}\right)_c \tag{A.420}$$

With the calculated cruise-climb angle γ_{CR}, the prescribed descent angle γ_{DE}, and the total cruise+descent remaining range $R_{\mathrm{total}} - R_c$, the end-of-cruise range and altitude is the intersection of the straight cruise-climb and descent paths, calculated as follows.

$$R_d \;=\; R_c \;+\; \frac{h_e - h_c - \gamma_{\mathrm{DE}}(R_{\mathrm{total}} - R_c)}{\gamma_{\mathrm{CR}} - \gamma_{\mathrm{DE}}} \tag{A.421}$$

$$h_d \;=\; h_c \;+\; \gamma_{\mathrm{CR}}(R_d - R_c) \tag{A.422}$$

Cruise-Climb

Because the cruise-climb segment proceeds at a fixed Mach number, the integrand in equation (A.414) can be assumed to be constant and equal to its value at start of cruise, so that an analytic integration is possible. The result is of course a form of the Breguet equation.

$$\frac{W_d}{W_c} \;=\; \exp\left[-\left(\frac{F'}{W}\frac{TSFC'}{V}\right)_c (R_d - R_c)\right] \tag{A.423}$$

$$t_d \;=\; t_c \;+\; \frac{R_d - R_c}{V} \tag{A.424}$$

59

Descent

The descent integration proceeds in much the same way as the climb, except that the descent angle is now prescribed, and the necessary thrust at each integration point i is computed from equation (A.413). The corresponding T_{t4} and all the other engine operating variables are the calculated via the engine model run in prescribed-thrust off-design mode 3.

$$F_e' = \frac{W}{n_{\text{eng}}} \left(\sin \gamma_{\text{DE}} + \frac{C_D'}{C_L} \cos \gamma_{\text{DE}} \right) \qquad (A.425)$$

$$\{T_{t_4} ; \mathit{TSFC}', \mathit{OPR}, \mathit{BPR}...\} = \mathcal{F}_{\text{eng3}}(F_e', A_2, A_5...; M_\infty, p_\infty, T_\infty, K_{\text{inl}}...) \qquad (A.426)$$

The end result of the integration is the final weight W_e and flight time t_e.

A.2.16   Mission fuel

From the final landing weight W_e, the fuel burn and takeoff fuel weight can then be obtained.

$$W_{\text{burn}} = W_b - W_e \qquad (A.427)$$

$$W_{\text{fuel}} = W_{\text{burn}} (1 + f_{\text{reserve}}) \qquad (A.428)$$

$$f_{\text{fuel}} = \frac{W_{\text{fuel}}}{W_{\text{MTO}}} \qquad (A.429)$$

Appendix B

Turbofan Sizing and Analysis with Variable $c_p(T)$

B.1 Summary

The turbofan model described here is used for two purposes:
1) Sizing of a turbofan engine to obtain a specified thrust at design conditions, and
2) Calculations for a given engine at off-design conditions, with a specified thrust or burner outlet temperature.

It is largely based on the formulation of Kerrebrock [11], with a number of modifications. Turbine cooling flow which bypasses the combustor is introduced, and a multi-constituent gas model with variable $c_{p(T)}$ is used for all the flowpath calculations.

B.2 Nomenclature

A	flowpath area
a	speed of sound ($= \sqrt{TRc_p/(c_p - R)}$)
F	thrust force
f	fuel mass flow fraction ($= \dot{m}_{\text{fuel}}/\dot{m}_{\text{core}}$)
M	Mach number ($= u/a$)
$\bar{m}$	component corrected mass flow ($= \dot{m}\sqrt{T_t/T_{\text{ref}}}/(p_t/p_{\text{ref}})$)
$\bar{N}$	component corrected rotation speed ($= N/\sqrt{T_t/T_{\text{ref}}}$)
h, h_t	static and total complete enthalpy
p, p_t	static and total pressure
T, T_t	static and total temperature
u	velocity
α	bypass ratio ($= \dot{m}_{\text{fan}}/\dot{m}_{\text{core}}$)
α_c	turbine-cooling bypass ratio ($= \dot{m}_{\text{cool}}/\dot{m}_{\text{core}}$)
$\Delta h_{()}$	total enthalpy jump across component ()
$\pi_{()}$	total pressure ratio across component ()
$\eta_{\text{pol}_{()}}$	polytropic efficiency of component ()
$\eta_{()}$	overall total-to-total efficiency of component ()
$c_{p_i(T)}$	specific heat of gas constituent i
$h_{i(T)}$	complete enthalpy of gas constituent i
$\sigma_{i(T)}$	entropy-complement function of gas constituent i ($= \int (c_{p_i}/T)dT$)
R_i	ideal-gas constant of constituent i
$\alpha_i, \beta_i, \lambda_i$	constituent i mass fractions for air, fuel vapor, combustion product
$(\ )_{\text{f}}$	fan quantity
$(\ )_{\text{lc}}$	low pressure compressor (LPC) quantity
$(\ )_{\text{hc}}$	high pressure compressor (HPC) quantity
$(\ )_{\text{ht}}$	high pressure turbine (HPT) quantity
$(\ )_{\text{lt}}$	low pressure turbine (LPT) quantity
$(\ )_{\text{fn}}$	fan nozzle quantity
$(\ )_{\text{tn}}$	turbine nozzle quantity
$(\ )_{\text{...D}}$	design-case quantity

The constituent property values and the mass fractions will also be denoted as a vector, e.g.

$$
\begin{aligned}
h_i &= \vec{h} \\
\alpha_i &= \vec{\alpha} \\
&\vdots
\end{aligned}
$$

B.2.1 Gas mixture properties

Overall gas-mixture functions $c_{p(T)}$, $h_{(T)}$, $\sigma_{(T)}$, R are computed using the individual $c_{p_i(T)}$, $h_{i(T)}$, $\sigma_{i(T)}$, R_i constituent functions and the mass fractions α_i, β_i, λ_i. For air we have the following.

$$
c_{p(T)} = \sum_i \alpha_i\, c_{p_i(T)} = \vec{\alpha} \cdot \vec{c}_{p(T)} \tag{B.1}
$$
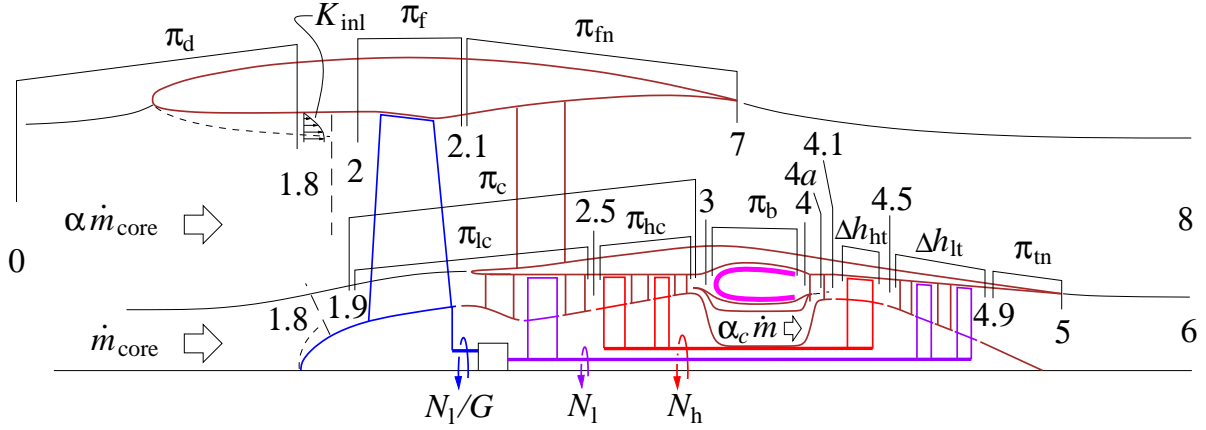
Figure B.1: Engine station numbers, total-pressure ratios, mass flows, and spool speeds.

$$h_{(T)} \;=\; \sum_i \alpha_i \, h_{i(T)} \;=\; \vec{\alpha} \cdot \vec{h}_{(T)} \tag{B.2}$$

$$\sigma_{(T)} \;=\; \sum_i \alpha_i \, \sigma_{i(T)} \;=\; \vec{\alpha} \cdot \vec{\sigma}_{(T)} \tag{B.3}$$

$$R \;=\; \sum_i \alpha_i \, R_i \;=\; \vec{\alpha} \cdot \vec{R} \tag{B.4}$$

For fuel vapor β_i is used instead of α_i, and for the combustion products λ_i is used instead of α_i. The combustion relations and the calculation of λ_i are described in detail in the related document "Thermally-Perfect Gas Calculations".

B.3 Pressure, Temperature, Enthalpy Calculations

B.3.1 Relations to be replaced

The standard constant–c_p equations connecting a baseline state T_o, h_o, p_o to some other state T, h, p are the familiar caloric and isentropic relations, with the latter possibly having a polytropic efficiency η_{pol} included to account for a non-isentropic process.

$$\Delta h \;\equiv\; h - h_o \;=\; c_p \, (T - T_o) \tag{B.5}$$

$$\pi \;\equiv\; \frac{p}{p_o} \;=\; \left(\frac{T}{T_o}\right)^{\eta_{\mathrm{pol}}^{\pm 1} c_p / R} \tag{B.6}$$

The $+1/-1$ exponent on η_{pol} indicates a compression/expansion process, respectively. For a gas or gas mixture with a temperature-dependent $c_{p(T)}$, these relations are no longer valid, and will not be used here. The replacement relations described in the subsequent sections will be used instead.

The function Jacobian derivatives $\partial(\text{output})/\partial(\text{input})$ will also be derived for each case. These are required for off-design performance calculations via the Newton method.

B.3.2 Enthalpy prescribed

Occasionally it is necessary to obtain the temperature from a specified enthalpy. This is performed by simply inverting the $h_{(T)}$ function via the Newton method.

$$\text{initial guess:} \quad T = T_{\text{guess}} \quad \text{(e.g. standard temperature)} \tag{B.7}$$

$$\text{solve:} \quad h_{(T)} - h_{\text{spec}} = 0 \quad \rightarrow \quad T \tag{B.8}$$

The overall calculation will be denoted by

$$T = \mathcal{F}_T\left(\vec{\alpha}, h_{\text{spec}}\,; T_{\text{guess}}\right) \tag{B.9}$$

where the $\vec{\alpha}$ argument is required to evaluate the $h_{(T)}$ function in (B.8), via (B.2).

The derivative of the calculated temperature is simply the inverse of the specific heat.

$$\frac{dT}{dh} = \frac{1}{c_{p(T)}} \tag{B.10}$$

B.3.3 Pressure ratio prescribed

For prescribed $p_o, T_o, \pi, \eta_{\text{pol}}$, the new state p, T, h after a compression/expansion process is computed as follows.

$$\sigma_o = \sigma_{(T_o)} \tag{B.11}$$

$$c_{p_o} = c_{p(T_o)} \tag{B.12}$$

$$\text{initial guess:} \quad T = T_o\,\pi^{R_o/(c_{p_o}\,\eta_{\text{pol}}{}^{\pm 1})} \tag{B.13}$$

$$\text{solve:} \quad \frac{\sigma_{(T)} - \sigma_o}{R} - \frac{\ln \pi}{\eta_{\text{pol}}{}^{\pm 1}} = 0 \quad \rightarrow \quad T \tag{B.14}$$

$$p = p_o\,\pi \tag{B.15}$$

$$h = h_{(T)} \tag{B.16}$$

The solution for T is via Newton iteration. The overall calculation will be denoted by

$$\{p, T, h\} = \mathcal{F}_p\left(\vec{\alpha}, p_o, T_o, \pi, \eta_{\text{pol}}{}^{\pm 1}\right) \tag{B.17}$$

The function Jacobian derivatives $\partial\{p, T, h\}/\partial\{p_o, T_o, \pi\}$ are obtained by first implicitly differentiating (B.14) with respect to the specified p_o, T_o, π.

$$\frac{1}{R}\frac{d\sigma}{dT}\frac{\partial T}{\partial p_o} = 0 \tag{B.18}$$

$$\frac{1}{R}\left(\frac{d\sigma}{dT}\frac{\partial T}{\partial T_o} - \frac{d\sigma_o}{dT_o}\right) = 0 \tag{B.19}$$

$$\frac{1}{R}\frac{d\sigma}{dT}\frac{\partial T}{\partial \pi} - \frac{1}{\eta_{\text{pol}}{}^{\pm 1}}\frac{1}{\pi} = 0 \tag{B.20}$$

Using $d\sigma/dT = c_{p(T)}/T$ these then give $\partial T/\partial(\ )$, and also the remaining p and h derivatives via the chain rule.

$$\frac{\partial T}{\partial p_o} = 0 \tag{B.21}$$

$$\frac{\partial T}{\partial T_o} = \frac{c_{p_o}}{T_o} \frac{T}{c_{p(T)}} \tag{B.22}$$

$$\frac{\partial T}{\partial \pi} = \frac{R}{\pi\,\eta_{\mathrm{pol}}{}^{\pm 1}} \frac{T}{c_{p(T)}} \tag{B.23}$$

$$\frac{\partial p}{\partial p_o} = \pi \tag{B.24}$$

$$\frac{\partial p}{\partial T_o} = 0 \tag{B.25}$$

$$\frac{\partial p}{\partial \pi} = p_o \tag{B.26}$$

$$\frac{\partial h}{\partial p_o} = \frac{dh}{dT}\frac{\partial T}{\partial p_o} = 0 \tag{B.27}$$

$$\frac{\partial h}{\partial T_o} = \frac{dh}{dT}\frac{\partial T}{\partial T_o} = c_{p(T)} \frac{c_{p_o}}{T_o} \frac{T}{c_{p(T)}} = \frac{c_{p_o}}{T_o} T \tag{B.28}$$

$$\frac{\partial h}{\partial \pi} = \frac{dh}{dT}\frac{\partial T}{\partial \pi} = c_{p(T)} \frac{R}{\pi} \frac{T}{c_{p(T)}} = \frac{R}{\pi\,\eta_{\mathrm{pol}}{}^{\pm 1}} T \tag{B.29}$$

B.3.4 Pure loss prescribed

A pure loss with no work or heat addition is the limiting case of a prescribed pressure ratio $\pi < 1$, with $\eta_{\mathrm{pol}} = 0$. The relations above then greatly simplify to the following.

$$p = p_o\,\pi \tag{B.30}$$
$$T = T_o \tag{B.31}$$
$$h = h_o \tag{B.32}$$

B.3.5 Enthalpy difference prescribed

For prescribed $p_o, T_o, \Delta h, \eta_{\mathrm{pol}}$, the new state p, T, h after a compression/expansion process is computed as follows.

$$h_o = h_{(T_o)} \tag{B.33}$$
$$\sigma_o = \sigma_{(T_o)} \tag{B.34}$$
$$c_{p_o} = c_{p(T_o)} \tag{B.35}$$
$$\text{initial guess:} \quad T = T_o + \Delta h/c_{p_o} \tag{B.36}$$
$$\text{solve:} \quad h_{(T)} - h_o - \Delta h = 0 \quad \rightarrow \quad T \tag{B.37}$$
$$p = p_o \exp\left(\eta_{\mathrm{pol}}{}^{\pm 1} \frac{\sigma_{(T)} - \sigma_o}{R}\right) \tag{B.38}$$
$$h = h_{(T)} \tag{B.39}$$

The solution for T is via Newton iteration. The overall calculation will be denoted by

$$\{p, T, h\} \;=\; \mathcal{F}_h\left(\vec{\alpha}, p_o, T_o, \Delta h, \eta_{\mathrm{pol}}^{\pm 1}\right) \tag{B.40}$$

The function Jacobian derivatives $\partial\{p, T, h\}/\partial\{p_o, T_o, \Delta h\}$ are obtained by first implicitly differentiating (B.37) with respect to the specified $p_o, T_o, \Delta h$.

$$\frac{dh}{dT}\frac{\partial T}{\partial p_o} \;=\; 0 \tag{B.41}$$

$$\frac{dh}{dT}\frac{\partial T}{\partial T_o} - \frac{dh_o}{dT_o} \;=\; 0 \tag{B.42}$$

$$\frac{dh}{dT}\frac{\partial T}{\partial \Delta h} - 1 \;=\; 0 \tag{B.43}$$

Using $dh/dT = c_{p(T)}$ these then give $\partial T/\partial(\ )$, and also the remaining p and h derivatives via the chain rule.

$$\frac{\partial T}{\partial p_o} \;=\; 0 \tag{B.44}$$

$$\frac{\partial T}{\partial T_o} \;=\; \frac{c_{p_o}}{c_{p(T)}} \tag{B.45}$$

$$\frac{\partial T}{\partial \Delta h} \;=\; \frac{1}{c_{p(T)}} \tag{B.46}$$

$$\frac{\partial p}{\partial p_o} \;=\; \frac{p}{p_o} + p\,\frac{\eta_{\mathrm{pol}}^{\pm 1}}{R}\left(\frac{d\sigma}{dT}\frac{\partial T}{\partial p_o}\right) \;=\; \frac{p}{p_o} \tag{B.47}$$

$$\frac{\partial p}{\partial T_o} \;=\; p\,\frac{\eta_{\mathrm{pol}}^{\pm 1}}{R}\left(\frac{d\sigma}{dT}\frac{\partial T}{\partial T_o} - \frac{d\sigma_o}{dT_o}\right) \;=\; p\,\frac{\eta_{\mathrm{pol}}^{\pm 1}}{R}\left(\frac{c_{p(T)}}{T} - \frac{c_{p_o}}{T_o}\right) \tag{B.48}$$

$$\frac{\partial p}{\partial \Delta h} \;=\; p\,\frac{\eta_{\mathrm{pol}}^{\pm 1}}{R}\frac{d\sigma}{dT}\frac{\partial T}{\partial \Delta h} \;=\; p\,\frac{\eta_{\mathrm{pol}}^{\pm 1}}{R}\frac{1}{T} \tag{B.49}$$

$$\frac{\partial h}{\partial p_o} \;=\; \frac{dh}{dT}\frac{\partial T}{\partial p_o} \;=\; 0 \tag{B.50}$$

$$\frac{\partial h}{\partial T_o} \;=\; \frac{dh}{dT}\frac{\partial T}{\partial T_o} \;=\; c_{p(T)}\frac{c_{p_o}}{c_{p(T)}} \;=\; c_{p_o} \tag{B.51}$$

$$\frac{\partial h}{\partial \Delta h} \;=\; \frac{dh}{dT}\frac{\partial T}{\partial \Delta h} \;=\; c_{p(T)}\frac{1}{c_{p(T)}} \;=\; 1 \tag{B.52}$$

B.3.6 Composition change prescribed

A composition change, such as due to combustion, is specified by the following mass fractions and input properties:

α_i constituent i mass fraction for air
β_i constituent i mass fraction for fuel vapor (assumed all burned)
γ_i constituent i mass fraction change in air due to combustion
T_o air temperature before combustion
T_{f} fuel vapor temperature before combustion
T temperature after combustion

The following quantities are computed:

f fuel/air mass ratio

λ_i constituent i mass fraction for combustion products

$$\vec{h}_o \;=\; h_{i(T_o)} \tag{B.53}$$

$$\vec{h} \;=\; h_{i(T)} \tag{B.54}$$

$$\vec{h}_{\mathrm{f}} \;=\; h_{i(T_{\mathrm{f}})} \tag{B.55}$$

The enthalpy balance across the combustor is

$$\dot{m}\,\vec{\alpha}\cdot\vec{h}_o \;+\; \dot{m}_{\mathrm{fuel}}\,\vec{\beta}\cdot\vec{h}_{\mathrm{f}} \;=\; \dot{m}\,\vec{\alpha}\cdot\vec{h} \;+\; \dot{m}_{\mathrm{fuel}}\,\vec{\gamma}\cdot\vec{h} \tag{B.56}$$

which can be solved for the fuel/air mass ratio.

$$f \;\equiv\; \frac{\dot{m}_{\mathrm{fuel}}}{\dot{m}_{\mathrm{core}}} \;=\; \frac{\vec{\alpha}\cdot\vec{h} - \vec{\alpha}\cdot\vec{h}_o}{\vec{\beta}\cdot\vec{h}_{\mathrm{f}} - \vec{\gamma}\cdot\vec{h}} \tag{B.57}$$

The mass fraction vector $\vec{\lambda}$ of the combustion products is obtained from the mass balance across the combustor.

$$\left[\,\dot{m}_{\mathrm{core}} + \dot{m}_{\mathrm{fuel}}\,\right]\vec{\lambda} \;=\; \dot{m}_{\mathrm{core}}\,\vec{\alpha} \;+\; \dot{m}_{\mathrm{fuel}}\,\vec{\gamma} \tag{B.58}$$

$$\vec{\lambda} \;=\; \frac{\vec{\alpha} + f\vec{\gamma}}{1+f} \tag{B.59}$$

The overall combustion-change calculation will be denoted by

$$\left\{f,\vec{\lambda}\right\} \;=\; \mathcal{F}_b\left(\vec{\alpha},\vec{\beta},\vec{\gamma},T_o,T_{\mathrm{f}},T\right) \tag{B.60}$$

The Jacobian derivatives of f and $\vec{\lambda}$ are obtained by direct differentiation of their definitions (B.57) and (B.59).

$$\frac{\partial f}{\partial T_o} \;=\; -\frac{\vec{\alpha}\cdot\vec{c}_{p_o}}{\vec{\beta}\cdot\vec{h}_{\mathrm{f}} - \vec{\gamma}\cdot\vec{h}} \tag{B.61}$$

$$\frac{\partial f}{\partial T_f} \;=\; -f\,\frac{\vec{\beta}\cdot\vec{c}_{p_{\mathrm{f}}}}{\vec{\beta}\cdot\vec{h}_{\mathrm{f}} - \vec{\gamma}\cdot\vec{h}} \tag{B.62}$$

$$\frac{\partial f}{\partial T} \;=\; \frac{\vec{\alpha}\cdot\vec{c}_p}{\vec{\beta}\cdot\vec{h}_{\mathrm{f}} - \vec{\gamma}\cdot\vec{h}} \tag{B.63}$$

$$\frac{\partial\vec{\lambda}}{\partial f} \;=\; \frac{\vec{\gamma} - \vec{\lambda}}{1+f} \tag{B.64}$$

$$\frac{\partial\vec{\lambda}}{\partial T_o} \;=\; \frac{\partial\vec{\lambda}}{\partial f}\frac{\partial f}{\partial T_o} \tag{B.65}$$

$$\frac{\partial\vec{\lambda}}{\partial T_{\mathrm{f}}} \;=\; \frac{\partial\vec{\lambda}}{\partial f}\frac{\partial f}{\partial T_{\mathrm{f}}} \tag{B.66}$$

$$\frac{\partial\vec{\lambda}}{\partial T} \;=\; \frac{\partial\vec{\lambda}}{\partial f}\frac{\partial f}{\partial T} \tag{B.67}$$

B.3.7 Mixing

Mixing between two streams is a simplified version of the combustion case above. No chemical reaction is assumed, so that $\vec{\gamma} = 0$. However, in general the two streams will have two different chemical compositions specified by their mass fraction vectors $\vec{\lambda}_a$ and $\vec{\lambda}_b$, two different temperatures T_a and T_b, and two different enthalpies $\vec{h}_a = h_{i(T_a)}$ and $\vec{h}_b = h_{i(T_b)}$. The species mass flow balance gives the composition mass fraction vector $\vec{\lambda}$ of the mixed gas, in terms of the convenient relative mass fractions f_a, f_b of the two streams.

$$f_a = \frac{\dot{m}_a}{\dot{m}_a + \dot{m}_b} \tag{B.68}$$

$$f_b = \frac{\dot{m}_b}{\dot{m}_a + \dot{m}_b} \tag{B.69}$$

$$\vec{\lambda} = f_a \vec{\lambda}_a + f_b \vec{\lambda}_b \tag{B.70}$$

Without any chemical reaction change term, the mixed enthalpy is

$$\vec{\lambda} \cdot \vec{h}_{(T)} \equiv h_{\mathrm{mix}} = f_a \vec{\lambda}_a \cdot \vec{h}_a + f_b \vec{\lambda}_b \cdot \vec{h}_b \tag{B.71}$$

which can be numerically inverted for the mixed temperature T, using the previously-defined $\mathcal{F}_T$ function.

$$T_{\mathrm{guess}} = f_a T_a + f_b T_b \tag{B.72}$$

$$T = \mathcal{F}_T \left(\vec{\lambda}, h_{\mathrm{mix}} \, ; \, T_{\mathrm{guess}} \right) \tag{B.73}$$

B.3.8 Mach number prescribed

For prescribed $p_o, T_o, M_o, M, \eta_{\mathrm{pol}}$, the new adiabatic-change state p, T, h corresponding to M is computed as follows.

$$\sigma_o = \sigma_{(T_o)} \tag{B.74}$$

$$c_{p_o} = c_{p(T_o)} \tag{B.75}$$

$$h_o = h_{(T_o)} \tag{B.76}$$

$$u_o^2 = M_o^2 \frac{c_{p_o} R_o}{c_{p_o} - R_o} T_o \tag{B.77}$$

$$\text{initial guess:} \quad T = T_o \frac{1 + \frac{R_o}{2(c_{p_o} - R_o)} M_o^2}{1 + \frac{R_o}{2(c_{p_o} - R_o)} M^2} \tag{B.78}$$

$$\text{solve:} \quad h_{(T)} + \frac{1}{2} M^2 \frac{c_{p(T)} R}{c_{p(T)} - R} T - h_o - \frac{1}{2} u_o^2 = 0 \quad \rightarrow \quad T \tag{B.79}$$

$$p = p_o \exp\left(\eta_{\mathrm{pol}}^{\pm 1} \frac{\sigma_{(T)} - \sigma_o}{R} \right) \tag{B.80}$$

$$h = h_{(T)} \tag{B.81}$$

The solution for T is via Newton iteration. The overall calculation will be denoted by

$$\{p, T, h\} = \mathcal{F}_M \left(\vec{\alpha}, p_o, T_o, M_o, M, \eta_{\mathrm{pol}}^{\pm 1} \right) \tag{B.82}$$

The convenient u^2 and u_o^2 derivatives are defined next.

$$u^2 \;=\; M^2 \frac{c_{p(T)} R}{c_{p(T)} - R} T \tag{B.83}$$

$$\frac{\partial u^2}{\partial M} \;=\; 2M \frac{c_{p(T)} R}{c_{p(T)} - R} T \tag{B.84}$$

$$\frac{\partial u^2}{\partial T} \;=\; M^2 \frac{R}{c_{p(T)} - R} \left(c_{p(T)} - \frac{R}{c_{p(T)} - R} c'_{p(T)} T \right) \tag{B.85}$$

$$\frac{\partial u_o^2}{\partial M_o} \;=\; 2M_o \frac{c_{p_o} R_o}{c_{p_o} - R_o} T_o \tag{B.86}$$

$$\frac{\partial u_o^2}{\partial T_o} \;=\; M_o^2 \frac{R_o}{c_{p_o} - R_o} \left(c_{p_o} - \frac{R_o}{c_{p_o} - R_o} c'_{p_o} T_o \right) \tag{B.87}$$

The function Jacobian derivatives $\partial \{p, T, h\} / \partial \{p_o, T_o, M_o, M\}$ are then obtained by first implicitly differentiating (B.79) with respect to the specified p_o, T_o, M_o, M.

$$\frac{dh}{dT} \frac{\partial T}{\partial p_o} + \frac{1}{2} \frac{\partial u^2}{\partial T} \frac{\partial T}{\partial p_o} \;=\; 0 \tag{B.88}$$

$$\frac{dh}{dT} \frac{\partial T}{\partial T_o} + \frac{1}{2} \frac{\partial u^2}{\partial T} \frac{\partial T}{\partial T_o} - \frac{\partial h_o}{\partial T_o} - \frac{\partial u_o^2}{\partial T_o} \;=\; 0 \tag{B.89}$$

$$\frac{dh}{dT} \frac{\partial T}{\partial M_o} + \frac{1}{2} \frac{\partial u^2}{\partial T} \frac{\partial T}{\partial M_o} - \frac{\partial u_o^2}{\partial M_o} \;=\; 0 \tag{B.90}$$

$$\frac{dh}{dT} \frac{\partial T}{\partial M} + \frac{1}{2} \frac{\partial u^2}{\partial T} \frac{\partial T}{\partial M} \;=\; 0 \tag{B.91}$$

Using $dh/dT = c_{p(T)}$ these then give $\partial T/\partial(\ )$, and also the remaining p and h derivatives via the chain rule.

$$\frac{\partial T}{\partial p_o} \;=\; 0 \tag{B.92}$$

$$\frac{\partial T}{\partial T_o} \;=\; \frac{c_{p_o}}{c_{p(T)}} \tag{B.93}$$

$$\frac{\partial T}{\partial \Delta h} \;=\; \frac{1}{c_{p(T)}} \tag{B.94}$$

$$\frac{\partial p}{\partial p_o} \;=\; \frac{p}{p_o} + p \frac{\eta_{\text{pol}}{}^{\pm 1}}{R} \left(\frac{d\sigma}{dT} \frac{\partial T}{\partial p_o} \right) \;=\; \frac{p}{p_o} \tag{B.95}$$

$$\frac{\partial p}{\partial T_o} \;=\; p \frac{\eta_{\text{pol}}{}^{\pm 1}}{R} \left(\frac{d\sigma}{dT} \frac{\partial T}{\partial T_o} - \frac{d\sigma_o}{dT_o} \right) \;=\; p \frac{\eta_{\text{pol}}{}^{\pm 1}}{R} \left(\frac{c_{p(T)}}{T} - \frac{c_{p_o}}{T_o} \right) \tag{B.96}$$

$$\frac{\partial p}{\partial \Delta h} \;=\; p \frac{\eta_{\text{pol}}{}^{\pm 1}}{R} \frac{d\sigma}{dT} \frac{\partial T}{\partial \Delta h} \;=\; p \frac{\eta_{\text{pol}}{}^{\pm 1}}{R} \frac{1}{T} \tag{B.97}$$

$$\frac{\partial h}{\partial p_o} \;=\; \frac{dh}{dT} \frac{\partial T}{\partial p_o} \;=\; 0 \tag{B.98}$$

$$\frac{\partial h}{\partial T_o} \;=\; \frac{dh}{dT} \frac{\partial T}{\partial T_o} \;=\; c_{p(T)} \frac{c_{p_o}}{c_{p(T)}} \;=\; c_{p_o} \tag{B.99}$$

$$\frac{\partial h}{\partial \Delta h} \;=\; \frac{dh}{dT} \frac{\partial T}{\partial \Delta h} \;=\; c_{p(T)} \frac{1}{c_{p(T)}} \;=\; 1 \tag{B.100}$$

69

B.3.9 Mass flux prescribed

It is occasionally useful to calculate the static quantities p, T, h corresponding to a specified stagnation state p_o, T_o, h_o, and a specified mass flux $\rho u = \dot{m}/A \equiv m'$. This is computed as follows, starting from some given initial guess specified by the Mach number M_{guess}, which also selects the subsonic or supersonic branch.

$$\sigma_o = \sigma_{(T_o)} \tag{B.101}$$

$$h_o = h_{(T_o)} \tag{B.102}$$

$$\text{initial guess:} \quad T = T_o / \left(1 + \frac{R_o}{2(c_{p_o} - R_o)} M_{\text{guess}}^2 \right) \tag{B.103}$$

$$\text{solve:} \quad \left(\frac{p_{(T)}}{RT} \right)^2 2 \left(h_o - h_{(T)} \right) - (m')^2 = 0 \quad \rightarrow \quad T \tag{B.104}$$

$$p = p_o \exp \left(\frac{\sigma_{(T)} - \sigma_o}{R} \right) \tag{B.105}$$

$$h = h_{(T)} \tag{B.106}$$

The solution for T is via Newton iteration. The overall calculation will be denoted by

$$\{p, T, h\} = \mathcal{F}_m \left(\vec{\alpha}, p_o, T_o, m' ; M_{\text{guess}} \right) \tag{B.107}$$

This function's Jacobian derivatives can be calculated by the same procedures used for the other functions.

B.4 Turbofan Component Calculations

Most of the calculations described in this section are common to both the design and the off-design cases. The design case requires only a single calculation pass, with the mass flow and component dimensions determined only at the end. In contrast, the off-design case requires multiple Newton-iteration passes to converge the component pressure ratios and mass flows.

B.4.1 Design case inputs

The following quantities are assumed to be known for the design-case calculation.

$$
\begin{array}{ll}
T_0, p_0 & \text{atmospheric properties} \\
M_0 & \text{flight Mach number} \\
T_{t4} & \text{burner exit total temperature} \\
\pi_{\mathrm{f}} & \text{fan pressure ratio} \\
\pi_{\mathrm{lc}} & \text{LPC pressure ratio} \\
\pi_{\mathrm{hc}} & \text{HPC pressure ratio} \\
\alpha & \text{fan bypass ratio} \\
\pi_{\mathrm{d}} & \text{diffuser pressure ratio} \\
\pi_{\mathrm{b}} & \text{burner pressure ratio} \\
\pi_{\mathrm{fn}} & \text{fan duct loss pressure ratio} \\
M_{4a} & \text{representative Mach number at start of HPT cooling-flow mixing zone} \\
T_{\mathrm{m}} & \text{HPT design metal temperature (if } \alpha_c \text{ is to be sized)} \\
\alpha_c & \text{cooling-flow bypass ratio (if previously sized)}
\end{array}
$$

B.4.2 Freestream properties

From the specified freestream static temperature, pressure, and Mach number, T_0, p_0, M_0, we can obtain the freesteam speed of sound and velocity.

$$
c_{p_0} \;=\; c_{p(T_0)} \tag{B.108}
$$

$$
a_0 \;=\; \sqrt{\dfrac{c_{p_0}}{c_{p_0} - R_0} \, R_0 T_0} \tag{B.109}
$$

$$
u_0 \;=\; M_0 \, a_0 \tag{B.110}
$$

B.4.3 Freestream-stagnation properties

The freestream stagnation quantities are computed using the specified enthalpy change procedure, with $\eta_{\mathrm{pol}} = 1$.

$$
\Delta h \;=\; \tfrac{1}{2} \, u_0^2 \tag{B.111}
$$

$$
\{p_{t0}, T_{t0}, h_{t0}\} \;=\; \mathcal{F}_h \left(\vec{\alpha}, p_0, T_0, \Delta h, 1 \right) \tag{B.112}
$$

The standard fixed-c_p relations could also be used here, since the stagnation-static temperature difference is sufficiently small for any non-hypersonic flight Mach number.

B.4.4 Fan and compressor quantities

Inlet conditions

The stagnation conditions $()_{t1.8}$ in the inlet inviscid flow (excluding the inlet BLs) are computed as the pure-loss case with a diffuser total/total pressure ratio π_{d}.

$$
p_{t\,1.8} \;=\; p_{t0} \, \pi_{\mathrm{d}} \tag{B.113}
$$

$$
T_{t\,1.8} \;=\; T_{t0} \tag{B.114}
$$

$$
h_{t\,1.8} \;=\; h_{t0} \tag{B.115}
$$

Normally $\pi_{\mathrm{d}} \simeq 1$, unless an inlet screen or other losses are present upstream.

Fan and LPC inlet conditions

The inlet BL is characterized by a kinetic energy defect K_{inl}.

$$K_{\mathrm{inl}} = \iint \frac{1}{2}(u_e^2 - u^2)\,\rho u\,dA \tag{B.116}$$

A low-speed approximation for the equivalent reduced total pressure $p_{t\,2}$ is obtained by a simple volume-flow average of p_t.

$$\dot{\mathcal{V}}_{\mathrm{inl}} \equiv \iint_{\mathrm{inl}} u\,dA \tag{B.117}$$

$$(p_{t\,2} - p_{t\,1.8})\,\dot{\mathcal{V}}_{\mathrm{inl}} = \iint_{\mathrm{inl}} (p_t - p_{t\,1.8})\,u\,dA$$

$$\simeq \iint_{\mathrm{inl}} \left(p + \tfrac{1}{2}\rho u^2 - p_e + \tfrac{1}{2}\rho_e u_e^2\right) u\,dA$$

$$= -\tfrac{1}{2}\rho_e u_e^3 \left(\Theta^* + \Delta^{**}\right)_{\mathrm{inl}} \simeq -\tfrac{1}{2}\rho_e u_e^3 \Theta_{\mathrm{inl}}^* = -K_{\mathrm{inl}} \tag{B.118}$$

$$p_{t\,2} = p_{t\,1.8} - \frac{K_{\mathrm{inl}}}{\dot{\mathcal{V}}_{\mathrm{inl}}} \tag{B.119}$$

$$T_{t\,2} = T_{t\,1.8} \tag{B.120}$$

$$h_{t\,2} = h_{t\,1.8} \tag{B.121}$$

A similar calculation is carried out for the LPC inlet state $()_{t\,1.9}$. Possible limiting cases are:

$$()_{t\,1.9} = \begin{cases} ()_{t\,1.8} & , \quad \text{(no significant BL ingestion)} \\ ()_{t\,2} & , \quad \text{(nacelle BL fills inlet flow)} \end{cases} \tag{B.122}$$

Fan exit conditions

The fan exit stagnation conditions are computed from the fan pressure ratio π_{f}. The polytropic efficiency is computed first using the appropriate assumed fan efficiency map.

$$\eta_{\mathrm{pol_f}} = \begin{cases} \mathcal{F}_\eta(\pi_{\mathrm{f}},\ \pi_{\mathrm{f}},\ 1,\ 1) & , \quad \text{(design case)} \\ \mathcal{F}_\eta(\pi_{\mathrm{f}},\ \pi_{\mathrm{fD}},\ \bar{m}_{\mathrm{f}}, \bar{m}_{\mathrm{fD}}) & , \quad \text{(off-design case)} \end{cases} \tag{B.123}$$

$$\{p_{t\,2.1}, T_{t\,2.1}, h_{t\,2.1}\} = \mathcal{F}_p\left(\vec{\alpha}, p_{t\,2}, T_{t\,2}, \pi_{\mathrm{f}}, \eta_{\mathrm{pol_f}}\right) \tag{B.124}$$

Fan nozzle exit conditions

Fan duct and fan nozzle losses are represented by the total pressure-drop ratio π_{fn} with no total enthalpy change.

$$p_{t\,7} = p_{t\,2.1}\,\pi_{\mathrm{fn}} \tag{B.125}$$

$$T_{t\,7} = T_{t\,2.1} \tag{B.126}$$

$$h_{t\,7} = h_{t\,2.1} \tag{B.127}$$

LPC exit conditions

The LPC calculation is the same as for the fan. But the inlet state can be either 2 or 1.8, depending on whether the LPC does or does not ingest the inlet BL fluid.

$$\eta_{\mathrm{pol_{lc}}} = \begin{cases} \mathcal{F}_\eta(\pi_{\mathrm{lc}},\ \pi_{\mathrm{lc}}\ ,\ 1\ ,\ 1\ ) & ,\quad \text{(design case)} \\ \mathcal{F}_\eta(\pi_{\mathrm{lc}}, \pi_{\mathrm{lcD}}\ ,\ \bar{m}_{\mathrm{lc}}, \bar{m}_{\mathrm{lcD}}) & ,\quad \text{(off-design case)} \end{cases} \tag{B.128}$$

$$\{p_{t\,2.5}, T_{t\,2.5}, h_{t\,2.5}\} = \mathcal{F}_p\left(\vec{\alpha}, p_{t\,1.9}, T_{t\,1.9}, \pi_{\mathrm{lc}}, \eta_{\mathrm{pol_{lc}}}\right) \tag{B.129}$$

HPC exit conditions

The HPC calculation procedure is the same as for the LPC and fan, except that the 2.5 station quantities from the LPC calculation above are used for the HPC inlet.

$$\eta_{\mathrm{pol_{hc}}} = \begin{cases} \mathcal{F}_\eta(\pi_{\mathrm{hc}},\ \pi_{\mathrm{hc}}\ ,\ 1\ ,\ 1\ ) & ,\quad \text{(design case)} \\ \mathcal{F}_\eta(\pi_{\mathrm{hc}}, \pi_{\mathrm{hcD}}\ ,\ \bar{m}_{\mathrm{hc}}, \bar{m}_{\mathrm{hcD}}) & ,\quad \text{(off-design case)} \end{cases} \tag{B.130}$$

$$\{p_{t\,3}, T_{t\,3}, h_{t\,3}\} = \mathcal{F}_p\left(\vec{\alpha}, p_{t\,2.5}, T_{t\,2.5}, \pi_{\mathrm{hc}}, \eta_{\mathrm{pol_{hc}}}\right) \tag{B.131}$$

Fan and compressor efficiencies

The equivalent isentropic states and overall efficiencies can be computed for the fan and compressors out of interest, although these are not required for any subsequent calculations.

$$\{p_{t\,2.1}, (T_{t\,2.1})_{is}, (h_{t\,2.1})_{is}\} = \mathcal{F}_p\left(\vec{\alpha}, p_{t\,2}, T_{t\,2}, \pi_{\mathrm{f}}, 1\right) \tag{B.132}$$

$$\{p_{t\,2.5}, (T_{t\,2.5})_{is}, (h_{t\,2.5})_{is}\} = \mathcal{F}_p\left(\vec{\alpha}, p_{t\,1.9}, T_{t\,1.9}, \pi_{\mathrm{lc}}, 1\right) \tag{B.133}$$

$$\{p_{t\,3}, (T_{t\,3})_{is}, (h_{t\,3})_{is}\} = \mathcal{F}_p\left(\vec{\alpha}, p_{t\,2.5}, T_{t\,2.5}, \pi_{\mathrm{hc}}, 1\right) \tag{B.134}$$

$$\eta_{\mathrm{f}} = \frac{(h_{t\,2.1})_{is} - h_{t\,2}}{h_{t\,2.1} - h_{t\,2}} \tag{B.135}$$

$$\eta_{\mathrm{lc}} = \frac{(h_{t\,2.5})_{is} - h_{t\,1.9}}{h_{t\,2.5} - h_{t\,1.9}} \tag{B.136}$$

$$\eta_{\mathrm{hc}} = \frac{(h_{t\,3})_{is} - h_{t\,2.5}}{h_{t\,3} - h_{t\,2.5}} \tag{B.137}$$

B.4.5   Cooling Mass Flow or Metal Temperature Calculations

Cooling-flow calculations consist of either

1) Determination of cooling mass flow ratio (cooling sizing), or
2) Determination of metal temperature (cooling analysis).

It should be noted that the cooling sizing case 1) may be performed for any operating point, and not necessarily the engine-sizing design point. For example, an engine whose design sizing case is the cruise condition will typically have its cooling flow ratio sized at the off-design takeoff condition.

Cooling Mass Flow Ratio Sizing

For the cooling-sizing case, the cooling mass flow ratios ε_1, $\varepsilon_2 \ldots$ for the hot-section blade rows are determined to obtain required blade-row metal temperatures $T_{m_1}, T_{m_2} \ldots$ as described in the document "Film Cooling Flow Loss Model". The function has the form

$$\{\varepsilon_1, \varepsilon_2, \ldots\} \;=\; \mathcal{F}_\varepsilon\left(T_{t3}, T_{t4}, T_{m_1}, T_{m_2} \ldots ; M_{\text{exit}}, \Delta T_{\text{streak}}, St_A, \theta_f, \eta\right) \qquad \text{(B.138)}$$

where $M_{\text{exit}} \ldots \eta$ are the various parameters in the cooling model. The overall cooling mass flow is the sum of the individual blade-row cooling mass flows.

$$\alpha_c \;=\; \varepsilon_1 + \varepsilon_2 + \ldots \qquad \text{(B.139)}$$

Metal Temperature Calculation

In this case the individual blade-row cooling mass flow ratios $\varepsilon_1, \varepsilon_2 \ldots$ and and the overall cooling mass flow ratio α_c are assumed to be known. The blade-row metal temperatures can then be determined from the cooling model relations, which are now recast into the following form.

$$\{T_{m_1}, T_{m_2}, \ldots\} \;=\; \mathcal{F}_{T_m}\left(T_{t3}, T_{t4}, \varepsilon_1, \varepsilon_2 \ldots ; M_{\text{exit}}, \Delta T_{\text{streak}}, St_A, \theta_f, \eta\right) \qquad \text{(B.140)}$$

These metal temperatures are not required for any subsequent calculations.

B.4.6 Combustor quantities

The combustor/IGV section possibly has cooling air flow which bypasses the combustor. The mass flows and control volumes are detailed in Figure B.2.
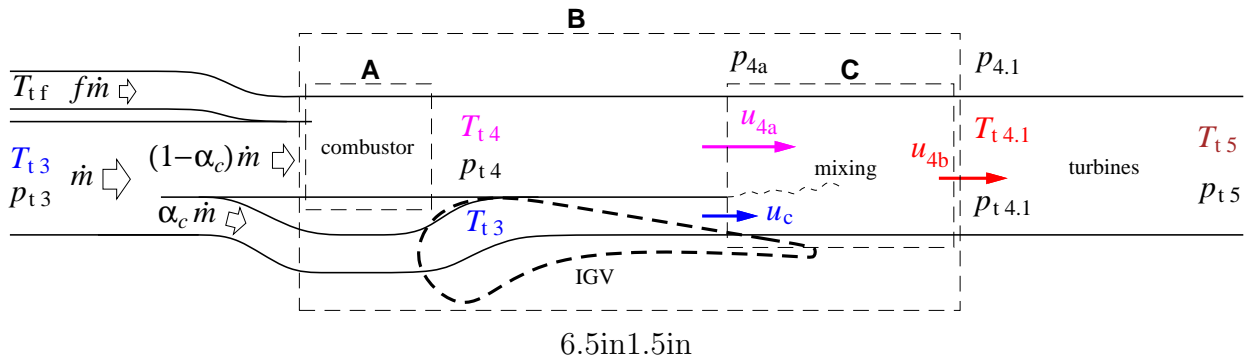
Figure B.2: Combustor and film-cooling flows, with mixing over and downstream of IGV. Dashed rectangles are control volumes.

Using control volume A in Figure B.2, the fuel/combustor-air mass flow fraction f_b and the combustion-product constituent mass fraction vector $\vec{\lambda}$ are obtained by using the compressor exit condition $()_{t3}$, together with the specified combustor exit total temperature T_{t4}. The fuel/core-air fraction f then follows.

$$\left\{f_b, \vec{\lambda}\right\} \;=\; \mathcal{F}_b\left(\vec{\alpha}, \vec{\beta}, \vec{\gamma}, T_{t3}, T_{t_f}, T_{t4}\right) \qquad \text{(B.141)}$$

$$f \;=\; f_b\left(1 - \alpha_c\right) \qquad \text{(B.142)}$$

74

The combustor exit conditions are then obtained using this $\vec{\lambda}$, together with the specified T_{t4} and the assumed combustor pressure ratio π_{b}.

$$h_{t4} = \vec{\lambda} \cdot \vec{h}_{(T_{t4})} \tag{B.143}$$

$$\sigma_{t4} = \vec{\lambda} \cdot \vec{\sigma}_{(T_{t4})} \tag{B.144}$$

$$p_{t4} = p_{t3} \, \pi_{\mathrm{b}} \tag{B.145}$$

B.4.7 Station 4.1 without IGV Cooling Flow

Without cooling flow ($\alpha_c = 0$), the 4.1 station quantities and constituent mass fraction at the first turbine rotor inlet are the same as the 4 station quantities at the combustor exit.

$$T_{t4.1} = T_{t4} \tag{B.146}$$

$$p_{t4.1} = p_{t4} \tag{B.147}$$

$$\vec{\lambda}' = \vec{\lambda} \tag{B.148}$$

The analysis can then skip the cooling flow mixing calculations below, and proceed directly to the **Turbine Quantities** section.

B.4.8 Station 4.1 with IGV Cooling Flow

The IGV pressure at the cooling flow exit is specified indirectly via the cooling-exit Mach M_{4a} at the combustor-exit stagnation conditions. The corresponding static conditions and velocity are calculated using the $\mathcal{F}_M$ function.

$$\{\, p_{4a}, T_{4a}, h_{4a} \,\} = \mathcal{F}_M\left(\vec{\lambda}, p_{t4}, T_{t4}, 0, M_{4a}, 1\right) \tag{B.149}$$

$$u_{4a} = \sqrt{2(h_{t4} - h_{4a})} \tag{B.150}$$

The cooling flow is assumed to exit the IGV at some fraction r_{u_c} of this u_{4a}.

$$u_{\mathrm{c}} = r_{u_c} \, u_{4a} \tag{B.151}$$

The combustor and cooling flows are assumed to be fully mixed at station 4.1. The mixed-out mass fraction vector $\vec{\lambda}'$ is calculated by the mass flow balance,

$$\vec{\lambda}' = \frac{1 - \alpha_c + f}{1 + f} \, \vec{\lambda} + \frac{\alpha_c}{1 + f} \, \vec{\alpha} \tag{B.152}$$

and is used for the downstream turbine and core exhaust calculations. Assuming a constant static pressure over the mixing region, a simple momentum balance gives the mixed-out velocity $u_{4.1}$.

$$p_{4.1} = p_{4a} \tag{B.153}$$

$$u_{4.1} = \frac{1 - \alpha_c + f}{1 + f} \, u_{4a} + \frac{\alpha_c}{1 + f} \, u_c \tag{B.154}$$

The enthalpy balance across control volume B in Figure B.2 gives the mixed-out total temperature $T_{t\,4.1}$ via the $\mathcal{F}_h$ function.

$$h_{(T_{t\,4.1})} \equiv h_{t\,4.1} = \frac{1 - \alpha_c + f}{1 + f}\,h_{t\,4} + \frac{\alpha_c}{1 + f}\,h_{t\,3} \tag{B.155}$$

$$T_{\text{guess}} = \frac{1 - \alpha_c + f}{1 + f}\,T_{t\,4} + \frac{\alpha_c}{1 + f}\,T_{t\,3} \tag{B.156}$$

$$T_{t\,4.1} = \mathcal{F}_T\left(\vec{\lambda}', h_{t\,4.1}\,;\, T_{\text{guess}}\right) \tag{B.157}$$

The total pressure is then obtained using the mixed-out velocity $u_{4.1}$, together with the $\mathcal{F}_h$ function.

$$h_{4.1} = h_{t\,4.1} - \frac{1}{2}\,u_{4.1}^2 \tag{B.158}$$

$$\Delta h = \frac{1}{2}\,u_{4.1}^2 \tag{B.159}$$

$$\{\,p_{t\,4.1}, T_{t\,4.1}, h_{t\,4.1}\,\} = \mathcal{F}_h\left(\vec{\lambda}', p_{4.1}, T_{4.1}, \Delta h, 1\right) \tag{B.160}$$

B.4.9 Turbine quantities

High Pressure Turbine

The HPT enthalpy drop is obtained by equating the turbine work with the HPC work.

$$\dot{m}_{\text{hc}}(1 + f)\,(h_{t\,4.1} - h_{t\,4.5}) = \dot{m}_{\text{hc}}\,(h_{t\,3} - h_{t\,2.5}) \tag{B.161}$$

$$h_{t\,4.5} - h_{t\,4.1} \equiv \Delta h_{\text{ht}} = \frac{-1}{1 + f}\left[h_{t\,3} - h_{t\,2.5}\right] \tag{B.162}$$

This enthalpy drop, together with an assumed polytropic efficiency, is then used to determine the HPT exit stagnation conditions.

$$\{p_{t\,4.5}, T_{t\,4.5}, h_{t\,4.5}\} = \mathcal{F}_h\left(\vec{\lambda}', p_{t\,4.1}, T_{t\,4.1}, \Delta h_{\text{ht}}, \eta_{\text{pol}_t}^{-1}\right) \tag{B.163}$$

Low Pressure Turbine (Design case)

The LPT enthalpy drop for the design case is obtained by equating the turbine work with the LPC plus fan work.

$$\dot{m}_{\text{hc}}(1 + f)\,(h_{t\,4.5} - h_{t\,4.9}) = \dot{m}_{\text{lc}}\,(h_{t\,2.5} - h_{t\,1.9}) + \dot{m}_{\text{fan}}\,(h_{t\,2.1} - h_{t\,2}) \tag{B.164}$$

$$h_{t\,4.9} - h_{t\,4.5} \equiv \Delta h_{\text{lt}} = \frac{-1}{1 + f}\frac{\dot{m}_{\text{lc}}}{\dot{m}_{\text{hc}}}\left[(h_{t\,2.5} - h_{t\,1.9}) + \alpha\,(h_{t\,2.1} - h_{t\,2})\right] \tag{B.165}$$

The $\dot{m}_{\text{lc}}/\dot{m}_{\text{hc}}$ mass flow ratio is known, and is unity if there's no bleed at the 2.5 station. The enthalpy drop calculated above, together with an assumed turbine polytropic efficiency,

is then used to determine all the station 4.9 LPT exit conditions. The turbine nozzle total pressure ratio π_{tn} then give the station 5 nozzle conditions.

$$\{p_{t\,4.9}, T_{t\,4.9}, h_{t\,4.9}\} = \mathcal{F}_h\left(\vec{\lambda}', p_{t\,4.5}, T_{t\,4.5}, \Delta h_{\text{lt}}, \eta_{\text{pol}_t}^{-1}\right) \tag{B.166}$$

$$p_{t\,5} = p_{t\,4.9}\,\pi_{\text{tn}} \tag{B.167}$$

$$T_{t\,5} = T_{t\,4.9} \tag{B.168}$$

$$h_{t\,5} = h_{t\,4.9} \tag{B.169}$$

Low Pressure Turbine (Off-Design case)

The relations above could be used to determine the $()_{t\,5}$ core exit quantities for the off-design case. However, this opens the possibility of $p_{t\,5}$ falling below the nozzle static pressure $p_5 = p_0$ during one Newton iteration. A common cause is the fan's enthalpy extraction term $\alpha(h_{t\,2.1} - h_{t\,2})$ in (B.165) being too large because of a momentarily excessive π_{f} and/or $\bar{m}_{\text{f}}$ values, so that Δh_{lt} is too negative which gives a small $p_{t\,5}$ in calculations (B.166) and (B.167).

Regardless of the cause, if $p_{t\,5} < p_5$ is a result then the nozzle velocity u_5 cannot be computed, and the subsequent nozzle mass flow and thrust relations cannot be imposed. This causes failure of the overall Newton iteration process. One solution is to underrelax an "excessive" Newton update so that $p_{t\,5}$ never falls below p_5. However, this is rather impractical since a very long calculation chain is required to reach the $p_{t\,5}$ evaluation operations (B.166) and (B.167), so the necessary underrelaxation factor cannot be determined without in effect performing and possibly discarding the calculations for one whole Newton iteration.

The solution taken here is to introduce $p_{t\,5}$ as a Newton variable, so that during the Newton update it can be easily monitored to ensure that it never falls below p_5. It also means that so that the $()_{t\,5}$ quantities are now computed by the alternative procedure of a specified pressure ratio as used for the compressors.

$$\pi_{\text{lt}} = \frac{p_{t\,4.9}}{p_{t\,4.5}} = \frac{1}{\pi_{\text{tn}}}\frac{p_{t\,5}}{p_{t\,4.5}} \tag{B.170}$$

$$\{p_{t\,4.9}, T_{t\,4.9}, h_{t\,4.9}\} = \mathcal{F}_p\left(\vec{\lambda}', p_{t\,4.5}, T_{t\,4.5}, \pi_{\text{lt}}, \eta_{\text{pol}_t}^{-1}\right) \tag{B.171}$$

$$p_{t\,5} = p_{t\,4.9}\,\pi_{\text{tn}} \tag{B.172}$$

$$T_{t\,5} = T_{t\,4.9} \tag{B.173}$$

$$h_{t\,5} = h_{t\,4.9} \tag{B.174}$$

The LPT work relation (B.165) will now play the role as a Newton equation which constrains $p_{t\,5}$. This overall procedure will of course produce the same final result as if $p_{t\,5}$ was calculated from (B.165), but its Newton iteration behavior is far more stable and reliable.

Turbine efficiencies

The turbine efficiencies (including cooling-air losses) can also be computed out of interest.

$$\{p_{t\,4.5}, (T_{t\,4.5})_{is}, (h_{t\,4.5})_{is}\} = \mathcal{F}_p\left(\vec{\lambda}', p_{t\,4}, T_{t\,4}, p_{t\,4.5}/p_{t\,4}, 1\right) \tag{B.175}$$

$$\{p_{t\,4.9}, (T_{t\,4.9})_{is}, (h_{t\,4.9})_{is}\} \;=\; \mathcal{F}_p\left(\vec{\lambda}', p_{t\,4.5}, T_{t\,4.5}, p_{t\,5}/p_{t\,4.5}, 1\right) \tag{B.176}$$

$$\eta_{\mathrm{ht}} \;=\; \frac{h_{t\,4.5} - h_{t\,4}}{(h_{t\,4.5})_{is} - h_{t\,4}} \tag{B.177}$$

$$\eta_{\mathrm{lt}} \;=\; \frac{h_{t\,4.9} - h_{t\,4.5}}{(h_{t\,4.9})_{is} - h_{t\,4.5}} \tag{B.178}$$

B.4.10 Fan exhaust quantities

The fan exhaust velocity is computed from the known $()_{t\,8}$ fan plume stagnation conditions, and the requirement of ambient exhaust pressure, $p_8 = p_0$.

$$p_{t\,8} \;=\; p_{t\,7} \tag{B.179}$$

$$T_{t\,8} \;=\; T_{t\,7} \tag{B.180}$$

$$\{p_8, T_8, h_8\} \;=\; \mathcal{F}_p\left(\vec{\alpha}, p_{t\,8}, T_{t\,8}, p_0/p_{t\,8}, 1\right) \tag{B.181}$$

$$u_8 \;=\; \sqrt{2(h_{t\,8} - h_8)} \tag{B.182}$$

B.4.11 Core exhaust quantities

The core exhaust velocity is computed from the known $()_{t\,6}$ core plume conditions and the requirement of ambient exhaust pressure, $p_6 = p_0$.

$$p_{t\,6} \;=\; p_{t\,5} \tag{B.183}$$

$$T_{t\,6} \;=\; T_{t\,5} \tag{B.184}$$

$$\{p_6, T_6, h_6\} \;=\; \mathcal{F}_p\left(\vec{\lambda}', p_{t\,6}, T_{t\,6}, p_0/p_{t\,6}, 1\right) \tag{B.185}$$

$$u_6 \;=\; \sqrt{2(h_{t\,6} - h_6)} \tag{B.186}$$

B.4.12 Overall engine quantities

The overall specific thrust is obtained from the total fan and core thrust forces.

$$\dot{m}_{\mathrm{core}} \;\equiv\; \bar{m}_{\mathrm{lc}} \frac{p_{t\,2}/p_{\mathrm{ref}}}{\sqrt{T_{t\,2}/T_{\mathrm{ref}}}} \tag{B.187}$$

$$F_8 \;=\; \alpha \dot{m}_{\mathrm{core}} \left[u_8 - u_0\right] \tag{B.188}$$

$$F_6 \;=\; \dot{m}_{\mathrm{core}} \left[(1+f)u_6 - u_0\right] \tag{B.189}$$

$$F \;=\; F_6 + F_8 \tag{B.190}$$

$$F_{\mathrm{sp}} \;\equiv\; \frac{F}{(1+\alpha)\,\dot{m}_{\mathrm{core}}\,a_0} \;=\; \frac{(1+f)u_6 - u_0 \;+\; \alpha(u_8 - u_0)}{(1+\alpha)\,a_0} \tag{B.191}$$

The overall specific impulse and thrust specific fuel consumption then follow.

$$I_{\mathrm{sp}} \;\equiv\; \frac{F}{\dot{m}_{\mathrm{fuel}}\,g} \;=\; \frac{F_{\mathrm{sp}}}{f}\frac{a_0}{g}(1+\alpha) \tag{B.192}$$

$$TSFC \;=\; \frac{1}{I_{\mathrm{sp}}} \tag{B.193}$$

B.5   Design Sizing Calculation

For the design case, the following quantities are specified.

F_D design thrust
M_2 fan-face, LPC-face axial Mach number
$M_{2.5}$ HPC-face axial Mach number

B.5.1   Mass Flow Sizing

This consists of finding the core mass flow to achieve the required thrust at at the design operating conditions p_0, a_0, M_0. This design core mass flow $\dot{m}_\mathrm{core}$ is obtained directly from relation (B.191), using the specified design thrust F_D.

$$\dot{m}_\mathrm{core} \;\; = \;\; \frac{F_\mathrm{D}}{F_\mathrm{sp}\, a_0 \,(1+\alpha)} \tag{B.194}$$

B.5.2   Component Area Sizing

Fan area

The fan-face static ρ_2 and a_2 are obtained from the specified-Mach procedure, with some specified fan-face Mach number M_2, and some $\eta_\mathrm{pol} = \eta_{\mathrm{pol_d}}$.

$$\{p_2, T_2, h_2\} \;\; = \;\; \mathcal{F}_M\left(\vec{\alpha}, p_0, T_0, M_0, M_2, \eta_{\mathrm{pol_d}}\right) \tag{B.195}$$

The fan area A_2 can then be computed from the design mass flow.

$$\rho_2 \;\; = \;\; \frac{p_2}{R_2 T_2} \tag{B.196}$$

$$u_2 \;\; = \;\; M_2 \sqrt{\frac{c_{p_2}\, R_2}{c_{p_2} - R_2}\, T_2} \tag{B.197}$$

$$A_2 \;\; = \;\; \frac{(1+\alpha)\, \dot{m}_\mathrm{core}}{\rho_2 u_2} \tag{B.198}$$

A specified hub/tip ratio HTR_f then also gives the fan diameter,

$$d_\mathrm{f} \;\; = \;\; \sqrt{\frac{4}{\pi} \frac{A_2}{1 - HTR_\mathrm{f}^2}} \tag{B.199}$$

although this is not required for any subsequent off-design analysis.

The HP compressor fan area $A_{2.5}$ is obtained in this same manner from a specified compressor-face Mach number $M_{2.5}$.

$$\{p_{2.5}, T_{2.5}, h_{2.5}\} \;\; = \;\; \mathcal{F}_M\left(\vec{\alpha}, p_{t\,2.5}, T_{t\,2.5}, 0, M_{2.5}, \eta_{\mathrm{pol_d}}\right) \tag{B.200}$$

$$\rho_{2.5} \;\; = \;\; \frac{p_{2.5}}{R_{2.5} T_{2.5}} \tag{B.201}$$

$$u_{2.5} = M_{2.5}\sqrt{\frac{c_{p2.5}\,R_{2.5}}{c_{p2.5}-R_{2.5}}\,T_{2.5}} \tag{B.202}$$

$$A_{2.5} = \frac{(1+\alpha)\,\dot{m}_{\text{core}}}{\rho_{2.5}u_{2.5}} \tag{B.203}$$

A specified hub/tip ratio HTR_{f} then also gives the HPC face diameter.

$$d_{\text{hc}} = \sqrt{\frac{4}{\pi}\frac{A_{2.5}}{1-HTR_{\text{hc}}^2}} \tag{B.204}$$

Fan nozzle area

The fan nozzle flow type can be determined from the fan-plume Mach number.

$$M_8 = u_8\Big/\sqrt{\frac{c_{p8}\,R_8}{c_{p8}-R_8}\,T_8} \tag{B.205}$$

If $M_8 < 1$ then the fan nozzle is assumed to be unchoked, and the nozzle conditions are obtained by using the specified pressure ratio function. The nozzle is assumed here to be at ambient static pressure, although any other pressure can be specified instead.

$$p_7 = p_0 \tag{B.206}$$
$$\{p_7, T_7, h_7\} = \mathcal{F}_p\left(\vec{\alpha}, p_{t7}, T_{t7}, p_7/p_{t7}, 1\right) \tag{B.207}$$

If $M_8 \geq 1$ the the fan nozzle is choked, and the nozzle conditions are obtained using the specified Mach function.

$$M_7 = 1 \tag{B.208}$$
$$\{p_7, T_7, h_7\} = \mathcal{F}_M\left(\vec{\alpha}, p_{t7}, T_{t7}, 0, M_7, 1\right) \tag{B.209}$$

In either case, the fan area follows directly.

$$u_7 = \sqrt{2(h_{t7} - h_7)} \tag{B.210}$$
$$\rho_7 = \frac{p_7}{R_7 T_7} \tag{B.211}$$
$$A_7 = \frac{\alpha\,\dot{m}_{\text{core}}}{\rho_7 u_7} \tag{B.212}$$

Core nozzle area

The core nozzle flow type is determined from the core-plume Mach number.

$$M_6 = u_6\Big/\sqrt{\frac{c_{p6}\,R_6}{c_{p6}-R_6}\,T_6} \tag{B.213}$$

If $M_6 < 1$ then the core nozzle is unchoked, and the nozzle conditions are obtained by using the specified pressure ratio function.

$$p_5 = p_0 \tag{B.214}$$
$$\{p_5, T_5, h_5\} = \mathcal{F}_p\left(\vec{\alpha}, p_{t5}, T_{t5}, p_5/p_{t5}, 1\right) \tag{B.215}$$

If $M_6 \geq 1$ the the fan nozzle is choked, and the nozzle conditions are obtained using the specified Mach function.

$$M_5 = 1 \tag{B.216}$$
$$\{p_5, T_5, h_5\} = \mathcal{F}_M\left(\vec{\alpha}, p_{t5}, T_{t5}, 0, M_5, 1\right) \tag{B.217}$$

The core nozzle area follows.

$$u_5 = \sqrt{2(h_{t5} - h_5)} \tag{B.218}$$
$$\rho_5 = \frac{p_5}{R_5 T_5} \tag{B.219}$$
$$A_5 = \frac{\dot{m}_{\text{core}}}{\rho_5 u_5} \tag{B.220}$$

B.5.3   Design corrected speeds and mass flows

Since only speed ratios will be considered in the off-design calculation, the LPC and HPC design spool speeds can be arbitrarily set to unity.

$$N_{\text{lcD}} = 1 \tag{B.221}$$
$$N_{\text{hcD}} = 1 \tag{B.222}$$

The design corrected spool speeds and high-pressure and low-pressure turbine corrected mass flows are defined in the usual manner.

$$\bar{N}_{\text{lD}} = N_{\text{lD}} \frac{1}{\sqrt{T_{t1.9}/T_{\text{ref}}}} \tag{B.223}$$
$$\bar{N}_{\text{hD}} = N_{\text{hD}} \frac{1}{\sqrt{T_{t2.5}/T_{\text{ref}}}} \tag{B.224}$$
$$\bar{m}_{\text{htD}} = (1+f)\,\dot{m}_{\text{core}} \frac{\sqrt{T_{t4.1}/T_{\text{ref}}}}{p_{t4.1}/p_{\text{ref}}} \tag{B.225}$$
$$\bar{m}_{\text{ltD}} = (1+f)\,\dot{m}_{\text{core}} \frac{\sqrt{T_{t4.5}/T_{\text{ref}}}}{p_{t4.5}/p_{\text{ref}}} \tag{B.226}$$

B.6   Off-Design Operation Calculation

For an off-design case, the following eight quantities which were assumed known at the start of the calculation pass are really unknowns, and must be updated.

π_{f} fan pressure ratio
π_{lc} LPC pressure ratio
π_{hc} HPC pressure ratio
$\bar{m}_{\text{f}}$ fan corrected mass flow
$\bar{m}_{\text{lc}}$ LPC corrected mass flow
$\bar{m}_{\text{hc}}$ HPC corrected mass flow
T_{t4} burner exit total temperature
p_{t5} core nozzle total pressure

The necessary eight constraining equations involve the spool speeds, which are calculated as described in the next section. The speed calculation is based on an assumed fan or compressor map, and has the following functional form.

$$\bar{N} = \mathcal{F}_N(\pi, \bar{m}) \tag{B.227}$$

This is used to compute the fan, LPC, and HPC speed from each component's current pressure ratio and corrected mass flows. The current station 1.9, 2, 2.5 stagnation conditions are also used, to compute the necessary $\bar{m}$ arguments for the $\mathcal{F}_N$ functions.

$$N_{\mathrm{f}} = \sqrt{T_{t2}/T_{\mathrm{ref}}} \; \mathcal{F}_N(\pi_{\mathrm{f}}, \bar{m}_{\mathrm{f}}) \tag{B.228}$$

$$N_{\mathrm{l}} = \sqrt{T_{t1.9}/T_{\mathrm{ref}}} \; \mathcal{F}_N(\pi_{\mathrm{lc}}, \bar{m}_{\mathrm{lc}}) \tag{B.229}$$

$$N_{\mathrm{h}} = \sqrt{T_{t2.5}/T_{\mathrm{ref}}} \; \mathcal{F}_N(\pi_{\mathrm{hc}}, \bar{m}_{\mathrm{hc}}) \tag{B.230}$$

Each of these three functions uses the appropriate map constants for that component, given in the component-map section.

The off-design fan face Mach number M_2 can be calculated from the fan-face mass flow relation.

$$\rho_2 u_2 A_2 = \bar{m}_{\mathrm{f}} \sqrt{\frac{T_{\mathrm{ref}}}{T_{t2}}} \frac{p_{t2}}{p_{\mathrm{ref}}} + \bar{m}_{\mathrm{lc}} \sqrt{\frac{T_{\mathrm{ref}}}{T_{t1.9}}} \frac{p_{t1.9}}{p_{\mathrm{ref}}} = (1+\alpha)\dot{m}_{\mathrm{core}} \tag{B.231}$$

This is solved for the implied M_2 (subsonic branch) using the $\mathcal{F}_m$ specified-mass function. The design M_2 value is a suitable initial guess.

$$M_{\mathrm{guess}} = (M_2)_{\mathrm{D}} \tag{B.232}$$

$$m' = (1+\alpha)\dot{m}_{\mathrm{core}}/A_2 \tag{B.233}$$

$$\{p_2, T_2, h_2\} = \mathcal{F}_m(\vec{\alpha}, p_{t2}, T_{t2}, h_{t2}, m'; M_{\mathrm{guess}}) \tag{B.234}$$

$$u_2 = \sqrt{2(h_{t2} - h_2)} \tag{B.235}$$

$$M_2 = u_2/\sqrt{\frac{c_{p2} R_2}{c_{p2} - R_2} T_2} \tag{B.236}$$

B.6.1 Constraint residuals

The eight residuals for constraining the eight operating unknowns are listed below.

Fan/LPC speed constraint

Equating the fan and LPC speeds, with some specified gear ratio G_{f}, defines the constraining equation residual.

$$\mathcal{R}_1 \equiv N_{\mathrm{f}} G_{\mathrm{f}} - N_{\mathrm{l}} = 0 \tag{B.237}$$

HPT mass flow

In lieu of a full turbine map, it is reasonable to assume that the high-pressure turbine IGV is always choked. The appropriate constraining residual is therefore a fixed corrected mass flow at station 4.1, equal to the design value.

$$\mathcal{R}_2 \; \equiv \; (1+f)\bar{m}_{\mathrm{hc}} \sqrt{\frac{T_{t\,4.1}}{T_{t\,2.5}}} \frac{p_{t\,2.5}}{p_{t\,4.1}} \; - \; \bar{m}_{\mathrm{htD}} \; = \; 0 \tag{B.238}$$

Note that this approximation means that the high spool speed N_{h} is not required in any of the calculations.

LPT mass flow

The low-pressure turbine IGV is also assumed to be choked. Again, the appropriate constraining residual is therefore a fixed corrected mass flow at station 4.5, equal to the design value.

$$\mathcal{R}_3 \; \equiv \; (1+f)\bar{m}_{\mathrm{hc}} \sqrt{\frac{T_{t\,4.5}}{T_{t\,2.5}}} \frac{p_{t\,2.5}}{p_{t\,4.5}} \; - \; \bar{m}_{\mathrm{ltD}} \; = \; 0 \tag{B.239}$$

Fan nozzle mass flow

The type of constraint imposed at the fan nozzle depends on whether or not the nozzle is choked. The fan nozzle trial static conditions and trial Mach number $\tilde{M}_7$ are first computed assuming a specified nozzle static pressure, equal to the freestream pressure.

$$\tilde{p}_7 \; = \; p_0 \tag{B.240}$$
$$\left\{ \tilde{p}_7, \tilde{T}_7, \tilde{h}_7 \right\} \; = \; \mathcal{F}_p \left(\vec{\alpha}, p_{t\,7}, T_{t\,7}, p_7/p_{t\,7}, 1 \right) \tag{B.241}$$
$$\tilde{u}_7 \; = \; \sqrt{2(h_{t\,7} - \tilde{h}_7)} \tag{B.242}$$
$$\tilde{M}_7 \; = \; \tilde{u}_7 / \sqrt{\frac{\tilde{c}_{p7}\,R_7}{\tilde{c}_{p7} - R_7}\tilde{T}_7} \tag{B.243}$$

If $\tilde{M}_7 \leq 1$, then the trial state is the actual state.

$$p_7 \; = \; \tilde{p}_7 \tag{B.244}$$
$$T_7 \; = \; \tilde{T}_7 \tag{B.245}$$
$$h_7 \; = \; \tilde{h}_7 \tag{B.246}$$

If $\tilde{M}_7 > 1$, then the trial state is incorrect, and a unity Mach number is imposed instead.

$$M_7 \; = \; 1 \tag{B.247}$$
$$\{p_7, T_7, h_7\} \; = \; \mathcal{F}_M \left(\vec{\alpha}, p_{t\,7}, T_{t\,7}, 0, M_7, 1 \right) \tag{B.248}$$

For either case, the velocity, density, and mass flow constraint residual is formulated the same way.

$$u_7 = \sqrt{2(h_{t\,7} - h_7)} \tag{B.249}$$

$$\rho_7 = \frac{p_7}{R_7 T_7} \tag{B.250}$$

$$\mathcal{R}_4 \equiv \bar{m}_\mathrm{f} \sqrt{\frac{T_\mathrm{ref}}{T_{t\,2}}} \frac{p_{t\,2}}{p_\mathrm{ref}} - \rho_7 u_7 A_7 = 0 \tag{B.251}$$

Core nozzle mass flow

The type of constraint imposed at the core nozzle depends on whether or not the nozzle is choked. The core nozzle trial static conditions and trial Mach number $\tilde{M}_5$ are first computed assuming a specified nozzle static pressure, equal to the freestream pressure.

$$\tilde{p}_5 = p_0 \tag{B.252}$$

$$\left\{ \tilde{p}_5, \tilde{T}_5, \tilde{h}_5 \right\} = \mathcal{F}_p\left(\vec{\alpha}, p_{t\,5}, T_{t\,5}, p_5/p_{t\,5}, 1\right) \tag{B.253}$$

$$\tilde{u}_5 = \sqrt{2(h_{t\,5} - \tilde{h}_5)} \tag{B.254}$$

$$\tilde{M}_5 = \tilde{u}_5 \Big/ \sqrt{\frac{\tilde{c}_{p5}\,R_5}{\tilde{c}_{p5} - R_5}\,\tilde{T}_5} \tag{B.255}$$

If $\tilde{M}_5 \leq 1$, then the trial state is the actual state.

$$p_5 = \tilde{p}_5 \tag{B.256}$$

$$T_5 = \tilde{T}_5 \tag{B.257}$$

$$h_5 = \tilde{h}_5 \tag{B.258}$$

If $\tilde{M}_5 > 1$, then the trial state is incorrect, and a unity Mach number is imposed instead.

$$M_5 = 1 \tag{B.259}$$

$$\{p_5, T_5, h_5\} = \mathcal{F}_M\left(\vec{\alpha}, p_{t\,5}, T_{t\,5}, 0, M_5, 1\right) \tag{B.260}$$

For either case, the velocity, density, and mass flow constraint residual is formulated the same way.

$$u_5 = \sqrt{2(h_{t\,5} - h_5)} \tag{B.261}$$

$$\rho_5 = \frac{p_5}{R_5 T_5} \tag{B.262}$$

$$\mathcal{R}_5 \equiv (1{+}f)\bar{m}_\mathrm{hc} \sqrt{\frac{T_\mathrm{ref}}{T_{t\,2.5}}} \frac{p_{t\,2.5}}{p_\mathrm{ref}} - \rho_5 u_5 A_5 = 0 \tag{B.263}$$

LPC/HPC mass flow constraint

Equating the LPC and HPC mass flows defines the sixth constraining equation residual.

$$\mathcal{R}_6 \equiv \bar{m}_\mathrm{lc} \sqrt{\frac{T_\mathrm{ref}}{T_{t\,1.9}}} \frac{p_{t\,1.9}}{p_\mathrm{ref}} - \bar{m}_\mathrm{hc} \sqrt{\frac{T_\mathrm{ref}}{T_{t\,2.5}}} \frac{p_{t\,2.5}}{p_\mathrm{ref}} = 0 \tag{B.264}$$

An offset term could be included here to model any bleed upstream of the 2.5 station.

Burner exit temperature constraint

One of two possible constraints on T_{t4} can be used.

$$\mathcal{R}_7 \equiv T_{t4} - (T_{t4})_{\text{spec}} = 0 \qquad (T_{t4} \text{ specified}) \tag{B.265}$$

$$\mathcal{R}_7 \equiv F - F_{\text{spec}} = 0 \qquad (\text{thrust specified}) \tag{B.266}$$

The thrust F is defined by relation (B.190), and is ultimately a function of the eight Newton variables.

Core exit total pressure constraint

The constraint on p_{t5} is obtained from the LPT work relations (B.165) and (B.166), which have not been used yet for the off-design case.

$$\Delta h_{\text{lt}} = \frac{-1}{1+f} \frac{\dot{m}_{\text{lc}}}{\dot{m}_{\text{hc}}} \left[(h_{t2.5} - h_{t1.9}) + \alpha \left(h_{t2.1} - h_{t2} \right) \right] \tag{B.267}$$

$$p_{t4.9} = \mathcal{F}_h \left(\vec{\lambda}', p_{t4.5}, T_{t4.5}, \Delta h_{\text{lt}}, \eta_{\text{pol}_{\text{t}}}^{-1} \right) \tag{B.268}$$

$$\mathcal{R}_8 \equiv p_{t5} - p_{t4.9}\, \pi_{\text{tn}} = 0 \tag{B.269}$$

The enthalpy drop Δh_{lt} is computed using (B.165).

B.6.2   Newton update

The eight residuals depend explicitly or implicitly on the eight unknowns. Newton changes are computed by forming and solving the 8×8 linear Newton system.

$$\left[\frac{\partial(\mathcal{R}_1, \mathcal{R}_2, \mathcal{R}_3, \mathcal{R}_4, \mathcal{R}_5, \mathcal{R}_6, \mathcal{R}_7, \mathcal{R}_8)}{\partial(\pi_{\text{f}}, \pi_{\text{lc}}, \pi_{\text{hc}}, \bar{m}_{\text{f}}, \bar{m}_{\text{lc}}, \bar{m}_{\text{hc}}, T_{t4}, p_{t5})} \right] \left\{ \begin{array}{c} \delta\pi_{\text{f}} \\ \delta\pi_{\text{lc}} \\ \delta\pi_{\text{hc}} \\ \delta\bar{m}_{\text{f}} \\ \delta\bar{m}_{\text{lc}} \\ \delta\bar{m}_{\text{hc}} \\ \delta T_{t4} \\ \delta p_{t5} \end{array} \right\} = - \left\{ \begin{array}{c} \mathcal{R}_1 \\ \mathcal{R}_2 \\ \mathcal{R}_3 \\ \mathcal{R}_4 \\ \mathcal{R}_5 \\ \mathcal{R}_6 \\ \mathcal{R}_7 \\ \mathcal{R}_8 \end{array} \right\} \tag{B.270}$$

The Newton changes are then used to update the variables,

$$\pi_{\text{f}} \leftarrow \pi_{\text{f}} + \omega\, \delta\pi_{\text{f}} \tag{B.271}$$

$$\pi_{\text{lc}} \leftarrow \pi_{\text{lc}} + \omega\, \delta\pi_{\text{lc}} \tag{B.272}$$

$$\pi_{\text{hc}} \leftarrow \pi_{\text{hc}} + \omega\, \delta\pi_{\text{hc}} \tag{B.273}$$

$$\bar{m}_{\text{f}} \leftarrow \bar{m}_{\text{f}} + \omega\, \delta\bar{m}_{\text{f}} \tag{B.274}$$

$$\bar{m}_{\text{lc}} \leftarrow \bar{m}_{\text{lc}} + \omega\, \delta\bar{m}_{\text{lc}} \tag{B.275}$$

$$\bar{m}_{\text{hc}} \leftarrow \bar{m}_{\text{hc}} + \omega\, \delta\bar{m}_{\text{hc}} \tag{B.276}$$

$$T_{t4} \leftarrow T_{t4} + \omega\, \delta T_{t4} \tag{B.277}$$

$$p_{t5} \leftarrow p_{t5} + \omega\, \delta p_{t5} \tag{B.278}$$

where $\omega \leq 1$ is possible underrelaxation factor set so that the resulting new variables stay within physically-dictated limits, e.g. $\pi > 1$, $p_{t5} > p_0$, etc. This is usually required only for the first few iterations where the Newton changes are large. Once the solution is approached and the changes become small, $\omega = 1$ is used.

After the update, all calculations are repeated for the next Newton iteration. Typically, 4–10 iterations are required for convergence to machine zero.

B.7 Fan and Compressor Maps

To enforce the fan/compressor speed matching requirement, the fan and compressor speeds are determined from their pressure ratios and mass flows. Also, it is desirable to obtain realistic degraded efficiencies away from the design point. These are implemented here using approximate canonincal compressor pressure-ratio maps and efficiency maps.

B.7.1 Pressure ratio map

The corrected speed and mass flow is defined in the usual way,

$$\bar{N} = N \frac{1}{\sqrt{T_{ti}/T_{\text{ref}}}} \tag{B.279}$$

$$\bar{m} = \dot{m} \frac{\sqrt{T_{ti}/T_{\text{ref}}}}{p_{ti}/p_{\text{ref}}} \tag{B.280}$$

where T_{ti}, p_{ti} are the face quantities, either T_{t2}, p_{t2} for the fan and the LPC, or $T_{t2.5}, p_{t2.5}$ for the HPC.

The fan and compressor maps are in turn defined in terms of these corrected values normalized by their design values.

$$\tilde{p} = \frac{\pi - 1}{\pi_{\text{D}} - 1} \tag{B.281}$$

$$\tilde{m} = \frac{\bar{m}}{\bar{m}_{\text{D}}} \tag{B.282}$$

$$\tilde{N} = \frac{\bar{N}}{\bar{N}_{\text{D}}} \tag{B.283}$$

The "spine" $\tilde{p}_s(\tilde{m}_s)$ on which the speed lines are threaded is parameterized by the corrected speed in the form

$$\tilde{m}_s(\tilde{N}) = \tilde{N}^b \tag{B.284}$$

$$\tilde{p}_s(\tilde{N}) = \tilde{m}_s^a = \tilde{N}^{ab} \tag{B.285}$$

where a controls the shape of the spine, and b controls the positioning of the speed lines along the spine.

The "knee" shape of each speed line is assumed to be a simple logarithmic function, translated to the $\tilde{m}_s, \tilde{p}_s$ position along the spine.

$$\tilde{p} - \tilde{p}_s \;=\; 2\tilde{N}\,k\,\ln\!\left(1 - \frac{\tilde{m} - \tilde{m}_s}{k}\right) \tag{B.286}$$

The constant k controls the sharpness of the logarithmic knee. Function (B.286) can be recast into an explicit form of a usual compressor map.

$$\pi\left(\bar{m}, \bar{N}\right) \;=\; 1 \;+\; (\pi_\mathrm{D} - 1)\left[\tilde{N}^{ab} \;+\; 2\tilde{N}\,k\,\ln\!\left(1 - \frac{\tilde{m} - \tilde{N}^b}{k}\right)\right] \tag{B.287}$$

Equation (B.287) is actually used here in inverse form, giving the fan or compressor corrected speed as a function of the pressure ratio and corrected mass flow.

$$\bar{N} \;=\; \mathcal{F}_N\left(\pi, \pi_\mathrm{D}, \bar{m}, \bar{m}_\mathrm{D}\right) \tag{B.288}$$

This is implemented by inverting the map (B.286) using the Newton method. To avoid problems with the extremely nonlinear logarithmic shape of each speed line curve, the Newton residual of (B.287) is formulated in one of two equivalent ways, depending on whether the specified $\tilde{m}, \tilde{p}$ point is above or below the spine curve (see Figure B.3).

$$\mathcal{R}_{(\tilde{N})} \;=\; \tilde{p}_s(\tilde{N}) \;+\; 2\tilde{N}\,k\,\ln\!\left(1 - \frac{\tilde{m} - \tilde{m}_s(\tilde{N})}{k}\right) \;-\; \tilde{p} \qquad (\text{if } \tilde{p} \geq \tilde{m}^a) \tag{B.289}$$

$$\mathcal{R}_{(\tilde{N})} \;=\; \tilde{m}_s(\tilde{N}) \;+\; k\left[1 \;-\; \exp\!\left(\frac{\tilde{p} - \tilde{p}_s(\tilde{N})}{2\tilde{N}k}\right)\right] \;-\; \tilde{m} \qquad (\text{if } \tilde{p} < \tilde{m}^a) \tag{B.290}$$

Residual (B.289), used above the spine curve, drives to the intersection of a speed line curve with a vertical constant-$\tilde{m}$ line. Residual (B.290), used below the spine curve, drives to the intersection of a speed line curve with a horizontal constant-$\tilde{p}$ line. In each case the intersection is nearly orthogonal, giving an extremely stable Newton iteration with rapid convergence in all cases.

B.7.2   Polytropic efficiency

The polytropic efficiency function is assumed to have the following form.

$$\eta_\mathrm{pol} \;=\; \mathcal{F}_\eta(\pi, \pi_\mathrm{D}, \bar{m}, \bar{m}_\mathrm{D}) \;=\; \eta_{\mathrm{pol}_o}\left(1 \;-\; C\left|\frac{\tilde{p}}{\tilde{m}^{a+\Delta a - 1}} - \tilde{m}\right|^c \;-\; D\left|\frac{\tilde{m}}{\tilde{m}_o} - 1\right|^d\right) \tag{B.291}$$

The maximum efficiency is η_{pol_o}, located at $\tilde{m}_o, \tilde{p}_o = \tilde{m}_o^{(a+\Delta a)}$ along the spine of the efficiency map. The exponent of the spine is $a + \Delta a$, which differs from the exponent of the pressure-map spine by the small amount Δa. Typically, Δa is slightly negative for single-stage fans, and slightly positive for multi-stage compressors. The c, d, C, D constants control the decrease of η_pol as $\tilde{m}, \tilde{p}$ move away from the $\tilde{m}_o, \tilde{p}_o$ point.

Table B.1: Pressure-ratio-map and efficiency-map constants for the E^3 fan.

π_D	a	b	k	η_{pol_o}	$\tilde{m}_o$	Δa	c	d	C	D
1.7	3.0	0.85	0.03	0.90	0.75	-0.5	3	6	2.5	15.0

B.7.3 Map calibration

The constants in Table B.1 give a realistic fan map, which is compared to the E^3 fan data. The resulting pressure-ratio contours are shown in Figure B.3, along with experimental data. The efficiency contours are shown in Figure B.4.

The constants in Table B.2 give a realistic high-pressure compressor map, which is compared to the E^3 compressor data. The resulting pressure-ratio contours are shown in Figure B.5,

Table B.2: Pressure-ratio-map and efficiency-map constants for the E^3 compressor.

π_D	a	b	k	η_{pol_o}	$\tilde{m}_o$	Δa	c	d	C	D
26.0	1.5	5	0.03	0.887	0.80	0.5	3	4	15.0	1.0

along with experimental data. The efficiency contours are shown in Figure B.6.
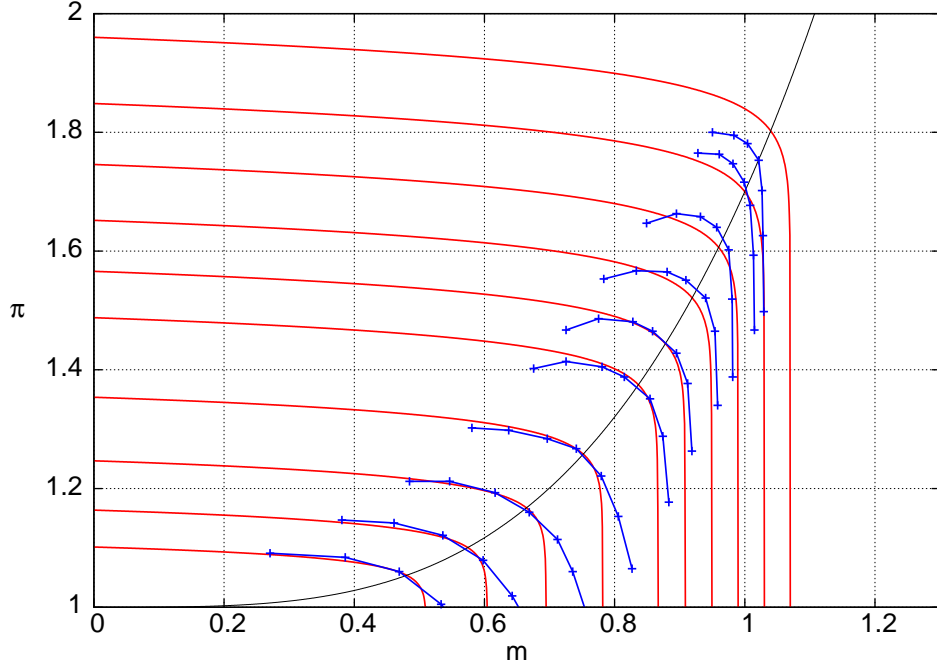
Figure B.3: Pressure ratio versus normalized corrected mass flow and corrected speed, for E^3 fan. Each red line is equation (B.287) with E^3 fan-model constants in Table B.1, and a specified experimental $\bar{N}$ value. Blue lines with symbols are measured data. Single black line is the "spine" curve $\tilde{p} = \tilde{m}^a$.
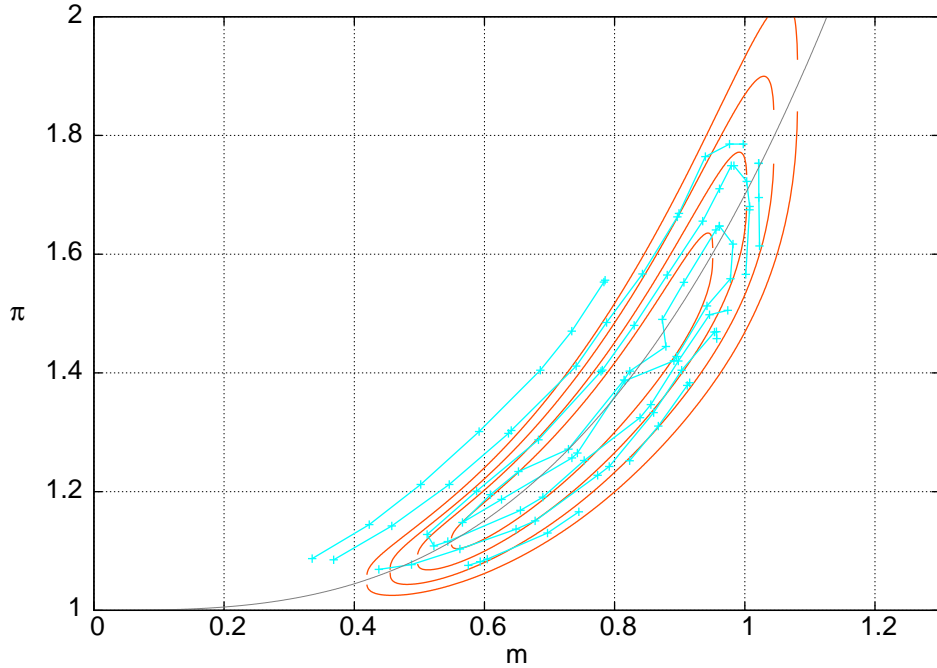

Figure B.4: Polytropic efficiency contours versus corrected mass flow and pressure ratio for E^3 fan. Red lines are isocontours of equation (B.291) with E^3 fan-model constants in Table B.1. Cyan lines with symbols are measured data. Single black line is the "spine" curve $\tilde{p} = \tilde{m}^{a+\Delta a}$.
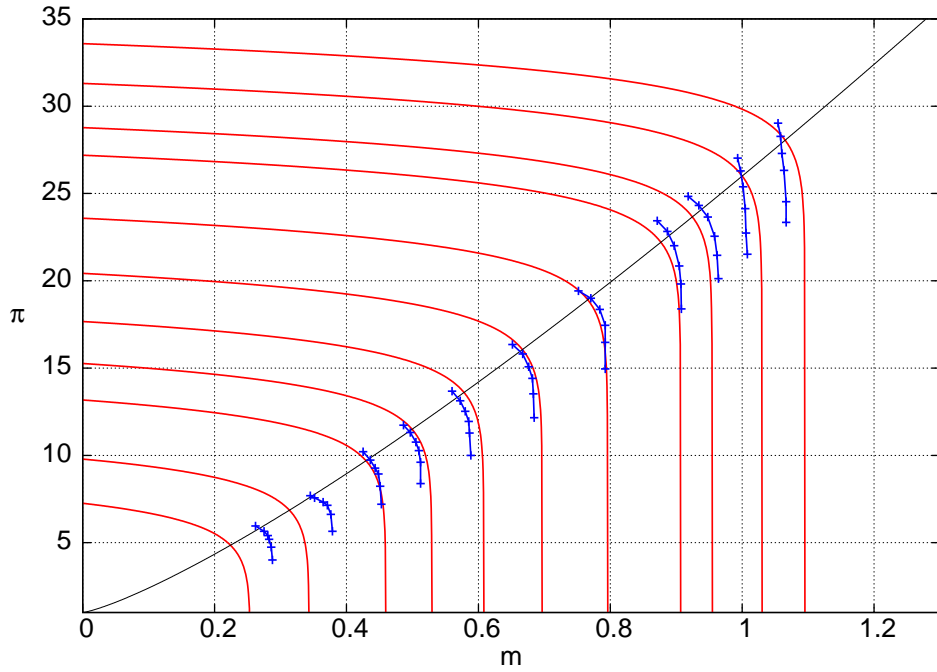
Figure B.5: Pressure ratio versus normalized corrected mass flow and corrected speed for E^3 compressor. Blue lines with symbols are measured data.
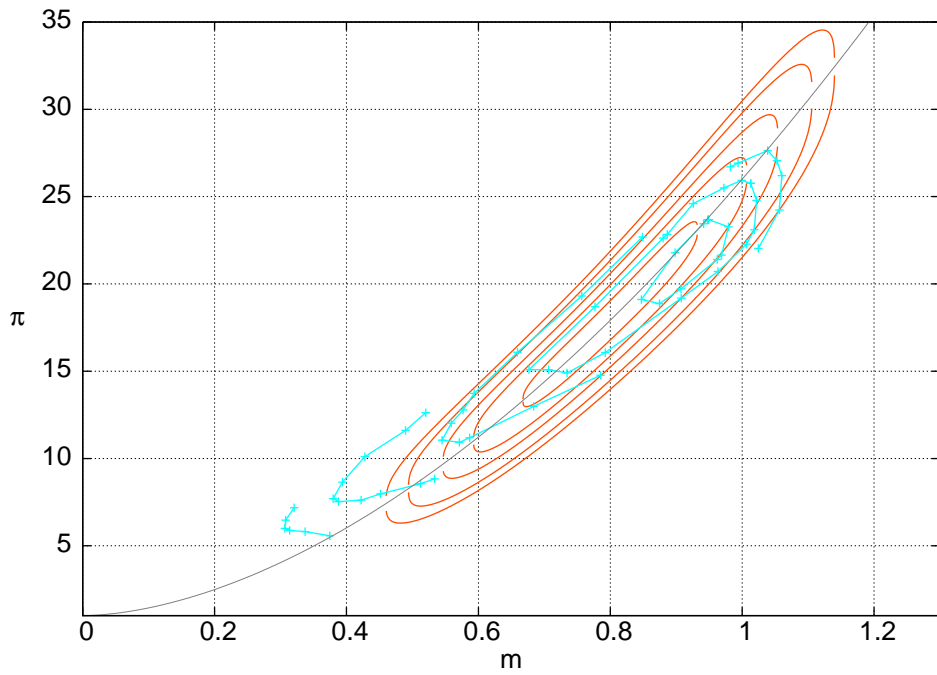

Figure B.6: Polytropic efficiency contours versus corrected mass flow and pressure ratio for E^3 compressor, for compressor-model constants in Table B.2. Cyan lines with symbols are measured data.

Appendix C

Film Cooling Flow Loss Model

C.1   Cooling mass flow calculation for one blade row

Figure C.1 shows the film-cooling model at the blade surface. The cooling gas flows into the blade at T_{ci}, and gets heated internally before issuing from the blade holes at T_{co}. The incoming hot gas at total temperature T_g is entrained into the film, and loses heat into the blade.
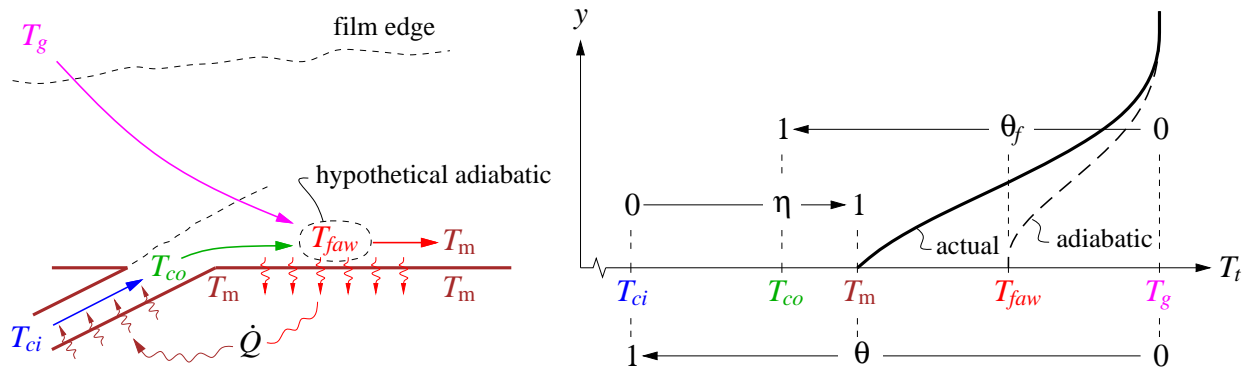

Figure C.1: Stream mixing, heat flow, and temperature profiles in film-cooling flow.

As analyzed by Horlock et al [19], the metal temperature T_m is characterized by the cooling effectiveness ratio θ,

$$\theta \;=\; \frac{T_r - T_\mathrm{m}}{T_g - T_{ci}} \;\simeq\; \frac{T_g - T_\mathrm{m}}{T_g - T_{ci}} \tag{C.1}$$

where T_r is the hot gas recovery temperature, T_m is the metal temperature, T_g is the hot gas inflow total temperature, and T_{ci} is the cooling-air inflow total temperature. The second approximate form in (C.1) makes the conservative assumption of full temperature recovery.

Since the cooling outlet holes cover only a fraction of the blade surface, the film fluid is a mixture of the cooling-fluid jets issuing at T_{co} and the entrained hot gas at T_g. In the

adiabatic (insulated wall) case, this temperature would be some T_{faw}, which is defined in terms of a film-effectiveness factor.

$$\theta_f \;=\; \frac{T_g - T_{faw}}{T_g - T_{co}} \;\simeq\; 0.4 \qquad\qquad \text{(C.2)}$$

The limiting cases would be

i) $\theta_f = 0$ or $T_{faw} = T_g$ if the cooling-fluid holes are absent, and

ii) $\theta_f = 1$ or $T_{faw} = T_{co}$ if the cooling-fluid holes completely cover the blade.

The experiments of Sargison et al [20] show that the $\theta_f \simeq 0.4$ value is a reasonable surface average for a typical blade.

The cooling efficiency

$$\eta \;=\; \frac{T_{co} - T_{ci}}{T_{\mathrm{m}} - T_{ci}} \;=\; 1 \;-\; \exp\!\left(-\frac{A_{cs}}{A_c}\,St_c\right) \;\simeq\; 0.7 \qquad\qquad \text{(C.3)}$$

indicates how much heat the cooling air has absorbed relative to the maximum possible amount before exiting the blade at temperature T_{co}. Horlock et al [19] indicate that for common internal heat transfer/flow area ratios A_{cs}/A_c and Stanton numbers St_c, the $\eta \simeq 0.7$ value is typical. This can be increased somewhat to reflect better cooling flowpath technology (e.g. improved pins, impingement, etc). However, increasing η closer to unity will also incur more total-pressure losses in the cooling flow, so $\eta < 1$ is clearly optimum from overall engine performance.

As indicated by Figure C.1, the outer-surface heat inflow from the film must be balanced by the internal heat outflow into the cooling flow. Equating these gives

$$\dot{Q} \;=\; A_{sg}\,St_g\,\rho_g V_g\,c_{p_g}(T_{faw} - T_{\mathrm{m}}) \;=\; \dot{m}_{c_1}\,c_{p_c}\,(T_{co} - T_{ci}) \qquad\qquad \text{(C.4)}$$

$$A_{sg}\,St_g\,\frac{\dot{m}_g}{A_g}\,c_{p_g}(T_{faw} - T_{\mathrm{m}}) \;=\; \dot{m}_{c_1}\,c_{p_c}\,(T_{co} - T_{ci}) \qquad\qquad \text{(C.5)}$$

where A_{sg} is the heat-transfer area of the hot gas, A_g is the flow area of the hot gas, and St_g is the external Stanton number. We now define the cooling/total mass flow ratio for one blade row,

$$\varepsilon \;=\; \frac{\dot{m}_{c_1}}{\dot{m}} \;=\; \frac{\dot{m}_{c_1}}{\dot{m}_g + \dot{m}_{c_1}} \qquad\qquad \text{(C.6)}$$

so that equation (C.4) becomes

$$\frac{\dot{m}_{c_1}}{\dot{m}_g} \;=\; \frac{\varepsilon}{1 - \varepsilon} \;=\; St_A\,\frac{T_{faw} - T_{\mathrm{m}}}{T_{co} - T_{ci}} \qquad\qquad \text{(C.7)}$$

$$\text{where} \qquad St_A \;\equiv\; \frac{c_{p_g}}{c_{p_c}}\,\frac{A_{sg}}{A_g}\,St_g \;\simeq\; 0.035 \qquad\qquad \text{(C.8)}$$

Horlock et al [19] argue that for typical blade solidities and aspect ratios, the assumed value for the weighted Stanton number $St_A \simeq 0.035$ is reasonable. This will typically need to be increased by a substantial safety factor of 2 or more to allow for parameter uncertainties, hotspots, etc. Improved cooling design would be represented by a decreased safety factor.

Using θ, θ_f, and η to eliminate T_{m}, T_{faw}, and T_{co} from (C.7) gives the following relation between all the dimensionless parameters.

$$\frac{\dot{m}_{c_1}}{\dot{m}_g} = \frac{\varepsilon}{1-\varepsilon} = St_A \frac{\theta(1-\eta\,\theta_f) - \theta_f(1-\eta)}{\eta\,(1-\theta)} \tag{C.9}$$

Design case

The design problem is to determine the cooling flow required to achieve a specified T_{m} at the maximum design T_g (e.g. $T_g = T_{t4}$ at the takeoff case). Since T_{ci} is also known for any operating point (e.g. $T_{ci} = T_{t3}$), then θ is fully determined from its definition (C.1). Equation (C.9) can then be solved for the required design cooling flow ratio for the engine.

$$\varepsilon = \left[1 + \frac{1}{St_A} \frac{\eta\,(1-\theta)}{\theta(1-\eta\,\theta_f) - \theta_f(1-\eta)}\right]^{-1} \tag{C.10}$$

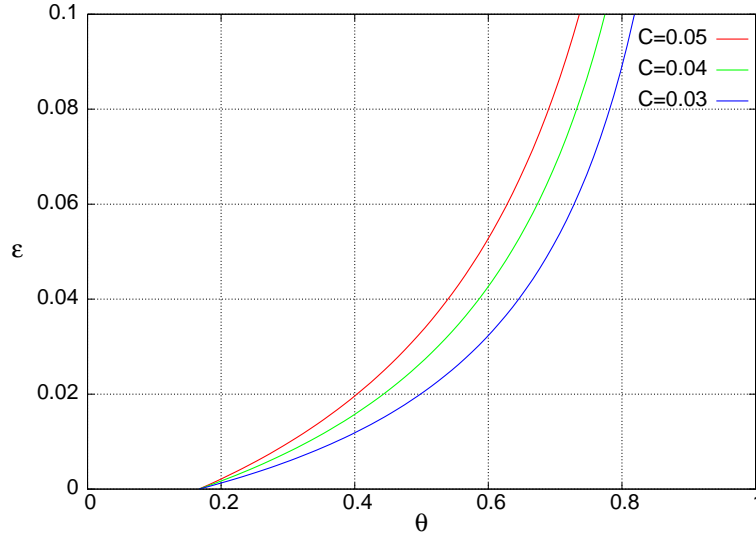Figure C.2 shows ε versus θ for three scaled Stanton numbers.

Figure C.2: Cooling mass flow ratio ε for one blade row, versus cooling effectiveness θ and Stanton number parameter C. Fixed parameters: $\eta = 0.7$, $\theta_f = 0.4$.

Off-design case

If the cooling mass flow is unregulated, it's reasonable to assume that ε will not change at off-design operation if the pressure ratios in the engine do not change appreciably. In that case, θ will not change either, and T_{m} can then be obtained from (C.1) for any specified T_g and T_{ci}. If the cooling flow ratio ε does change for whatever reason, it's then of interest to determine the resulting metal temperature. Hence, we now solve equation (C.9) for the new resulting θ in terms of a specified new ε.

$$\theta = \frac{\varepsilon\,\eta + St_A\,\theta_f(1-\eta)(1-\varepsilon)}{\varepsilon\,\eta + St_A\,(1-\eta\,\theta_f)(1-\varepsilon)} \tag{C.11}$$

C.2 Total Cooling Flow Calculation

The turbine cooling-flow bypass ratio is defined as follows.

$$\alpha_c = \frac{\dot{m}_{\text{cool}}}{\dot{m}} \qquad (C.12)$$

This represents the total cooling mass flow of all the blade rows which receive cooling flow. The calculations will assume the following quantities are specified, or known from other (e.g. compressor, combustor) calculations:

h_{fuel}	fuel heating value
T_{tf}	fuel total temperature
T_{t3}	compressor exit total temperature
p_{t3}	compressor exit total pressure
T_{t4}	turbine inlet total temperature
p_{t4}	turbine inlet total pressure $(= p_{t3}\pi_{\text{b}})$
T_{m}	metal temperature (for design case)
α_c	total cooling-flow bypass ratio (for off-design case)
St_A	area-weighted external Stanton number
M_{exit}	turbine blade-row exit Mach number
M_{4a}	representative Mach number at start of mixing zone
r_{u_c}	cooling-flow velocity ratio $(= u_c/u_{4a})$

To estimate the blade-relative hot-gas total temperature T_g incoming into each blade row, it is assumed that the inlet Mach number for that blade row is neglible. Hence, the inlet total temperature for a blade row is the same as the static exit temperature of the upstream blade row.

$$T_g \simeq (T_{\text{exit}})_{\text{upstream}} \qquad (C.13)$$

Specifying the burner exit temperature T_{t4} and a typical blade-relative exit Mach number M_{exit} is then sufficient to determine the blade-relative hot-gas temperatures $T_{g1}, T_{g2}, T_{g3} \ldots$ for all downstream blade rows.

$$T_{g1} = T_{t4} + \Delta T_{\text{streak}} \qquad (C.14)$$

$$T_{g2} = T_{t4}\left(1 + \frac{\gamma_t - 1}{2}M_{\text{exit}}^2\right)^{-1} \qquad (C.15)$$

$$T_{g3} = T_{t4}\left(1 + \frac{\gamma_t - 1}{2}M_{\text{exit}}^2\right)^{-2} \qquad (C.16)$$

$$\vdots$$

The added ΔT_{streak} for T_{g1} is a hot-streak temperature allowance for the first IGV row. According to Koff [21], assuming $\Delta T_{\text{streak}} \simeq 200°K$ is realistic.

With the row T_g's defined, relation (C.1) gives the required cooling effectiveness ratio for each blade row,

$$\theta_1 = \frac{T_{g1} - T_{\text{m}}}{T_{g1} - T_{ci}} \qquad (C.17)$$

$$\theta_2 \;\; = \;\; \frac{T_{g2} - T_{\mathrm{m}}}{T_{g2} - T_{ci}} \tag{C.18}$$

$$\vdots$$

and relation (C.11) gives the corresponding cooling mass flow $\varepsilon_1, \varepsilon_2, \varepsilon_3 \ldots$ for each blade row. These are computed until $\varepsilon_{()} < 0$ is reached, indicating that cooling is no longer required. The total cooling mass flow ratio is then the sum of the individual blade-row mass flow ratios.

$$\alpha_c \;\; = \;\; \varepsilon_1 \,+\, \varepsilon_2 \,+\, \varepsilon_3 \ldots \tag{C.19}$$

C.3 Mixed-out Flow and Loss Calculation

C.3.1 Loss Model Assumptions

The introduction of cooling air into the flowpath reduces the total pressure seen by the turbine. Strictly speaking, it is necessary to perform separate cooling-flow, mixing-loss, and rotor-work calculations separately for each cooled stator and rotor blade row.

To avoid this complication, a much simpler model will be used: The cooling air for all blade rows is assumed to be discharged entirely over the first IGV, and to fully mix out before flow enters the first turbine rotor. This seems to be a reasonable simplification given that the first IGV blade row typically requires the bulk of the cooling flow. The main motivation is that this model does not require work calculations to be performed for individual turbine stages, greatly simplifying the matching of overall compressor+fan and turbine work.

C.3.2 Loss Calculation

Figure C.3 shows the core and cooling mass flow paths assumed for the mixed-out state calculation. The cooling air is assumed to be bled off at the compressor exit, which defines the cooling-flow total temperature.

$$T_{ci} \;\; = \;\; T_{t3} \tag{C.20}$$

The cooling air is assumed to re-enter the flowpath over the first IGV.

The heat flow $\dot{Q}$ from the core flow to the metal and then to the cooling flow does not need to be considered here, since this heat flow is purely internal to the control volume spanning stations 4 and 4.1, for example.

The cooling flow is assumed to remain unmixed until some representative station 4a (e.g. somewhere between stagnation and IGV exit Mach), where it has velocity $u_c = r_{u_c} u_{4a}$, and the local static pressure p_{4a}. The mixing then occurs between 4a and 4.1, producing a total-pressure drop and ultimately resulting in a reduced core-flow exhaust velocity at station 6.

For clarity and convenience, the equations shown assume a constant c_p. In practice, the calculations would be performed using their equivalent variable-c_p forms.
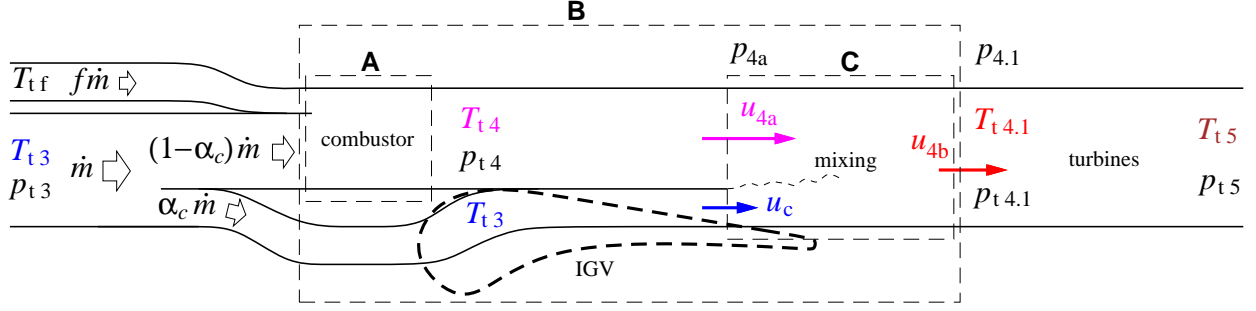
Figure C.3: Combustor and film-cooling flows, with mixing over and downstream of IGV. Dashed rectangles are control volumes.

Using control volume A, the heat-balance equation for the fuel/core mass flow ratio $f = \dot{m}_{\text{fuel}}/\dot{m}$ is as follows.

$$h_{\text{fuel}} f \dot{m} = \bar{c}_p \left(T_{t\,4} - T_{t\,3} \right) \left(1 - \alpha_c \right) \dot{m} + \bar{c}_p \left(T_{t\,4} - T_{t\,\text{f}} \right) f \dot{m} \tag{C.21}$$

$$f = \frac{\bar{c}_p \left(T_{t\,4} - T_{t\,3} \right) \left(1 - \alpha_c \right)}{h_{\text{fuel}} - \bar{c}_p \left(T_{t\,4} - T_{t\,\text{f}} \right)} \tag{C.22}$$

Using control volume B, the heat-balance equation for the mixed-out total temperature $T_{t\,4.1}$ is as follows.

$$h_{\text{fuel}} f \dot{m} = \bar{c}_p \left(T_{t\,4.1} - T_{t\,3} \right) \dot{m} + \bar{c}_p \left(T_{t\,4.1} - T_{t\,\text{f}} \right) f \dot{m} \tag{C.23}$$

$$T_{t\,4.1} = \frac{h_{\text{fuel}} f / \bar{c}_p + T_{t\,3} + T_{t\,\text{f}} f}{1 + f} \tag{C.24}$$

The core and cooling flow velocities u_{4a}, u_c are obtained from the specified M_{4a} and the velocity ratio r_{u_c}.

$$u_{4a} = \frac{M_{4a}}{\sqrt{1 + \frac{\gamma - 1}{2} M_{4a}^2}} \sqrt{\gamma R T_{t\,4}} \tag{C.25}$$

$$u_c = r_{u_c} u_{4a} \tag{C.26}$$

Neglecting the mixing pressure rise over control volume C, a momentum balance gives the mixed-out velocity $u_{4.1}$.

$$p_{4.1} \simeq p_{4a} = p_{t\,4} \left(1 + \frac{\gamma - 1}{2} M_{4a}^2 \right)^{-\gamma/(\gamma-1)} \tag{C.27}$$

$$(1 + f)\, \dot{m}\, u_{4.1} = (1 - \alpha_c + f)\, \dot{m}\, u_{4a} + \alpha_c\, \dot{m}\, u_c \tag{C.28}$$

$$u_{4.1} = u_{4a} \frac{(1 - \alpha_c + f) u_{4a} + \alpha_c\, u_c}{1 + f} \tag{C.29}$$

The mixed-out static temperature and total pressure then follow.

$$T_{4.1} = T_{t\,4.1} - \frac{1}{2} \frac{u_{4.1}^2}{c_p} \tag{C.30}$$

$$p_{t\,4.1} = p_{4.1} \left(\frac{T_{t\,4.1}}{T_{4.1}} \right)^{\gamma/(\gamma-1)} \tag{C.31}$$

These can now be used as effective turbine inlet conditions for turbine-work and pressure-drop calculations.

Appendix D

Thermally-Perfect Gas Calculations

D.1 Governing equations

Starting equations, with some assumed known $c_{p(T)}$:

$$dh - v\,dp = T\,ds \tag{D.1}$$
$$pv = RT \tag{D.2}$$
$$dh = c_{p(T)}\,dT \tag{D.3}$$

D.2 Complete enthalpy calculation

The complete enthalpy function is obtained by integration of the known $c_{p(T)}$ function,

$$h_{(T)} \equiv \Delta h_f + \int_{T_s}^{T} c_{p(T)}\,dT \tag{D.4}$$

where Δh_f is the heat of formation, and T_s is the standard condition at which Δh_f is defined, typically $T_s = 298\,\mathrm{K}$.

D.3 Pressure calculation

For an adiabatic compressor or turbine, the entropy change is specified via a polytropic efficiency

$$T\,ds = \left(1 - \eta_{\mathrm{pol}}{}^{\pm 1}\right) c_p\,dT \tag{D.5}$$

with $\eta_{\mathrm{pol}}{}^{+1}$ used when $dT > 0$ as in a compressor, and $\eta_{\mathrm{pol}}{}^{-1}$ used when $dT < 0$ as in a turbine, so that ds is always positive. All the above relations above are combined into the definition of an entropy-complement variable $\sigma_{(T)}$, which then defines $p_{(T)}$.

$$\frac{dp}{p} = \eta_{\mathrm{pol}}{}^{\pm 1}\frac{c_p}{R}\frac{dT}{T} = \eta_{\mathrm{pol}}{}^{\pm 1}\frac{d\sigma}{R} \tag{D.6}$$

$$\sigma_{(T)} \;\equiv\; \int_{T_s}^{T} c_{p(T)} \frac{dT}{T} \;=\; \int_{\ln T_s}^{\ln T} c_{p(\ln T)} \, d(\ln T) \tag{D.7}$$

$$p_{(T)} \;=\; p_0 \, \exp\!\left(\eta_{\mathrm{pol}}^{\pm 1} \frac{\sigma_{(T)} - \sigma_{(T_0)}}{R} \right) \tag{D.8}$$

The compression or expansion process is assumed to occur over $p_0 \ldots p$ and $T_0 \ldots T$.

D.4 Properties of a gas mixture

A gas mixture is specified with the mass fraction vector $\vec{\alpha}$, whose components are the mass fractions of the mixture constituents. Similarly, the components of $\vec{R}$, $\vec{c}_p$, $\vec{h}$, $\vec{\sigma}$ are gas properties of the constituents. The overall properties are then

$$R \;=\; \vec{\alpha} \cdot \vec{R} \tag{D.9}$$

$$c_{p(T)} \;=\; \vec{\alpha} \cdot \vec{c}_{p(T)} \tag{D.10}$$

$$h_{(T)} \;=\; \vec{\alpha} \cdot \vec{h}_{(T)} \tag{D.11}$$

$$\sigma_{(T)} \;=\; \vec{\alpha} \cdot \vec{\sigma}_{(T)} \tag{D.12}$$

D.5 Calculations for turbomachine components

The $()_t$ total-quantity subscript will be omitted here for convenience.

D.5.1 Compressor

In a compressor, the total-pressure ratio

$$\pi_{\mathrm{c}} \;=\; \frac{p_3}{p_2}$$

is typically specified. The inlet conditions p_2 and T_2 are also assumed known. The objective here is to determine the corresponding exit total temperature T_3.

We first recast the specified pressure ratio definition in residual form.

$$\ln \pi_{\mathrm{c}} \;=\; \ln \frac{p_3}{p_2} \;=\; \frac{\eta_{\mathrm{pol}}}{R} \left(\sigma_3 - \sigma_2 \right) \tag{D.13}$$

$$\mathcal{R}_{(T_3)} \;\equiv\; \frac{\sigma_{(T_3)}}{R} - \frac{\sigma_2}{R} - \frac{\ln \pi_{\mathrm{c}}}{\eta_{\mathrm{pol}}} \;=\; 0 \tag{D.14}$$

$$\mathcal{R}'_{(T_3)} \;\equiv\; \frac{d\mathcal{R}}{dT}_{(T_3)} \;=\; \frac{c_{p(T_3)}}{RT_3} \tag{D.15}$$

This is then solved for the unknown T_3 by the standard Newton method, with the sequence of progressively better iterates $T_3^1, T_3^2 \ldots T_3^n$. A good initial guess T_3^0 is obtained by assuming

a fixed isentropic exponent $(\gamma-1)/\gamma = R/c_p$ taken from the known $()_2$ condition.

$$c_{p2} = c_{p(T_2)} \tag{D.16}$$

$$T_3^0 = T_2\, \pi_c^{R/(c_{p2}\eta_{\mathrm{pol}})} \tag{D.17}$$

$$T_3^{n+1} = T_3^n - \frac{\mathcal{R}_{(T_3^n)}}{\mathcal{R}'_{(T_3^n)}} \tag{D.18}$$

After convergence, the exit h_3 is evaluated directly.

$$h_3 = h_{(T_3)} \tag{D.19}$$

D.5.2 Combustor

In a combustor, both the inlet and outlet temperatures T_3, T_4 are typically specified. The objective is to determine the fuel mass fraction.

It will be assumed that the fuel has the chemical form

$$C_{x_C}\, H_{x_H}\, O_{x_O}\, N_{x_N}$$

and the combustion reaction is limited to the fuel and atmospheric oxygen, and is complete (i.e. nitrogen oxide and carbon monoxide production is neglected).

$$C_{x_C}\, H_{x_H}\, O_{x_O}\, N_{x_N}\ +\ n_{O_2}\, O_2\ \rightarrow\ n_{CO_2}\, CO_2\ +\ n_{H_2O}\, H_2O\ +\ n_{N_2}\, N_2 \tag{D.20}$$

Equating the atom numbers gives the reaction mole numbers.

$$n_{O_2} = x_C + x_H/4 - x_O/2 \tag{D.21}$$

$$n_{CO_2} = x_C \tag{D.22}$$

$$n_{H_2O} = x_H/2 \tag{D.23}$$

$$n_{N_2} = x_N/2 \tag{D.24}$$

Using mole numbers together with the atomic masses

$$m_C = 12.01$$
$$m_H = 1.01$$
$$m_O = 16.00$$
$$m_N = 14.01$$

gives the reactant masses.

$$M_{O_2} = n_{O_2}\,(2m_O) \tag{D.25}$$

$$M_{CO_2} = n_{CO_2}\,(m_C + 2m_O) \tag{D.26}$$

$$M_{H_2O} = n_{H_2O}\,(2m_H + m_O) \tag{D.27}$$

$$M_{N_2} = n_{N_2}\,(2m_N) \tag{D.28}$$

$$M_{\mathrm{fuel}} = x_C\, m_C + x_H\, m_H + x_O\, m_O + x_N\, m_N \tag{D.29}$$

The following mass fraction vector components are then calculated.

	i	α_i	β_i	γ_i
N_2	1	0.781	0	M_{N_2}/M_{fuel}
O_2	2	0.209	0	$-M_{O_2}/M_{\text{fuel}}$
CO_2	3	0.0004	0	M_{CO_2}/M_{fuel}
H_2O	4	0	0	M_{H_2O}/M_{fuel}
Ar	5	0.0096	0	0
fuel	6	0	1	0

Here, β_i gives the composition of the fuel, while γ_i gives the air constituent fractional changes over the reaction. The fraction vector component sums are all exactly $\sum \alpha_i = 1$, $\sum \beta_i = 1$, $\sum \gamma_i = 1$.

The total enthalpies of all the constituents are known from the specified T_3 and T_4, and also at the known fuel temperature T_{f}.

$$\vec{h}_3 = h_{i(T_3)} \tag{D.30}$$

$$\vec{h}_4 = h_{i(T_4)} \tag{D.31}$$

$$\vec{h}_{\text{f}} = h_{i(T_{\text{f}})} \tag{D.32}$$

The enthalpy balance across the combustor is

$$\dot{m}_{\text{air}}\, \vec{\alpha} \cdot \vec{h}_3 \;+\; \dot{m}_{\text{fuel}}\, \vec{\beta} \cdot \vec{h}_{\text{f}} \;=\; \dot{m}_{\text{air}}\, \vec{\alpha} \cdot \vec{h}_4 \;+\; \dot{m}_{\text{fuel}}\, \vec{\gamma} \cdot \vec{h}_4 \tag{D.33}$$

so that the fuel mass fraction is obtained directly.

$$f \equiv \frac{\dot{m}_{\text{fuel}}}{\dot{m}_{\text{air}}} = \frac{\vec{\alpha} \cdot \vec{h}_4 - \vec{\alpha} \cdot \vec{h}_3}{\vec{\beta} \cdot \vec{h}_{\text{f}} - \vec{\gamma} \cdot \vec{h}_4} \tag{D.34}$$

The mass fraction vector $\vec{\lambda}$ of the combustion products is obtained from the mass balance across the combustor,

$$(\dot{m}_{\text{air}} + \dot{m}_{\text{fuel}})\, \vec{\lambda} \;=\; \dot{m}_{\text{air}}\, \vec{\alpha} \;+\; \dot{m}_{\text{fuel}}\, \vec{\gamma} \tag{D.35}$$

$$\vec{\lambda} = \frac{\vec{\alpha} + f\vec{\gamma}}{1 + f} \tag{D.36}$$

which can then be used to obtain the net properties of the combustion products.

$$R_4 = \vec{\lambda} \cdot \vec{R}_4 \tag{D.37}$$

$$c_{p4} = \vec{\lambda} \cdot \vec{c}_{p4} \tag{D.38}$$

D.5.3 Mixer

Mixing will typically occur between the combustor discharge flow and the turbine cooling flow. In general, the two streams will have two different chemical compositions specified by their mass fraction vectors $\vec{\lambda}_a$ and $\vec{\lambda}_b$, two different temperatures T_a and T_b, and two different

enthalpies $\vec{h}_a = h_{i(T_a)}$ and $\vec{h}_b = h_{i(T_b)}$. The species mass flow balance gives the composition mass fraction vector $\vec{\lambda}$ of the mixed gas.

$$(\dot{m}_a + \dot{m}_b)\,\vec{\lambda} = \dot{m}_a\,\vec{\lambda}_a + \dot{m}_b\,\vec{\lambda}_b \tag{D.39}$$

$$\vec{\lambda} = \frac{\dot{m}_a\,\vec{\lambda}_a + \dot{m}_b\,\vec{\lambda}_b}{\dot{m}_a + \dot{m}_b} \tag{D.40}$$

Assuming no chemical reaction takes place, the enthalpy balance equation is

$$(\dot{m}_a + \dot{m}_b)\,\vec{\lambda}\cdot\vec{h}_{(T)} = \dot{m}_a\,\vec{\lambda}_a\cdot\vec{h}_a + \dot{m}_b\,\vec{\lambda}_b\cdot\vec{h}_b \tag{D.41}$$

which can be numerically inverted for the mixed temperature T.

D.5.4   Turbine

In a turbine, the total-enthalpy difference is typically known from the compressor–turbine work balance.

$$(\dot{m}_{\text{air}} + \dot{m}_{\text{fuel}})(h_5 - h_4) = \dot{m}_{\text{air}}(h_2 - h_3) \tag{D.42}$$

$$\Delta h \equiv h_5 - h_4 = \frac{h_2 - h_3}{1 + f} \tag{D.43}$$

The objective here is to determine the corresponding total-pressure ratio.

$$\pi_{\text{t}} = \frac{p_5}{p_4} \tag{D.44}$$

The procedure is similar to that for the compressor, except that $h_{(T)}$ is used in the Newton residual.

$$\mathcal{R}_{(T_5)} \equiv h_{(T_5)} - h_4 - \Delta h = 0 \tag{D.45}$$

$$\mathcal{R}'_{(T_5)} \equiv \frac{d\mathcal{R}}{dT}_{(T_5)} = c_{p(T_5)} \tag{D.46}$$

The Newton method is started by assuming a fixed c_p taken from the known $()_4$ condition.

$$c_{p_4} = c_{p(T_4)} \tag{D.47}$$

$$T_5^0 = T_4 + \Delta h/c_{p_4} \tag{D.48}$$

$$T_5^{n+1} = T_5^n - \frac{\mathcal{R}_{(T_5^n)}}{\mathcal{R}'_{(T_5^n)}} \tag{D.49}$$

After convergence, the total-pressure ratio and p_5 are evaluated directly.

$$\pi_{\text{t}} = \exp\left(\frac{1}{\eta_{\text{pol}}}\frac{\sigma_{(T_5)} - \sigma_{(T_4)}}{R}\right) \tag{D.50}$$

$$p_5 = p_4\,\pi_{\text{t}} \tag{D.51}$$

D.5.5 Inlet or Nozzle

An inlet or nozzle with losses can be considered as a turbine with zero efficiency, and is typically specified via a total-pressure drop ratio.

$$\pi_i = \frac{p_2}{p_0} \tag{D.52}$$

In the limit $\eta_{\mathrm{pol}} \to 0$, the turbine case above then reduces to the trivial relations

$$p_2 = p_0 \, \pi_i \tag{D.53}$$
$$T_2 = T_0 \tag{D.54}$$
$$h_2 = h_{(T_2)} = h_0 \tag{D.55}$$

with no need for Newton iteration.

Appendix: Spline representations

General

A cubic spline representation of a function $y_{(x)}$ requires the following discrete values at $i = 1, 2 \ldots N$ nodes:

x_i spline parameter values
y_i function values
y'_i function derivative values, $(dy/dx)_i$

On each interval $i - 1 \ldots i$, the four end values $y_{i-1}, y_i, y'_{i-1}, y'_i$ uniquely define a cubic-polynomial $y_{(x)}$ over that interval. The union of all intervals then defines the overall $y_{(x)}$ function.

The derivative values y'_i are obtained from x_i, y_i by solving a linear system of equations expressing 2nd-derivative continuity across all the interior nodes $i = 2, 3 \ldots N-1$, together with two zero 3rd-derivative end conditions at $i = 1, N$. This system of equations produces a tridiagonal matrix which is very rapidly solved in $\mathcal{O}(N)$ arithmetic operations.

Current application

Two splines are first generated using the tabulated values T_i, c_{p_i}:

1) $c_{p(T)}$ spline:

$$
\begin{aligned}
x_i &= T_i & \text{(table values)} \\
y_i &= c_{p_i} & \text{(table values)} \\
y'_i &= (dc_p/dT)_i & \text{(via spline system solution)}
\end{aligned}
$$

2) $c_{p(\ln T)}$ spline:

$$
\begin{aligned}
x_i &= \ln(T_i) & \text{(table values)} \\
y_i &= c_{p_i} & \text{(table values)} \\
y'_i &= (dc_p/d\ln T)_i & \text{(via spline system solution)}
\end{aligned}
$$

Then two related splines $h_{(T)}$, $\sigma_{(\ln T)}$ are constructed as follows, with Δh_f being the heat of formation.

3) $h_{(T)}$ spline:

$$
\begin{aligned}
x_i &= T_i \\
y'_i &= c_{p_i} \\
y_i &= \Delta h_f + \int_{T_s}^{T_i} c_{p(T)} \, dT
\end{aligned}
$$

4) $\sigma_{(\ln T)}$ spline:

$$
\begin{aligned}
x_i &= \ln(T_i) \\
y'_i &= c_{p_i} \\
y_i &= \int_{\ln T_s}^{\ln T_i} c_{p(\ln T)} \, d(\ln T)
\end{aligned}
$$

Since the splined $c_{p(T)}$ and $c_{p(\ln T)}$ are piecewise-cubic, exact integrations can be used here to give perfect consistency between the related splines.

Appendix E

Simplified Viscous/Inviscid Analysis for Nearly-Axisymmetric Bodies

E.1 Summary

The method described here uses a compressible extension of the old Von Karman airship method [22] to describe the potential flow, and an axisymmetric version of the integral boundary layer formulation of XFOIL [23] to describe the surface boundary layer and trailing wake. The two formulations are strongly coupled and solved simultaneously using the XFOIL methodology. Effects such as flow separation can thus be captured. The intent of this strongly-coupled viscous/inviscid method is to obtain reasonable drag prediction accuracy together with extreme computational speed.

E.2 Geometry

The body geometry is described by the area $A_{(x)}$ and perimeter $b_{0(x)}$ distributions, as shown in Figure E.1, with x being the axial coordinate. For a body of circular cross-section these are related by

$$4\pi A \;\; = \;\; b_0^2 \qquad\qquad \text{(round body)} \qquad\qquad \text{(E.1)}$$

but considering them to be independent allows reasonably accurate drag calculation of bodies which are slender but not axisymmetric.

E.3 Potential Flow Calculation

To compute the potential flow, an equivalent axisymmetric body of radius $R_{(x)}$ is first defined.

$$R_{(x)} \;\; = \;\; \sqrt{\frac{A_{(x)}}{\pi}} \qquad\qquad\qquad \text{(E.2)}$$
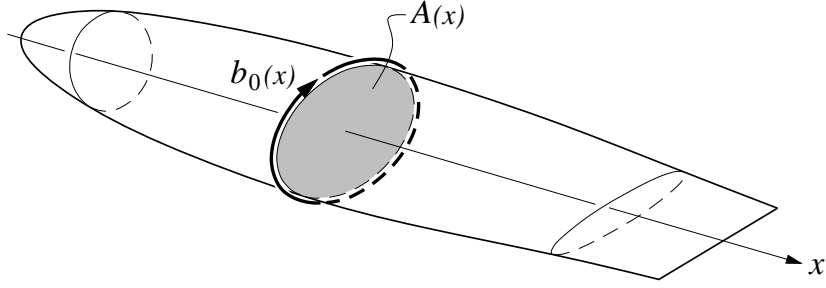
Figure E.1: Slender body with cross-sectional area $A_{(x)}$ and perimeter $b_{0(x)}$.
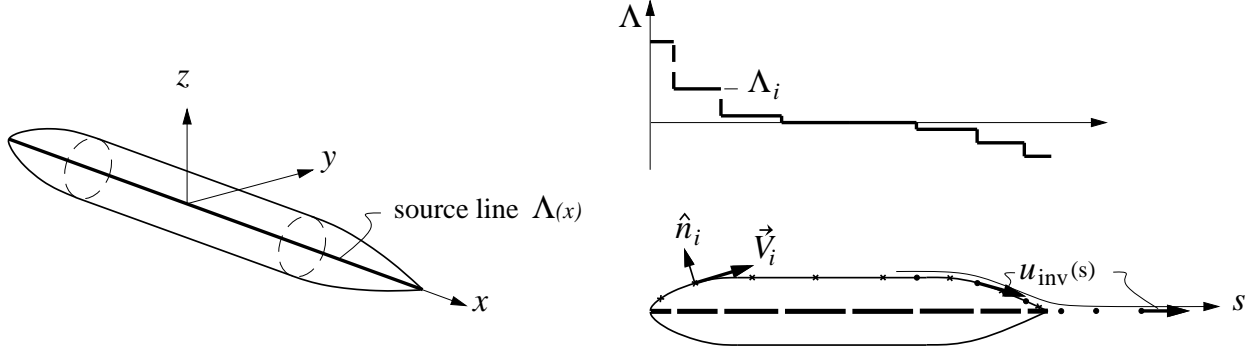

Figure E.2: Fuselage potential flow model using compressible source line on axis.

The compressible potential flow about this body is represented with piecewise-constant line sources placed on the axis, as sketched in Figure E.2.

The cartesian perturbation velocities of $i = 1, 2 \ldots n$ such segments located between points $x_1, x_2, \ldots x_{n+1}$ are

$$u(x, y, z) \;=\; \sum_{i=1}^{n} \frac{\Lambda_i}{4\pi\,\beta^2} \left(\frac{1}{r_{i+1}} - \frac{1}{r_i} \right) \tag{E.3}$$

$$v(x, y, z) \;=\; \sum_{i=1}^{n} \frac{\Lambda_i}{4\pi\,\beta} \left(\frac{x_{i+1}-x}{r_{i+1}} - \frac{x_i-x}{r_i} \right) \frac{\beta y}{(\beta y)^2 + (\beta z)^2} \tag{E.4}$$

$$w(x, y, z) \;=\; \sum_{i=1}^{n} \frac{\Lambda_i}{4\pi\,\beta} \left(\frac{x_{i+1}-x}{r_{i+1}} - \frac{x_i-x}{r_i} \right) \frac{\beta z}{(\beta y)^2 + (\beta z)^2} \tag{E.5}$$

$$\text{where} \qquad \beta^2 \;\equiv\; 1 - M_\infty^2 \tag{E.6}$$

$$r_i(x, y, z) \;\equiv\; \sqrt{(x-x_i)^2 + (\beta y)^2 + (\beta z)^2} \tag{E.7}$$

$$r_{i+1}(x, y, z) \;\equiv\; \sqrt{(x-x_{i+1})^2 + (\beta y)^2 + (\beta z)^2} \tag{E.8}$$

Setting flow tangency at each of the n control points on the actual body surface with normal vectors $\hat{n}_i$

$$\left[(V_\infty + u)\,\hat{\imath} \,+\, v\,\hat{\jmath} \,+\, w\,\hat{k} \right]_i \cdot \hat{n}_i \;=\; 0 \tag{E.9}$$

gives a $n \times n$ linear system for the source strengths Λ_i. Because the control points are not immediately adjacent to the source elements, this system becomes increasingly ill-conditioned

as n is increased, especially with non-slender bodies. However, with the cosine spacing sketched in Figure E.2, essentially converged results are obtained for $n = 25$ or less, with very great computational economy.

A proper axisymmetric panel method is of course an alternative to the present approach, but would greatly increase the code complexity, and also the system setup time which would dominate the system solution time for these small number of unknowns. These additional drawbacks favor the simple present approach.

E.4 Viscous Flow Calculation

E.4.1 Axisymmetric boundary layer and wake equations

All viscous calculations are performed in the meridional arc length coordinate s, defined from the equivalent $R_{(x)}$ distribution.

$$s_{(x)} = \int^x \sqrt{1 + (dR/dx)^2} \, dx \tag{E.10}$$

This is continued into the wake where $R = 0$ is specified.

The axisymmetric momentum and kinetic energy boundary layer equations governing the viscous boundary layers and wake are as follows.

$$\frac{d \left(\rho_e u_e^2 \Theta \right)}{ds} = b \frac{\tau_w}{2} - \rho_e u_e \Delta^* \frac{du_e}{ds} \tag{E.11}$$

$$\frac{d \left(\frac{1}{2} \rho_e u_e^3 \Theta^* \right)}{ds} = (b\mathcal{D}) - \rho_e u_e^2 \Delta^{**} \frac{du_e}{ds} \tag{E.12}$$

Here, b is an effective perimeter shown in Figure E.3 which arises when the various areas Δ^*, Θ etc. in the equations above are approximated with their 2D equivalents.

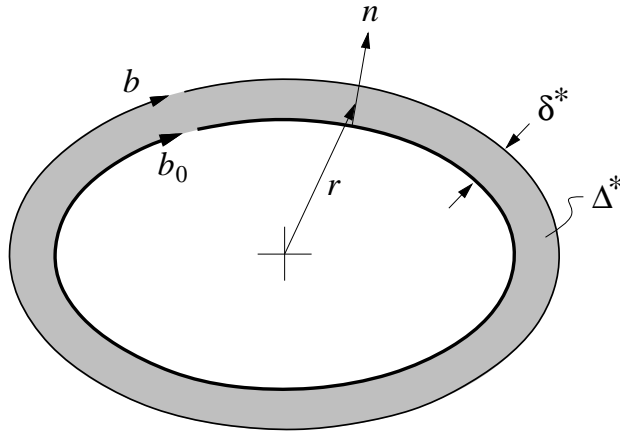Figure E.3: Body perimeter b_0, displacement area Δ^*, and effective perimeter b.

For example, the definition of the displacement area is

$$\Delta^* = \int_0^{n_e} \left(1 - \frac{\rho u}{\rho_e u_e} \right) 2\pi r \, dn \tag{E.13}$$

107

which has the somewhat awkward radius r inside the integral. This is suitably approximated by its average value over the layer thickness, by using the 2D displacement thickness itself,

$$2\pi r \simeq b_0 + 2\pi\delta^* \equiv b \tag{E.14}$$

so that the modified perimeter b is taken as a suitable approximate value for the local perimeter $2\pi r_{(n)}$ over the integral. This allows all the viscous areas to be expressed in terms of the more familar 2D integral thicknesses as follows.

$$\delta^* = \int_0^{n_e} \left(1 - \frac{\rho u}{\rho_e u_e}\right) dn \tag{E.15}$$

$$\theta = \int_0^{n_e} \left(1 - \frac{u}{u_e}\right) \frac{\rho u}{\rho_e u_e} dn \tag{E.16}$$

$$\theta^* = \int_0^{n_e} \left(1 - \frac{u^2}{u_e^2}\right) \frac{\rho u}{\rho_e u_e} dn \tag{E.17}$$

$$\delta^{**} = \int_0^{n_e} \left(1 - \frac{u^2}{u_e^2}\right) \frac{\rho u}{\rho_e u_e} dn \tag{E.18}$$

$$\Delta^* = \int_0^{n_e} \left(1 - \frac{\rho u}{\rho_e u_e}\right) 2\pi r \, dn \simeq b\,\delta^* \tag{E.19}$$

$$\Theta = \int_0^{n_e} \left(1 - \frac{u}{u_e}\right) \frac{\rho u}{\rho_e u_e} 2\pi r \, dn \simeq b\,\theta \tag{E.20}$$

$$\Theta^* = \int_0^{n_e} \left(1 - \frac{u^2}{u_e^2}\right) \frac{\rho u}{\rho_e u_e} 2\pi r \, dn \simeq b\,\theta^* \tag{E.21}$$

$$\Delta^{**} = \int_0^{n_e} \left(1 - \frac{\rho}{\rho_e}\right) \frac{u}{u_e} 2\pi r \, dn \simeq b\,\delta^{**} \tag{E.22}$$

The dissipation integral is also defined in terms of its 2D form.

$$\mathcal{D} = \int_0^{n_e} \tau \frac{\partial u}{\partial n} \, dn \tag{E.23}$$

$$(b\mathcal{D}) = \int_0^{n_e} \tau \frac{\partial u}{\partial n} 2\pi r \, dn \simeq b\,\mathcal{D} \tag{E.24}$$

Using the approximate area definitions above, equations (E.11) and (E.12) are put in their equivalent logarithmic differential forms.

$$d\ln\theta + d\ln b = \frac{s}{\theta}\frac{C_f}{2} d\ln s - \left(H + 2 - M_e^2\right) d\ln u_e \tag{E.25}$$

$$d\ln H^* = \left(\frac{s}{\theta}\frac{2C_{\mathcal{D}}}{H^*} - \frac{s}{\theta}\frac{C_f}{2}\right) d\ln s - \left(\frac{2H^{**}}{H^*} + 1 - H\right) d\ln u_e \tag{E.26}$$

Equation (E.26) is actually the difference between the logarithmic forms of equations (E.12) and (E.11). The usual 2D shape parameter is defined as

$$H = \frac{\delta^*}{\theta} \tag{E.27}$$

and the 2D integral relations

$$\frac{\tau_w}{\frac{1}{2}\rho_e u_e^2} = C_f(H, Re_\theta, M_e^2) \tag{E.28}$$

$$\frac{\mathcal{D}}{\rho_e u_e^3} = C_{\mathcal{D}}(H, Re_\theta, M_e^2) \tag{E.29}$$

$$\frac{\theta^*}{\theta} = H^*(H, Re_\theta, M_e^2) \tag{E.30}$$

$$\frac{\delta^{**}}{\theta} = H^{**}(H, Re_\theta, M_e^2) \tag{E.31}$$

are used to close the equations. Except for the trivial additional term $d\ln b$ in (E.25), all these relations are identical to their 2D forms, so that an existing 2D implementation can be used with only minimal modification.

E.4.2 Direct BL solution

In the classical BL formulation, $u_{e(s)}$ is prescribed to be the inviscid velocity, e.g.

$$u_e = u_{\text{inv}} \tag{E.32}$$

This can be obtained from the Λ_i strengths computed above, by using them in the u, v, w summations (E.3,E.4,E.5) to compute the inviscid surface tangential velocities $u_{\text{inv}(s)}$ along the surface and also into the wake.

$$u_{\text{inv}(s)} = \sqrt{u^2 + v^2 + w^2} \tag{E.33}$$

Once $u_{e(s)}$ is specified, then equations (E.25) and (E.26) can in principle be solved for the boundary layer variables $\theta_{(s)}, \delta^*_{(s)}$ by usual downstream ODE integration. However, if separation is encountered this integration will fail, since $dH^*/dH \simeq 0$ at separation, and equation (E.26) cannot then be used to obtain the necessary $d\delta^*/ds$ form for integration.

E.4.3 Viscous/Inviscid interacted solution

The present method eliminates the separation problem by the usual viscous/inviscid interaction formulation. Using the wall-blowing concept, the actual viscous edge velocities $u_{e(s)}$ seen by the boundary layer and wake are modified by adding contributions from the apparent wall-blowing sources, assumed to be axisymmetric point sources at the $j \ldots j{+}1$ interval midpoints.

$$u_{e_i} = u_{\text{inv}_i} + \frac{1}{\rho_{e_i}} \sum_j \frac{1}{4\pi} \frac{m_{j+1} - m_j}{\left| s_i - \frac{1}{2}(s_{j+1}{+}s_j) \right| \left(s_i - \frac{1}{2}(s_{j+1}{+}s_j) \right)} \tag{E.34}$$

Here, m is the axisymmetric mass defect, defined by

$$m = \rho_e u_e \Delta^* = \int_0^{n_e} (\rho_e u_e - \rho u)\, 2\pi r\, dn \simeq \rho_e u_e \delta^*(b_0 + 2\pi\delta^*) \tag{E.35}$$

which is a quadratic equation giving δ^* in terms of m and u_e.

$$\delta^* = \frac{1}{4\pi}\left(-b_0 + \sqrt{b_0^2 + \frac{8\pi\,m}{\rho_e u_e}}\right) \tag{E.36}$$

The summation (E.34) can be put into a more concise form by precomputation of the mass-influence matrix d_{ij} which depends only on the geometry.

$$u_{e_i} = u_{\text{inv}_i} + \frac{1}{\rho_{e_i}}\sum_j d_{ij}\,m_j \tag{E.37}$$

$$d_{ij} = \frac{1}{4\pi}\left[\frac{1}{\left|s_i - \frac{1}{2}(s_j+s_{j-1})\right|\left(s_i - \frac{1}{2}(s_j+s_{j-1})\right)}\right.$$
$$\left. - \frac{1}{\left|s_i - \frac{1}{2}(s_{j+1}+s_j)\right|\left(s_i - \frac{1}{2}(s_{j+1}+s_j)\right)}\right] \tag{E.38}$$

In the viscous/inviscid solution scheme, the boundary layer equations (E.25) and (E.26) are solved together with the u_e definition equation (E.37), to obtain the overall solution $\theta_{(s)}$, $\delta^*_{(s)}$, $u_{e(s)}$. Only the inviscid velocity $u_{\text{inv}(s)}$ is prescribed. Because equation (E.37) has global influence, the equations are not solved by marching, but instead are solved "everywhere" at once by a global Newton iteration. An initial maching calculation with $u_e = u_{\text{inv}}$ prescribed (and necessarily modified at separation) is still used to obtain a good initial guess to start the Newton cycle.

E.4.4 Drag and dissipation calculation

In the absence of any boundary layer ingestion, the body profile drag is simply the momentum defect at the end of the wake.

$$D = (\rho_e u_e^2 \Theta)_{\text{wake}} \tag{E.39}$$

$$C_D = \frac{2\Theta_{\text{wake}}}{S_{\text{ref}}} \tag{E.40}$$

The overall surface + wake viscous dissipation is the kinetic energy defect at the end of the wake, with a density-flux thickness correction.

$$\Phi_{\text{surf}} + \Phi_{\text{wake}} = \int_0^\infty b\mathcal{D}\,ds = (\rho_e u_e^3 \Theta^*)_{\text{wake}} + \int_0^\infty b\rho_e u_e^2 \Delta^{**}\frac{du_e}{ds}\,ds \tag{E.41}$$

$$= DV_\infty \tag{E.42}$$

The overall calculation gives reliable fuselage drag and dissipation predictions for any reasonable fuselage shape, without the need to rely on effective wetted area correlations, closure-angle correlations, or effective fineness-ratio correlations. For example, if the rear closure of the body is too rapid, the present method will simply predict separation off the back and into the wake, together with the increased dissipation leading to an increase in the downstream wake defect which reflects the larger drag.

It's useful to note that the individual 2D thicknesses θ, δ^* significantly depend on exactly how the effective perimeter b is defined. For example, in the wake where $b_0 = 0$, the momentum and kinetic energy area breakdowns become

$$\Theta \; = \; b\,\theta \; = \; 2\pi\delta^*\,\theta \tag{E.43}$$

$$\Theta^* \; = \; b\,\theta^* \; = \; 2\pi\delta^*\,\theta^* \tag{E.44}$$

So for example if the factor of 2π in the b definition (E.14) is modified somewhat because of a non-circular body cross section, then the θ, θ^* and δ^* values will change somewhat. However, because equations (E.11) and (E.12) evolve the full momentum and K.E. defects, these defects are extremely insensitive to how they are broken down into the θ, θ^*, and δ^* components in (E.43) and (E.44). So the computed drag and dissipation are also insensitive to such modeling ambiguities, since they depends only on the overall Θ and Θ^*. This justifies the somewhat ad-hoc definitions of b in the various integral area approximations.

For related reasons, the present drag and dissipation calculation method is surprisingly accurate for bodies which are not quite axisymmetric. If the flow is slender but not quite axisymmetric, the local 2D momentum defect $\rho_e u_e^2 \theta$ might vary considerably at any given x location. In Figure E.3, for example, the corresponding δ^* might be very nonuniform around the perimeter. A typical cause is redistribution of the viscous fluid via crossflow, from a small angle of attack, for instance. However, the circumferential integral of $\rho_e u_e^2 \theta$ will average out this redistribution, and since this integral is simply the total momentum defect,

$$\int \rho_e u_e^2\, \theta \; db \; = \; \rho_e u_e^2\, \Theta \tag{E.45}$$

the overall drag will also be very insensitive to such redistribution. The same argument follows for the kinetic energy thicknesses. Hence, accurate drag and dissipation predictions are still expected for weakly non-axisymmetric flows.

Appendix F

Power Accounting with Boundary Layer Ingestion

F.1   General Power Balance

The general power balance relation for an aircraft is written as follows.

$$(P_{K_\text{inl}} + P_V) + (P_{K_\text{out}} - \Phi_\text{jet}) = \Phi_\text{surf} + \Phi_\text{wake} + \dot{E}_\text{v} + W\dot{h} \tag{F.1}$$

F.2   Isolated–Propulsor Case

For an isolated-propulsion case without Boundary Layer Ingestion (BLI) all the terms above reduce as follows.

$$P_{K_\text{inl}} + P_V = 0 \tag{F.2}$$

$$P_{K_\text{out}} - \Phi_\text{jet} = \iint_\text{out} \rho V_\infty u \, (V_\infty + u) \, dA = \iint_\text{out} V_\infty u \, d\dot{m} = F V_\infty \tag{F.3}$$

$$\Phi_\text{surf} + \Phi_\text{wake} = D_p V_\infty \tag{F.4}$$
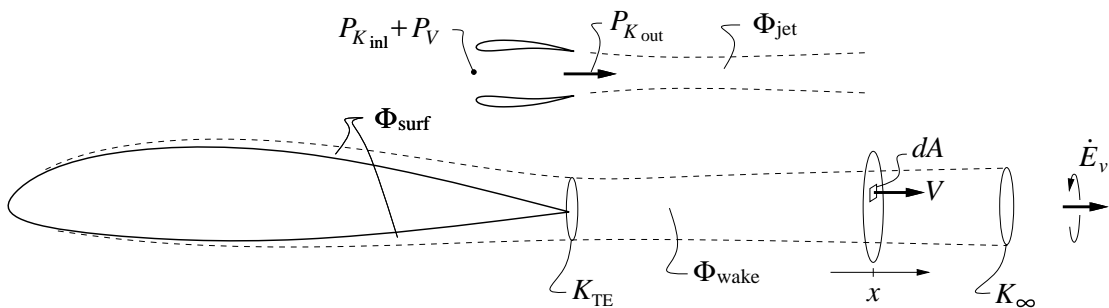
$$\dot{E}_\text{v} = D_i V_\infty \tag{F.5}$$

Figure F.1: Power terms in non-ingesting airframe and propulsion system.

As expected for this case, the above can then be combined into the usual force-balance relation.

$$FV_\infty = D_p V_\infty + D_i V_\infty + W\dot{h} \qquad \text{(F.6)}$$

which is compared term-by-term with (F.1) in the top half of Figure F.2. Equation (F.6) can be considered as a formula for the thrust F necessary to achieve a required climb rate $\dot{h}$, or as a formula for the climb rate $\dot{h}$ which results from a given thrust and total drag, at a given flight speed. Corresponding interpretations will be made for the equivalent equation in the BL-ingesting case, considered next.
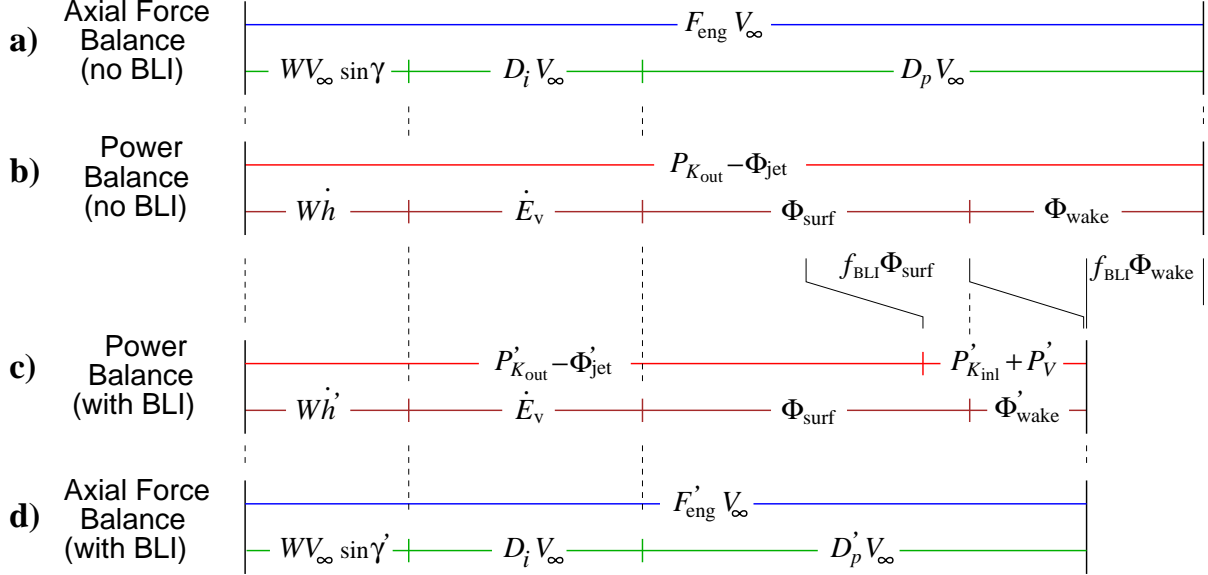

Figure F.2: Force balance compared to power balance (top half of figure). Power balance readily addresses the BLI case, and can be interpreted as equivalent forces (bottom half of figure). Primes $(\,)'$ denote quantities which are significantly modified by the BLI.

It's useful to first define the viscous kinetic energy defect K, and the density-flux defect Q,

$$K_{(x)} \equiv \iint \tfrac{1}{2}\left(V_e^2 - V^2\right)\rho V\, dA = \tfrac{1}{2}\rho_e V_e^3 \Theta^* \qquad \text{(F.7)}$$

$$Q_{(x)} \equiv \iint (\rho_e - \rho) V\, dA = \rho_e V_e \Delta^{**} \qquad \text{(F.8)}$$

where Θ^* is the kinetic energy area and Δ^{**} is the density-flux area. The integrals are over a plane in the viscous layer, normal to the flow at some x location, shown in Figure F.1.

For the incompressible case, where $Q = \Delta^{**} = 0$, K is simply related to the various terms in (F.1) as follows.

$$\Phi_{\text{surf}} = K_{TE} \qquad \text{(F.9)}$$

$$\Phi_{\text{wake}} = K_\infty - K_{TE} \qquad \text{(F.10)}$$

$$D_p V_\infty = K_\infty \qquad \text{(F.11)}$$

If density variations and hence Q are significant, then surface integrals of Q must be included:

$$\Phi_{\text{surf}} = K_{TE} + \int_{\text{surf}} Q\, V_e \frac{\partial V_e}{\partial x}\, dx \qquad \text{(F.12)}$$

113

$$\Phi_{\text{wake}} \;\; = \;\; K_\infty \;-\; K_{TE} \;+\; \int_{\text{wake}} Q\, V_e \frac{\partial V_e}{\partial x}\, dx \tag{F.13}$$

The Q contributions scale as the local M_e^2, and for typical high subsonic flows contribute perhaps $\sim 5\%$ to the total Φ_{surf} and Φ_{wake}. They will be omitted here for physical clarity.

F.3 Ingesting–Propulsor Case

Primes $(\;)'$ will now be used to denote ingestion-case quantities, which will be expressed in terms of the non-ingestion-case quantities above.
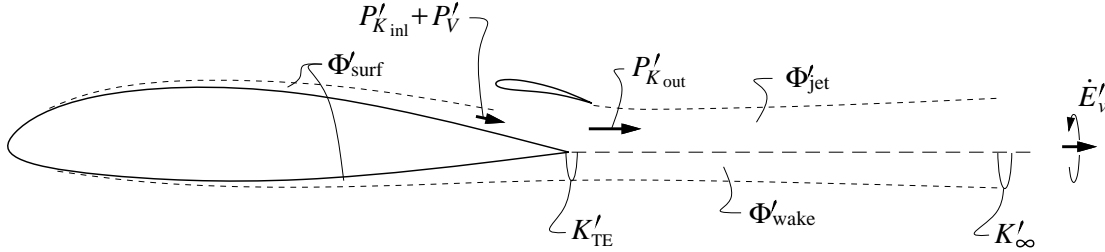

Figure F.3: Power terms in ingesting airframe and propulsion system.

The propulsor is assumed to ingest a fraction f_{BLI} of the body's kinetic energy defect at the trailing edge, so that the inlet P_K term is now no longer zero.

$$(P_{K_{\text{inl}}} \;+\; P_V)' \;\; = \;\; f_{\text{BLI}} K_{TE} \;\; = \;\; f_{\text{BLI}}\, \Phi_{\text{surf}} \tag{F.14}$$

Furthermore, the defect flowing into the wake is reduced by the same amount, so that the amount of rotational fluid flowing into the wake, and the associated wake dissipation are reduced correspondingly.

$$K'_{TE} \;\; = \;\; (1-f_{\text{BLI}}) K_{TE} \tag{F.15}$$
$$\Phi'_{\text{wake}} \;\; = \;\; (1-f_{\text{BLI}})\, \Phi_{\text{wake}} \tag{F.16}$$

In contrast, the surface dissipation occurs upstream of the propulsor and hence is largely unaffected. The trailing vortex system and hence the induced power are also unaffected.

$$\Phi'_{\text{surf}} \;\; = \;\; \Phi_{\text{surf}} \tag{F.17}$$
$$\dot{E}'_{\text{v}} \;\; = \;\; \dot{E}_{\text{v}} \tag{F.18}$$

Inserting all these primed quantities into the general power balance relation (F.1) gives

$$\boxed{(P_{K_{\text{inl}}} + P_V)' \;+\; (P_{K_{\text{out}}} - \Phi_{\text{jet}})' \;\; = \;\; \Phi'_{\text{surf}} \;+\; \Phi'_{\text{wake}} \;+\; \dot{E}'_{\text{v}} \;+\; W\dot{h}'} \tag{F.19}$$

or $\quad (P_{K_{\text{inl}}} + P_V)' \;+\; (P_{K_{\text{out}}} - \Phi_{\text{jet}})' \;\; = \;\; \Phi_{\text{surf}} \;+\; (1-f_{\text{BLI}})\Phi_{\text{wake}} \;+\; \dot{E}_{\text{v}} \;+\; W\dot{h}'$ (F.20)

Replacing these Φ and $\dot{E}_{\text{v}}$ in terms of the more familiar drag quantities (all defined for the non-ingesting case), we have the following force-balance equation.

$$\boxed{F'V_\infty \;\; = \;\; D_p V_\infty \;-\; f_{\text{BLI}}\Phi_{\text{wake}} \;+\; D_i V_\infty \;+\; W\dot{h}'} \tag{F.21}$$

Although the equivalent-force relation (F.21) is usable, it has a potential problem in that D_p and Φ_{wake} are both hypothetical for the BLI case, in that they correspond to the non-BLI case which really does not exist. Hence, it would be difficult to apply to high-fidelity calculations since both the BLI and non-BLI cases would then need to be computed, even though the non-BLI case is geometrically different and may be unrealizable. In contrast, the power-balance relation (F.19) is given only in term of the BLI-case quantities which really exist.

Setting aside such interpretation or computability issues, equation (F.21) can be treated as a formula for either F' or $\dot{h}'$. However, the modified thrust F' needs more careful consideration. By definition, it is credited with the normally positive inlet defect $f_{\text{BLI}}K_{TE}$.

$$
\begin{aligned}
F'V_\infty &\equiv (P_{K_{\text{inl}}} + P_V)' + (P_{K_{\text{out}}} - \Phi_{\text{jet}})' \\
&\simeq f_{\text{BLI}}K_{TE} + \iint_{\text{out}} \rho V_\infty u' (V_\infty + u')\, dA \\
&= f_{\text{BLI}}K_{TE} + \iint_{\text{out}} V_\infty u'\, d\dot{m}'
\end{aligned}
\tag{F.22}
$$

This is consistent with a basic momentum argument, that as the velocity into a propulsor is reduced with the power input fixed, the "ram drag" is reduced and the net thrust will naturally increase.

However, when u' and $\dot{m}'$ in (F.22) are computed with an engine-cycle calculation, it is necessary to account for the ingested defect $f_{\text{BLI}}K_{TE}$, via a reduced inlet total pressure for example. The resulting engine parameters will then be different from the non-ingesting case, hence the primes on u' and $\dot{m}'$ above. Additional distortion-related component losses may also be included if deemed appropriate. In any case, this inlet defect will definitely have a fuel-burn penalty which can more than offset the otherwise large gain of the $f_{\text{BLI}}K_{TE}$ credit term in the final thrust power $F'V_\infty$ in (F.22). If this cancellation is perfect, then the only gain of ingestion is the $-f_{\text{BLI}}\Phi_{\text{wake}}$ term in the overall power-balance equation (F.21).

F.4 Incorporation into Range Equation

Starting from the general power balance equation (F.1), with $\dot{h} = 0$, the corresponding Breguet-type equation is obtained as follows. First we define the total dissipation and vortex energy-rate coefficients C_Φ, C_{E_v}, the usual lift coefficient C_L, and the net effective propulsive power P and associated power-specific fuel consumption $PSFC$.

$$
C_\Phi \equiv \frac{\Phi_{\text{surf}} + \Phi_{\text{wake}}}{\frac{1}{2}\rho V_\infty^3 S}
\tag{F.23}
$$

$$
C_{E_v} \equiv \frac{\dot{E}_v}{\frac{1}{2}\rho V_\infty^3 S}
\tag{F.24}
$$

$$
C_L \equiv \frac{L}{\frac{1}{2}\rho V_\infty^2 S}
\tag{F.25}
$$

$$
P \equiv (P_{K_{\text{inl}}} + P_V) + (P_{K_{\text{out}}} - \Phi_{\text{jet}}) = \Phi_{\text{surf}} + \Phi_{\text{wake}} + \dot{E}_v
\tag{F.26}
$$

$$
P = \frac{1}{2}\rho V_\infty^3 S (C_\Phi + C_{E_v})
\tag{F.27}
$$

$$PSFC \equiv \frac{\dot{m}_{\text{fuel}}\, g}{P} \tag{F.28}$$

The weight rate of change can be related to the fuel flow rate and hence the power, and also to the weight/range gradient via the velocity for nearly-level flight.

$$\frac{dW}{dt} = -\dot{m}_{\text{fuel}}\, g = -P\; PSFC \tag{F.29}$$

$$\frac{dW}{dt} = \frac{dW}{dR}\frac{dR}{dt} = \frac{dW}{dR}\, V_\infty \tag{F.30}$$

Equating these two weight rate relations, inserting $W/L = 1$ for level flight, and invoking the coefficient definitions above gives

$$\frac{dW}{dR} = -\frac{P}{V_\infty}\, PSFC = -W\frac{P}{V_\infty L}\, PSFC \tag{F.31}$$

$$\frac{dW}{dR} = -W\frac{C_\Phi + C_{E_{\text{v}}}}{C_L}\, PSFC \tag{F.32}$$

This is then integrated over the mission to give the mission range in terms of the fuel-burned weight W_{f}, and the final aircraft weight W_{e}.

$$R = \frac{C_L}{C_\Phi + C_{E_{\text{v}}}}\frac{1}{PSFC}\ln\!\left(\frac{W_{\text{e}} + W_{\text{f}}}{W_{\text{e}}}\right) \tag{F.33}$$

F.4.1 Non-ingesting case

For the non-BLI isolated propulsion case, the following relations hold.

$$P = FV_\infty \tag{F.34}$$

$$PSFC = TSFC/V_\infty \tag{F.35}$$

$$C_\Phi = C_{D_p} \tag{F.36}$$

$$C_{E_{\text{v}}} = C_{D_i} \tag{F.37}$$

$$C_\Phi + C_{E_{\text{v}}} = C_D \tag{F.38}$$

The power-based Breguet equation (F.33) is then exactly equivalent to its usual thrust-based form as expected:

$$R = \frac{C_L}{C_D}\frac{V_\infty}{TSFC}\ln\!\left(\frac{W_{\text{e}} + W_{\text{f}}}{W_{\text{e}}}\right) \tag{F.39}$$

F.4.2 Ingesting case

For the ingesting case, the corresponding derivations above give

$$P' \equiv (P_{K_{\text{inl}}} + P_V) + (P_{K_{\text{out}}} - \Phi_{\text{jet}})' = \Phi'_{\text{surf}} + \Phi'_{\text{wake}} + \dot{E}_{\text{v}} \tag{F.40}$$

$$R = \frac{C_L}{C'_\Phi + C_{E_{\text{v}}}}\frac{1}{PSFC'}\ln\!\left(\frac{W_{\text{e}} + W_{\text{f}}}{W_{\text{e}}}\right) \tag{F.41}$$

where the BLI-case dissipation coefficient is defined as before in (F.23),

$$C'_\Phi \quad \equiv \quad \frac{\Phi'_{\text{surf}} + \Phi'_{\text{wake}}}{\frac{1}{2}\rho V_\infty^3 S} \tag{F.42}$$

$$\simeq \quad C_{D_p} - \frac{f_{\text{BLI}}\Phi_{\text{wake}}}{\frac{1}{2}\rho_\infty V_\infty^3 S}$$

$$= \quad C_{D_p} - f_{\text{BLI}}\frac{K_\infty - K_{TE}}{\rho_\infty V_\infty^3 S} \tag{F.43}$$

with the second approximate form using values from the non-ingesting case and may be useful in some applications. Similarly, $PSFC'$ is defined as

$$PSFC' \quad = \quad \frac{\dot{m}'_{\text{fuel}}\, g}{P'} \tag{F.44}$$

where it's essential to remember that P' and corresponding $\dot{m}'_{\text{fuel}}$ must be computed in the presence of the implied inlet kinetic energy defect $f_{\text{BLI}}K_{TE}$ and equivalent inlet total pressure loss. The range for the BLI case is then given simply by the power-based Breguet equation using the primed parameters.

$$R' \quad = \quad \frac{C_L}{C'_\Phi + C_{E_v}}\frac{1}{PSFC'}\,\ln\!\left(\frac{W_e + W_f}{W_e}\right) \tag{F.45}$$

F.5   Thrust and Drag Accounting

The presence of boundary layer ingestion makes the definition of "thrust" and "drag" somewhat ambiguous. However, the above definitions of F' and C'_Φ are reasonable choices for comparing against non-ingesting alternatives, since they reduce to the usual F and C_{D_p} definitions in the non-ingesting case. Furthermore, these choices closely reflect what really happens to the flowfield when boundary layer ingestion is introduced, and can be explained using common engine terminology.

- The dissipation of the removed wake is excluded from C'_Φ

- The reduced velocities into the engine inlet are both beneficial (from a "ram drag" argument), and detrimental (from a cycle efficiency argument). The net benefit can be either positive or negative, depending on a number of secondary factors.

F.6   Inlet Total Pressure Calculation

For engine-cycle calculations, it is necessary to define a suitably-averaged inlet total pressure p_{t2} from the inlet boundary layer properties.

F.6.1 Low speed flow case

For low speed flow, a suitable method is to perform a volume-flow weighted average of the total pressure.

$$\dot{\mathcal{V}}_{\text{inl}} \equiv \iint_{\text{inl}} V \, dA \tag{F.46}$$

$$
\begin{aligned}
(p_{t\,2} - p_{t\,\infty}) \, \dot{\mathcal{V}}_{\text{inl}} &= \iint_{\text{inl}} (p_t - p_{t\,\infty}) V \, dA \\
&\simeq \iint_{\text{inl}} \left(p + \tfrac{1}{2}\rho V^2 - p_e + \tfrac{1}{2}\rho_e V_e^2 \right) V \, dA \\
&= -\tfrac{1}{2}\rho_e V_e^3 \left(\Theta^* + \Delta^{**} \right)_{\text{inl}} \\
&= -f_{\text{BLI}} \left(K_{TE} + \tfrac{1}{2} V_e^2 Q_{TE} \right) \simeq -f_{\text{BLI}} K_{TE}
\end{aligned}
\tag{F.47}
$$

$$p_{t\,2} = p_{t\,\infty} - \frac{f_{\text{BLI}} K_{TE}}{\dot{\mathcal{V}}_{\text{inl}}} \tag{F.48}$$

F.6.2 High speed flow case

An alternative approach, more justifiable for the high speed case, is to employ a mass weighted average of the entropy. The adiabatic boundary layer is assumed to have some known velocity profile a constant total temperature $T_t = T_{t_e} = T_{t_\infty}$, and the usual assumption of a constant profile static pressure $p = p_e$ is also made. This gives the following temperature and entropy profiles in terms of the velocity profile $V_{(y)}$.

$$T_{(y)} = T_{t_e} - \frac{V_{(y)}^2}{2\,c_p} \tag{F.49}$$

$$s_{(y)} = \ln \frac{(T_{(y)}/T_{t_\infty})^{\frac{\gamma}{\gamma-1}}}{p_{(y)}/p_{t_\infty}} = \ln \frac{(T_{(y)}/T_e)^{\frac{\gamma}{\gamma-1}}}{p_{(y)}/p_e} = \frac{\gamma}{\gamma-1} \ln \frac{T_{(y)}}{T_e} \tag{F.50}$$

For modest heat transfer and near-unity Prandtl numbers, the Stewartson temperature profile is quite accurate.

$$\frac{V_{(y)}}{V_e} \equiv U_{(y)} \tag{F.51}$$

$$\frac{T_{(y)}}{T_e} = 1 + \frac{T_w - T_{aw}}{T_e}(1 - U) + r\frac{\gamma-1}{2} M_e^2 \left(1 - U^2\right) \tag{F.52}$$

$$= 1 + r\frac{\gamma-1}{2} M_e^2 \left(1 - U^2\right) \qquad \text{(for adiabatic flow)} \tag{F.53}$$

$$r \simeq Pr^{1/2} \simeq 0.9 \qquad \text{(for air)} \tag{F.54}$$

For a typical fan, $M_e \simeq 0.6$, so that the compressibility factor is quite small compared to unity.

$$r\frac{\gamma-1}{2} M_e^2 \simeq 0.065 \ll 1 \qquad \text{(for } M_e = 0.6) \tag{F.55}$$

The entropy profile can then be simplified using the logarithm's Taylor series,

$$\ln(1+\epsilon) = \epsilon - \frac{1}{2}\epsilon^2 + \frac{1}{3}\epsilon^3 - \ldots \quad (F.56)$$

$$\frac{s(y)}{c_p} = \frac{\gamma}{\gamma-1} \ln\left[1 + r\frac{\gamma-1}{2}M_e^2\left(1-U^2\right)\right] \simeq r\frac{\gamma}{2}M_e^2\left(1-U^2\right) \quad (F.57)$$

which is accurate to roughly 3% for the $M_e = 0.6$ case.

The mass-weighted entropy flux and the associated average entropy $\bar{s}$ are then computed as follows.

$$\dot{m}_{\text{inl}} \equiv \iint_{\text{inl}} \rho V\, dA \quad (F.58)$$

$$\bar{s}\,\dot{m}_{\text{inl}} = \iint s\, d\dot{m} = \iint s\,\rho V\, dA = \rho_e V_e\, r\frac{\gamma}{2}M_e^2 \iint \left(1-U^2\right) RU\, dA \quad (F.59)$$

$$\bar{s} = \frac{\rho_e V_e \Theta_{\text{inl}}^*}{\dot{m}_{\text{inl}}}\, r\frac{\gamma}{2}M_e^2 \quad (F.60)$$

Substituting $\gamma M_e^2 = \rho_e V_e^2/p_e$ and for Θ_{inl}^* in terms of K_{inl} gives

$$\bar{s} = \frac{K_{\text{inl}}}{\dot{m}_{\text{inl}}}\, r\frac{\rho_e}{p_e} \quad (F.61)$$

Finally, the equivalent average total pressure is computed from this $\bar{s}$ via the entropy definition (F.50).

$$p_{t2} = p_{t\infty}\, \exp(-\bar{s}) \quad (F.62)$$

Bibliography

[1] J. Roskam. *Airplane Design*. DAR Corporation, Lawrence, Kansas, 2000.

[2] E. Torrenbeek. *Synthesis of Subsonic Airplane Design*. Delft University Press, 1988.

[3] D.P. Raymer. *Aircraft Design: A Conceptual Approach*. AIAA Education Series. AIAA, 1992.

[4] S. Jayaram, A. Myklebust, and P. Gelhausen. ACSYNT — A standards-based system for parametric computer aided conceptual design of aircraft. AIAA Paper 92-1268, Feb 1992.

[5] W.H. Mason and T.K. Arledge. ACSYNT aerodynamic estimation — An examination and validation for use in conceptual design. AIAA Paper 93-0973, Feb 1993.

[6] M.D. Ardema, M.C. Chambers, A.P. Patron, A.S. Hahn, M. Hirokazu, and M.D. Moore. Analytical fuselage and wing weight estimation of transport aircraft. NASA TM 110392, May 1996.

[7] B. Knapp, Matt. Applications of a nonlinear wing planform design program. Master's thesis, MIT, Aug 1996.

[8] S. Wakayama. *Lifting Surface Design Using Multidisciplinary Optimization*. PhD thesis, Stanford, June 1994.

[9] S. Wakayama. Blended-wing-body optimization setup. AIAA Paper 00-4740, Sept 2000.

[10] I. Kroo. PASS, program for aircraft synthesis studies. Software Package, Desktop Aeronautics, Palo Alto, CA, 2005.

[11] J.L. Kerrebrock. *Aircraft Engines and Gas Turbines, 2nd Ed.* The MIT Press, Cambridge, 1996.

[12] M. Drela. Power balance in aerodynamic flows. *AIAA Journal*, 47(7):1761–1771, July 2009. Also AIAA Paper 09-3762, San Antonio Conference, June 2009.

[13] J.K.C. Low. Ultra-high bypass ratio jet noise. NASA Contractor Report NASA CR-195394, NASA, 1994.

[14] J.R. Stone, D.E. Groesbeck, and C.L. Zola. Conventional profile coaxial jet noise prediction. *AIAA Journal*, 21(3), Mar 1983.

[15] M.R. Fink. Airframe noise prediction method. Report FAA-RD-77-29, FAA, 1977.

[16] J. Wolkovitch. The joined wing: An overview. *Journal of Aircraft*, 23(3), Mar 1986.

[17] R. Liebeck. Design of the blended wing body subsonic transport. *Journal of Aircraft*, 41(1), Jan 2004.

[18] M. Drela and M.B. Giles. Viscous-inviscid analysis of transonic and low Reynolds number airfoils. *AIAA Journal*, 25(10):1347–1355, Oct 1987.

[19] J.H. Horlock, D.T. Watson, and T.V. Jones. Limitations on gas turbine performance imposed by large turbine cooling flows. *Journal of Engineering for Gas Turbines and Power*, 123:487–494, Jul 2001.

[20] J.E. Sargison, S.M. Guo, M.L.G. Oldfield, G.D. Lock, and A.J. Rawlinson. A converging slot-hole film-cooling geometry — part 2: Transonic nozzle guide vane heat transfer and loss. *Journal of Turbomachinery*, 124:461–471, July 2002.

[21] B.L. Koff. Gas turbine technology evolution: A designer's perspective. *Journal of Propusion and Power*, 20(4):577–595, Jul–Aug 2004.

[22] T. Von Karman. Calculation of pressure distribution on airship hulls. Technical Memorandum 574, NACA, 1930.

[23] M. Drela. XFOIL: An analysis and design system for low Reynolds number airfoils. In T.J. Mueller, editor, *Low Reynolds Number Aerodynamics*. Springer-Verlag, Jun 1989. Lecture Notes in Engineering, No. 54, http://raphael.mit.edu/xfoil/.